

TECHNICAL REPORT STANDARD PAGE

1. Title and Subtitle
Design and Analysis Procedures for Asphalt Mixtures Containing High RAP Contents and/or RAS
2. Author(s)
Louay Mohammad, Ph.D., P.E. (WY), Wei Cao, Ph.D.,
Peyman Barghabany
3. Performing Organization Name and Address
Louisiana Transportation Research Center
Louisiana State University
Baton Rouge, LA 70808
4. Sponsoring Agency Name and Address
Louisiana Department of Transportation and Development
P.O. Box 94245
Baton Rouge, LA 70804-9245
5. Report No.
FHWA/LA.17/639
6. Report Date
April 2021
7. Performing Organization Code
LTRC Project Number: 14-5PF
SIO Number: DOTLT1000002
8. Type of Report and Period Covered
Final Report
Enter Date: 11/2014 – 10/2019
9. No. of Pages
128
10. Supplementary Notes
Conducted in Cooperation with the U.S. Department of Transportation, Federal Highway Administration
11. Distribution Statement
Unrestricted. This document is available through the National Technical Information Service, Springfield, VA 21161.
12. Key Words
RAP; RAS; WMA; cracking resistance; rheology; chemistry; mechanistic performance tests
13. Abstract
Asphalt recycling has been implemented as a cost-effective and environmentally friendly technique in pavement construction activities. Currently, the most widely used recycled asphalts are contributed from reclaimed asphalt pavement (RAP) and recycled asphalt shingles (RAS). In order to accommodate the recycled asphalts that are oxidatively aged, techniques such as warm-mix asphalt (WMA) processes and use of soft base binder have proven effective to attain the desired performance. With the increasing complexity in material composition, however, the design of asphalt mixtures has relied on the Superpave method, which is based on volumetric principles and is not directly related to performance. Mechanistic performance testing is needed to complement the Superpave approach that was originally developed for virgin materials. The objectives of this research project were to: (1) assess the impact of RAP/RAS binders on the chemical and rheological properties of their blends with virgin binders in relation to cracking resistance; (2) evaluate the asphalt mixture cracking resistance using a variety of testing methods; and (3) compare the mixture testing methods by developing a comprehensive score card system to provide a guideline for selecting the optimum testing methods.

In order to achieve the objectives, a total of 16 plant-produced loose mixtures contributed from four participating agencies of FHWA accelerated loading facility (ALF), Colorado DOT, Florida DOT, and Louisiana DOTD (referred to as ALF, CO, FL, and LA mixtures, respectively) were collected and characterized in the LTRC asphalt laboratory. These mixtures incorporated different RAP percentages, RAS, WMA technologies, and different soft base binders. The asphalt mixture tests employed consisted of simplified viscoelastic continuum damage (S-VECD), Texas overlay, four-point bending beam fatigue, semi-circular bend, indirect tension, and Illinois flexibility index (I-FIT) tests. Prior to testing, all compacted samples were subjected to long-term aging in a forced draft convection oven at 85°C for 120 hours. Data analysis was based on the test standard, or the developed approaches, to obtain the evaluation parameters for cracking resistance. Asphalt binders were extracted from the long-term aged, tested asphalt mixture samples. Rheological characterization included Superpave performance grading, frequency sweep, and linear amplitude sweep (LAS) tests. Chemical evaluation consisted of saturates, aromatics, resins, and asphaltenes (SARA) fractionation, gel permeation chromatography (GPC), and Fourier transform infrared (FTIR) spectroscopy. With respect to material composition, in general all the evaluation parameters for asphalt mixtures and extracted asphalt binders provided consistent observations with respect to cracking resistance. Increase in RAP percentage or use of RAS reduced the cracking resistance; use of the two WMA technologies (water foaming and Evotherm additive) with RAP was found to produce mixtures with comparable cracking performance with conventional hot-mix asphalt (HMA) mixtures; and use of soft base binder was found to be more effective in accommodating the recycled asphalts from (high) RAP than from RAS. In addition, incorporation of more recycled asphalt binders yielded increased percentages of asphaltenes (SARA fractionation) and high molecular weight (HMW) fractions (GPC), and higher values of carbonyl index (FTIR), which corresponded to reduced cracking resistance.

Correlations among the evaluation parameters were investigated. The S-VECD parameter provided the strongest correlation with the results from the remaining test methods, followed by the Texas overlay and SCB tests. Generally, good to strong relationships were observed among the rheological and chemical parameters of the extracted asphalt binders. The asphaltenes percentage (SARA) yielded the highest correlation with the rheological properties, while the critical temperature difference T_c determined from Superpave performance grading tests exhibited the highest correlation with the chemical properties. Relationship between the evaluation parameters of asphalt mixtures and extracted asphalt binders were also examined. Reasonable trends were noted, but the correlation was in general not strong. The lack of strong correlation was attributed to the complicating role of aggregate structure in resisting deformation and cracking.

Relationship between the laboratory asphalt mixture performance test results and field fatigue measurements on the ALF full-scale test lanes was evaluated. For this purpose, a strategy was developed to accommodate the structural variations in construction of the ALF lanes and the adjusted field performance was obtained. Based on the numerical and ranking correlations between the laboratory performance parameters and the adjusted ALF performance, the Texas overlay, S-VECD, and SCB tests were recommended as routine tools for evaluating the intermediate-temperature cracking resistance. These three methodologies demonstrated adequate mixture discriminating capabilities and good ranking agreement with the field performance. The beam fatigue test also proved to be an adequate test method despite its lengthy test time and relatively high variability. The IDT and I-FIT tests were not recommended as both showed weak mixture discriminating

potential and did not correlate well with the ranking of the ALF experiment. The preliminary test criteria for each mixture performance test were established based upon the field performance of the ALF lanes. Finally, a score card system was developed for comparing the six asphalt mixture performance tests, which considered 14 factors related to testing, data analysis, and correlation with field performance. This score card was evaluated independently by two asphalt laboratories from LTRC and Paragon Technical Services, Inc., both having sufficient experience with each test method to provide reliable scores. According to the scoring results, both laboratories considered the SCB and I-FIT tests the most desired testing methods for evaluating cracking resistance of asphalt mixtures, primarily given their high test efficiency and easy data analysis and interpretation. In this system, each factor was considered with the same weight, but certainly some factors (e.g., sensitivity to material composition, data analysis, and correlation with field performance) would be more emphasized in comparing the tests. Therefore, this score card result was only for the purpose of complementing the performance-based comparison of the test methods in selecting the appropriate methodologies in practice.

Project Review Committee

Each research project will have an advisory committee appointed by the LTRC Director. The Project Review Committee is responsible for assisting the LTRC Administrator or Manager in the development of acceptable research problem statements, requests for proposals, review of research proposals, oversight of approved research projects, and implementation of findings.

LTRC appreciates the dedication of the following Project Review Committee Members in guiding this research study to fruition.

LTRC Administrator/Manager

Samuel B Cooper, III, Ph.D., P.E.
Materials Research Administrator

Members

Aziz Khan
Jim Musselman
Danny Smith
Don Weathers
Chris Abadie
Scott Nelson

Directorate Implementation Sponsor

Christopher P. Knotts, P.E.
DOTD Chief Engineer

Design and Analysis Procedures for Asphalt Mixtures Containing High RAP Contents and/or RAS

By

Louay Mohammad, Ph.D., P.E. (WY)

Wei Cao, Ph.D., Peyman Barghabany

Department of Civil and Environmental Engineering

Louisiana State University

Louisiana Transportation Research Center

Baton Rouge, LA 70808

LTRC Project No. 14-5PF

SIO No. DOTLT1000002

conducted for

Louisiana Department of Transportation and Development

Louisiana Transportation Research Center

The contents of this report reflect the views of the author/principal investigator who is responsible for the facts and the accuracy of the data presented herein.

The contents do not necessarily reflect the views or policies of the Louisiana Department of Transportation and Development, the Federal Highway Administration or the Louisiana Transportation Research Center. This report does not constitute a standard, specification, or regulation.

April 2021

Abstract

Asphalt recycling has been implemented as a cost-effective and environmentally friendly technique in pavement construction activities. Currently, the most widely used recycled asphalts are contributed from reclaimed asphalt pavement (RAP) and recycled asphalt shingles (RAS). In order to accommodate the recycled asphalts that are oxidatively aged, techniques such as warm-mix asphalt (WMA) processes and use of soft base binder have proven effective to attain the desired performance. With the increasing complexity in material composition, the design of asphalt mixtures has been relying on the Superpave method, which is based on volumetric principles and is not directly related to performance. Mechanistic performance testing is needed to complement the Superpave approach that was originally developed for virgin materials. The objectives of this research project were to: (1) assess the impact of RAP/RAS binders on the chemical and rheological properties of their blends with virgin binders in relation to cracking resistance; (2) evaluate the asphalt mixture cracking resistance using a variety of testing methods; and (3) compare the mixture testing methods by developing a comprehensive score card system to provide a guideline for selecting the optimum testing methods.

In order to achieve the objectives, a total of 16 plant-produced loose mixtures contributed from four participating agencies of FHWA accelerated loading facility (ALF), Colorado DOT, Florida DOT, and Louisiana DOTD (referred to as ALF, CO, FL, and LA mixtures, respectively) were collected and characterized in the LTRC asphalt laboratory. These mixtures incorporated different RAP percentages, RAS, WMA technologies, and different soft base binders. The asphalt mixture tests employed consisted of simplified viscoelastic continuum damage (S-VECD), Texas overlay, four-point bending beam fatigue, semi-circular bend, indirect tension, and Illinois flexibility index (I-FIT) tests. Prior to testing, all compacted samples were subjected to long-term aging in a forced draft convection oven at 85°C for 120 hours. Data analysis was based on the test standard or the developed approaches to obtain the evaluation parameters for cracking resistance. Asphalt binders were extracted from the long-term aged, tested asphalt mixture samples. Rheological characterization included Superpave performance grading, frequency sweep, and linear amplitude sweep (LAS) tests. Chemical evaluation consisted of saturates, aromatics, resins, and asphaltenes (SARA) fractionation, gel permeation chromatography (GPC), and Fourier transform infrared (FTIR) spectroscopy.

With respect to material composition, in general, all the evaluation parameters for asphalt mixtures and extracted asphalt binders provided consistent observations with respect to cracking resistance. Increase in RAP percentage or use of RAS reduced the cracking resistance; use of the two WMA technologies (water foaming and Evotherm additive) with RAP was found to produce mixtures with comparable cracking performance with conventional hot-mix asphalt (HMA) mixtures; and use of soft base binder was found to be more effective in accommodating the recycled asphalts from (high) RAP than from RAS. In addition, incorporation of more recycled asphalt binders yielded increased percentages of asphaltenes (SARA fractionation) and high molecular weight (HMW) fractions (GPC), and higher values of carbonyl index (FTIR), which corresponded to reduced cracking resistance.

The correlations among the evaluation parameters were investigated. The S-VECD parameter provided the strongest correlation with the results from the remaining test methods, followed by the Texas overlay and SCB tests. Generally good to strong relationships were observed among the rheological and chemical parameters of the extracted asphalt binders. The asphaltenes percentage (SARA) yielded the highest correlation with the rheological properties, while the critical temperature difference T_c determined from Superpave performance grading tests exhibited the highest correlation with the chemical properties. Relationship between the evaluation parameters of asphalt mixtures and extracted asphalt binders were also examined. Reasonable trends were noted, but the correlation was in general not strong. The lack of strong correlation was attributed to the complicating role of aggregate structure in resisting deformation and cracking.

The relationship between the laboratory asphalt mixture performance test results and field fatigue measurements on the ALF full-scale test lanes was evaluated. For this purpose, a strategy was developed to accommodate the structural variations in construction of the ALF lanes, and the adjusted field performance was obtained. Based on the numerical and ranking correlations between the laboratory performance parameters and the adjusted ALF performance, the Texas overlay, S-VECD, and SCB tests were recommended as routine tools for evaluating the intermediate-temperature cracking resistance. These three methodologies demonstrated adequate mixture discriminating capability and also good ranking agreement with the field performance. The beam fatigue test also proved to be an adequate test method despite its lengthy test time and relatively high variability. The IDT and I-FIT tests were not recommended as both showed weak mixture discriminating potential and did not correlate well with the ranking of the ALF experiment. The

preliminary test criteria for each mixture performance tests were established based upon the field performance of the ALF lanes.

Finally, a score card system was developed for comparing the six asphalt mixture performance tests, which considered 14 factors related to testing, data analysis, and correlation with field performance. This score card was evaluated independently by two asphalt laboratories from LTRC and Paragon Technical Services, Inc., both having sufficient experience with each test method to provide reliable scores. According to the scoring results, both laboratories considered the SCB and I-FIT tests the most desired testing methods for evaluating cracking resistance of asphalt mixtures, primarily given their high test efficiency and easy data analysis and interpretation. In this system, each factor was considered with the same weight, but certainly some factors (e.g., sensitivity to material composition, data analysis, and correlation with field performance) would be more emphasized in comparing the tests. Therefore, this score card result was only for the purpose of complementing the performance-based comparison of the test methods in selecting the appropriate methodologies in practice.

Acknowledgments

The authors would like to acknowledge the support provided by Federal Highway Administration (FHWA), Louisiana Transportation Research Center (LTRC), Louisiana Department of Transportation and Development, Colorado DOT, and Florida DOT. The assistance of Jack Youtcheff, Ph.D., Nelson Gibson, Ph.D., and Xinjun Li in obtaining the technical data of the ALF test lanes is greatly appreciated. The assistance of Paragon Technical Services, Inc., in notching the I-FIT specimens is appreciated.

Implementation Statement

It is anticipated that the results from this study will provide guidance to state agencies in the selection of a fatigue/fracture performance test to incorporate during asphalt mixture design containing high-RAP and/or RAS materials. Incorporating a performance test as part of asphalt mixture design will address durability concerns of the produced mixture contained recycled brittle asphalt binder.

Table of Contents

Technical Report Standard Page	1
Project Review Committee	4
LTRC Administrator/Manager	4
Members	4
Directorate Implementation Sponsor	4
Design and Analysis Procedures for Asphalt Mixtures Containing High RAP Contents and/or RAS.....	5
Abstract	6
Acknowledgments.....	9
Implementation Statement	10
Table of Contents	11
List of Tables.....	12
List of Figures.....	13
Introduction.....	15
Objective	17
Scope.....	18
Methodology	19
Asphalt Mixture Testing and Data Analysis Methods	23
Asphalt Binder Testing and Data Analysis Methods	40
Discussion of Results.....	49
Asphalt Mixture Testing.....	49
Asphalt Binder Testing.....	70
Correlation of Evaluation Parameters between Asphalt Binders and Mixtures	88
Correlation between Laboratory and Field Fatigue Performance.....	90
Score Card ranking for Asphalt Mixture Test Methods	100
Conclusions.....	104
Recommendations.....	108
Acronyms, Abbreviations, and Symbols.....	109
References.....	112
Appendix.....	124
A. Score Card System for Asphalt Mixture Test Methods.....	124

List of Tables

Table 1. Asphalt mixture composition for the ALF materials.....	20
Table 2. Structural information of the ALF lanes	21
Table 3. Asphalt mixture composition for the CO, FL, and LA materials	22
Table 4. Relationships between parameters indicating asphalt mixture cracking resistance.....	68
Table 5. Relationships among the asphalt binder parameters	87
Table 6. Tensile strain responses and fatigue performance of the ALF lanes	91
Table 7. Ranking results for the ALF mixtures.....	98

List of Figures

Figure 1. Aggregate gradation of the ALF mixtures	21
Figure 2. Aggregate gradation curves of the CO, FL, and LA mixtures.....	22
Figure 3. Illustration of MFS calculation procedure.....	31
Figure 4. Development of the CCPR parameter	34
Figure 5. Illustration of calculation of DCSE	37
Figure 6. Dynamic modulus master curves for the ALF mixtures.....	50
Figure 7. Dynamic modulus master curves for the CO, FL, and LA mixtures	51
Figure 8. Damage characteristic curves of the ALF mixtures	53
Figure 9. Damage characteristic curves of the CO, FL, and LA mixtures.....	53
Figure 10. The MFS parameter from the S-VECD test for all the asphalt mixtures	54
Figure 11. Fatigue life results of the Texas overlay test for all the asphalt mixtures.....	55
Figure 12. Critical fracture energy results for all the asphalt mixtures.....	56
Figure 13. Crack progression rates and corrected crack progression rates for all the asphalt mixtures	57
Figure 14. Relationship of fatigue life $N_{f,BF}$ versus strain level for the ALF mixtures	58
Figure 15. Relationship of fatigue life $N_{f,BF}$ versus strain level for the CO, FL, and LA mixtures	58
Figure 16. Fatigue life $N_{f,BF}$ results at 340 microstrain for all the asphalt mixtures	59
Figure 17. The J_c parameter from the SCB test for all the asphalt mixtures	60
Figure 18. Dissipated creep strain energy results for all the asphalt mixtures.....	61
Figure 19. Flexibility index results for all the asphalt mixtures	62
Figure 20. Normalized parameters for evaluating the effect of RAP/RAS on the ALF mixtures (HMA with PG 64-22 base binder).....	64
Figure 21. Normalized parameters for evaluating the effect of RAP on the CO, FL, and LA mixtures	65
Figure 22. Normalized parameters for evaluating the effect of WMA technologies on the ALF mixtures containing: (a) 40% RAP with PG 58-28 base binder, and (b) 20% RAP with PG 64-22 base binder.....	66
Figure 23. Normalized parameters for evaluating the effect of soft base binder on the ALF mixtures containing: (a) 40% RAP, and (b) 20% RAS.....	67
Figure 24. The highest correlations among the parameters: (a) CCPR versus $N_{f,OT}$, and (b) J_c versus MFS	70
Figure 25. Superpave PG results of all the extracted asphalt binders.....	71
Figure 26. The ΔT_c parameter for all the extracted binders	73

Figure 27. Dynamic shear modulus master curves for the ALF extracted binders.....	74
Figure 28. Dynamic shear modulus master curves for the CO, FL, and LA extracted binders.....	74
Figure 29. The R parameter for all the extracted asphalt binders	75
Figure 30. Damage characteristic curves for the ALF extracted binders.....	77
Figure 31. Damage characteristic curves for the CO, FL, and LA extracted binders	77
Figure 32. The A_{LAS} parameter for all the extracted asphalt binders.....	78
Figure 33. SARA fractionation results for all the extracted asphalt binders	79
Figure 34. GPC fractionation results for all the extracted binders	81
Figure 35. Carbonyl index results for all the extracted asphalt binders.....	82
Figure 36. Normalized parameters for evaluating the effect of RAP/RAS on the ALF extracted binders	83
Figure 37. Normalized parameters for evaluating the effect of RAP/RAS on the CO, FL, and LA extracted binders	84
Figure 38. Normalized parameters for evaluating the effect of WMA technologies on the extracted binders from the ALF mixtures containing: (a) 40% RAP with PG 58-28 base binder, and (b) 20% RAP with PG 64-22 base binder	85
Figure 39. Normalized parameters for evaluating the effect of soft base binder for the extracted binders from the ALF mixtures containing: (a) 40% RAP, and (b) 20% RAS.....	86
Figure 40. Correlations among the selected parameters for asphalt mixtures and extracted asphalt binders	89
Figure 41. Relationship between MFS and the adjusted ALF performance.	93
Figure 42. Relationships between the Texas overlay parameters and the adjusted ALF performance	94
Figure 43. Relationship between $N_{f,BF}$ and the adjusted ALF performance.....	95
Figure 44. Relationship between J_c and the adjusted ALF performance.	96
Figure 45. Relationship between DCSE and the adjusted ALF performance.....	96
Figure 46. Relationships between FI and the adjusted ALF performance.....	97
Figure 47. Rank correlation coefficients for all mixture evaluation parameters with reference to the adjusted ALF fatigue life	99
Figure 48. Summary of scoring results for the asphalt mixture test methods.....	101

Introduction

Asphalt recycling has become an important instrument used to minimize production costs of new pavements as well as to mitigate its impacts on the environment. Some of the benefits of utilizing recycled materials include the conservation of nonrenewable natural resources such as virgin aggregates and asphalt binder, reduction in the amount of construction debris disposed of in landfills, decrease of the variability in material expenditures, and potential reduction of the overall life-cycle cost. Recycling also helps to cut greenhouse gas emissions by reducing the energy spent on the extraction and processing of petroleum products and aggregates. Moreover, the increasing price of asphalt binder along with more restrictive environmental legislation has forced the highway agencies and contractors to search for novel materials and construction techniques. Such efforts are aimed at fulfilling the current sustainability needs without compromising the pavement quality and performance. There is, at this time, considerable emphasis on the use of reclaimed asphalt pavement (RAP) as preferred recycled material for roadway construction due to its abundance and successful prior experiences. Recycled asphalt shingles (RAS) has also become another promising recycling candidate due to their potential use in asphalt mixtures. However, to ensure successful use of RAP and/or RAS, their impact on the engineering performance of asphalt mixtures should be addressed. It is generally found that use of RAP/RAS in asphalt mixtures would improve stiffness and rutting resistance while attaining a satisfactory or reduced moisture susceptibility [1, 2]. Yet, the introduced oxidized asphalt binders tend to embrittle the mixture, reduce the stress relaxation capability, and increase the mixtures' propensity to cracking [3, 4, 5]. To address this inadequacy, strategies such as the use of WMA technologies, soft base binder, and recycling agents have demonstrated the potential in accommodating the recycled asphalts to produce mixtures with similar performance as compared to conventional hot-mix asphalt mixtures [6, 7, 8, 9].

Despite the increasing complexity of material composition, the design of asphalt mixtures has been following the conventional volumetrics-based Superpave method that is essentially not related to performance. To ensure adequate pavement performance, the Superpave design method should be complemented with advanced performance tests. So far, a number of performance evaluation tests have been developed and implemented by researchers and practitioners for the design phase, as well as quality assurance and forensic study. Examples include the cyclic test methods such as simplified viscoelastic continuum damage (S-VECD), Texas overlay, and four-point bending beam tests, and

monotonic test methods such as semi-circular bend (SCB), and indirect tension (IDT), and Illinois flexibility index (I-FIT) tests.

As a composite material, asphalt mixture consists of aggregate, asphalt binder, and air voids. It is generally believed that asphalt binder plays a dominant role in resisting cracking by acting as an adhesive binding agent. With the increasing complexity in material composition, evaluation of asphalt binders extracted and recovered from mixtures is expected to provide insights into the mechanical performance of asphalt mixtures. Asphalt binder can be assessed for its chemical and rheological properties as related to the effect of oxidative aging and use of additives. Typical chemical evaluation approaches include the saturates, aromatics, resins, and asphaltenes (SARA) fractionation, gel permeation chromatography (GPC) test for molecular size distribution, and Fourier transformation infrared (FTIR) characterization for identifying the oxidation related functional groups. Typical rheological characterization methods include the Superpave performance grading, frequency sweep test for linear viscoelastic properties, and linear amplitude sweep (LAS) test for fatigue evaluation.

Despite recent advancements in the design and performance evaluation of asphalt mixtures containing RAP/RAS, many states are still cautious in their regulations to avoid premature fatigue cracking related to the use of these recycled materials. In many states, RAP is currently not allowed in highest-class asphalt mixtures and in polymer modified asphalt products. In addition, high percentages of RAP exceeding 25% are not commonly used in practice. Meanwhile, other state agencies are taking a more aggressive approach by considering increasing the allowable percentages of RAP in asphalt mixture to take full advantage of this promising technology. For instance, up to 50% RAP has been used in some asphalt mixtures, which produced an acceptable level of performance [1]. In order to establish confidence and promote the use of RAP/RAS in asphalt pavement, it is necessary to assess the existing, well-established performance evaluation test methods and to develop proper criteria to ensure adequate field performance of asphalt mixtures against fatigue cracking. It is also beneficial for material design to understand the effect of aged binder on the chemical and rheological properties of asphalt binders.

Objective

The objectives of this research project were to:

- Investigate the effect of oxidatively aged asphalt binder contributed from RAP/RAS on the chemical and rheological properties of their blends with virgin binders in relation to fatigue/fracture resistance;
- Establish mechanistic test criteria that ensures pavement fatigue performance for hot- and warm-mix asphalt mixtures containing high percentages of RAP or RAS; and
- Conduct a comparative study of the various mixture performance test methods and develop a score card ranking system for a comprehensive comparison that provides a guideline for selection of the optimum test methods.

Scope

The research study involved four participating federal/state agencies: Federal Highway Administration (FHWA), Colorado Department of Transportation (DOT), Florida DOT, and Louisiana Department of Transportation and Development (DOTD). Each agency contributed one field project including a minimum of two plant-produced asphalt mixtures consisting of a convention (or low RAP percentage) mixture and a mixture containing high RAP or RAS. If available, the field fatigue cracking performance data were collected. Each asphalt mixture was characterized in the Louisiana Transportation Research Center (LTRC) asphalt laboratory using the performance tests of S-VECD (including dynamic modulus test as part of the procedure), Texas overlay, four-point bending beam, SCB, IDT, and I-FIT tests. The extracted asphalt binders were characterized using the SARA fractionation, GPC, FTIR, Superpave performance grading, frequency sweep, and LAS tests for their chemical and rheological properties. Analysis of the test data followed the standard test methods, and in certain cases, new analysis methods were developed and new performance parameters proposed. The obtained results were discussed with respect to the material composition and were also compared to evaluate the interrelationships among them. The asphalt mixture performance parameters were correlated with the measured field fatigue data, and based on the resulting relationships, a design criterion was established for each parameter. Finally, all the asphalt mixture performance tests were compared in a total of 14 aspects as included in the score card ranking system.

Methodology

This chapter presents descriptions of the asphalt materials involved in this study and the testing methods for asphalt mixtures and binders. For each test, a brief review of its background, application, and data analysis are also provided. In certain cases, new data analysis approaches and evaluation parameters were proposed during the course of this study and are presented in details.

Materials

Asphalt materials used in this study consisted of loose mixtures provided by four participating agencies/facility: FHWA Accelerated Loading Facility, Colorado DOT, Florida DOT, and Louisiana DOTD.

The ALF materials were acquired during an experiment conducted on the full-scale test lanes at FHWA ALF in McLean, Virginia, in 2013. This experiment is a part of an ongoing FHWA Project FHWA-PROJ-11-0070 titled *Advance Use of Recycled Asphalt in Flexible Pavement Infrastructure: Develop and Deploy Framework for Proper Use and Evaluation of Recycled Asphalt in Asphalt Mixtures*. In total, 10 lanes using various RAP/RAS contents and warm-mix technologies were constructed. For all mixtures, the aggregate source, type, and gradation were kept constant in mixture design with a nominal maximum aggregate size (NMAS) of 12.5 mm. Table 1 provides the material composition information for the ten ALF mixtures. The volumetric properties were measured on cores taken from the lanes after construction. Despite the same design with the optimum asphalt content of 5.0%, the actual air voids, voids in the mineral aggregate (VMA), and binder content varied slightly due to production and placement variabilities, as can be seen in Table 1. Figure 1 provides the aggregate gradation obtained from the produced mixtures. Note that Lane 10 was excluded from this study due to construction issues. The content of recycled materials was expressed in terms of recycled binder ratio (RBR), which is defined as the percentage of recycled asphalt in the total asphalt binder of the mixture. As shown in Table 1, the RAP content used provided RBR of 20% and 40% in the mixtures, whereas the RAS content utilized yielded an RBR of 20% in HMA mixtures. The asphalt binder extracted and recovered from the RAP source was graded as PG 89-22, while the asphalt from RAS had a high-temperature PG well above 140°C (exceeding the limit of the test equipment). In addition, two warm-mix technologies

(water foaming and Evotherm) and two base binder grades (PG 58-28 and PG 64-22) were used.

Table 2 provides the structural information of the ALF test lanes, including asphalt layer thickness, and moduli of the crushed aggregate base (CAB) and subgrade. The average asphalt layer thickness for all lanes was 11.1 cm, and each asphalt layer was built on top of a 56-cm CAB layer. The base and subgrade moduli were obtained from back calculation using falling weight deflectometer (FWD) measurements. Each lane was loaded using a single wide-base tire with 63.2 kN wheel load and 689 kPa contact pressure. The wheel speed was 4.9 m/s and the asphalt layer temperature was maintained at 20°C during loading. Other details regarding the ALF mixtures and lanes can be found in Li and Gibson [10].

Table 1. Asphalt mixture composition for the ALF materials

Mix Designation	Air Void (%)	VMA (%)	Asphalt Content (%)	RAP RBR (%)	RAS RBR (%)	Virgin Binder PG	HMA/WMA Process
L1	4.3	16.1	5.08	--	--	64-22	HMA
L2	4.3	16.1	5.07	40	--	58-28	Water foam
L3	3.3	14.6	4.98	--	20	64-22	HMA
L4	4.4	15.6	4.95	20	--	64-22	Evotherm
L5	5.2	15.9	4.60	40	--	64-22	HMA
L6	3.6	14.9	4.91	20	--	64-22	HMA
L7	4.1	15.3	4.91	--	20	58-28	HMA
L8	4.9	16.4	4.95	40	--	58-28	HMA
L9	3.7	15.1	4.98	20	--	64-22	Water foam
L11	4.9	16.5	4.89	40	--	58-28	Evotherm

Note: VMA: voids in the mineral aggregate; RBR: recycled binder ratio; PG: performance grade; -- : not applicable.

Figure 1. Aggregate gradation of the ALF mixtures

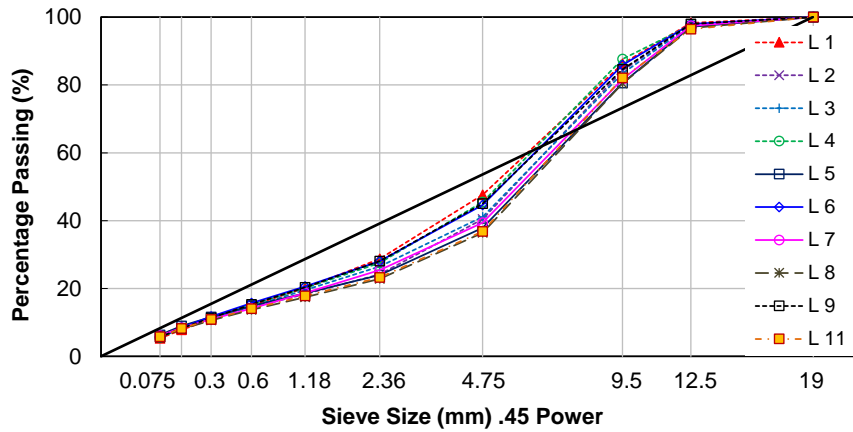


Table 2. Structural information of the ALF lanes

Lane	Asphalt Layer Thickness (cm)	CAB Modulus (MPa)	Subgrade Modulus (MPa)
L1	11.7	115.1	71.0
L2	11.7	109.6	81.4
L3	11.2	103.4	54.5
L4	11.6	83.4	72.4
L5	10.4	96.5	49.0
L6	11.7	82.7	103.4
L7	10.8	83.4	126.2
L8	11.4	85.5	61.4
L9	10.5	111.0	57.9
L11	10.3	90.3	57.2

Note: CAB = crushed aggregate base

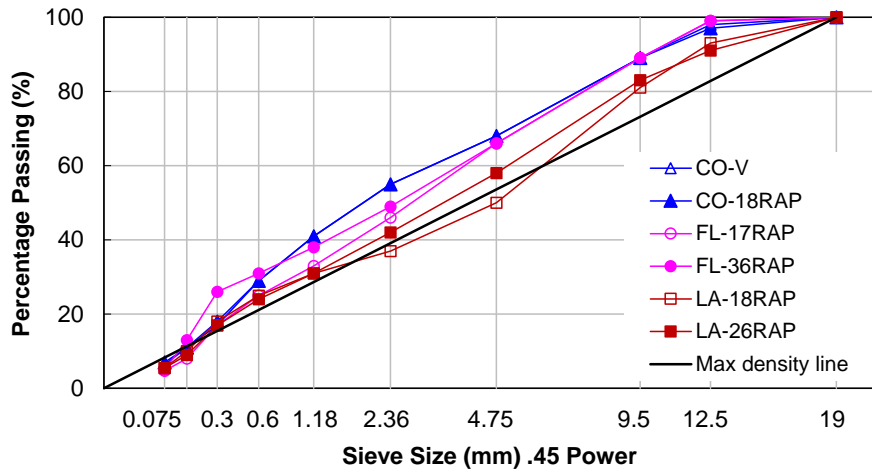
Table 3 and Figure 2 present the mixture composition and aggregate gradation, respectively, of the other three material sources, all with an NMAS of 12.5 mm. Two mixtures were provided by the Colorado DOT, which contained 0% and 18% RAP by RBR (designated as CO-V and CO-18RAP, respectively). A softer base binder was utilized to accommodate the 18% RAP incorporation. Florida DOT provided two asphalt

mixtures containing 17% and 36% RAP by RBR, denoted as FL-17RAP and FL-36RAP, respectively. A softer base binder was utilized to accommodate the 36% RAP incorporation. Louisiana DOTD provided two mixtures containing 18% and 26% RAP, denoted as LA-18RAP and LA-26RAP, respectively. The same base asphalt binder graded as PG 70-22 was used in both mixtures. Some minor differences were noted in the gradation curves of the produced FL and LA mixtures, but the same RAP source was employed within each mixture group.

Table 3. Asphalt mixture composition for the CO, FL, and LA materials

Mix Designation	RAP RBR	PG of Base Binder	Asphalt Content (%)
CO-V	0	64-22	5.3
CO-18RAP	18%	58-28	5.3
FL-17RAP	17%	58-22	5.2
FL-36RAP	36%	52-28	5.0
LA-18RAP	18%	70-22	5.0
LA-26RAP	26%	70-22	5.3

Figure 2. Aggregate gradation curves of the CO, FL, and LA mixtures



Asphalt Mixture Testing and Data Analysis Methods

Asphalt mixtures were first characterized using the dynamic modulus test for their linear viscoelastic properties. The cyclic fatigue characterization included simplified viscoelastic continuum damage (S-VECD), Texas overlay, and four-point bending beam fatigue tests. Three monotonic fracture tests were employed for the cracking resistance evaluation: semi-circular bend (SCB), indirect tension (IDT), and Illinois Flexibility Index (I-FIT) tests. All specimens were prepared with air voids within $7\% \pm 0.5\%$ unless otherwise stated, and were then long-term oven aged at 85°C for 120 hours in accordance with AASHTO R30 [11] prior to testing.

Dynamic Modulus Test

Dynamic modulus test was performed to ascertain the linear viscoelastic properties of asphalt mixtures. The loose mixtures were reheated and compacted using a Superpave Gyrotory Compactor (SGC) in the LTRC asphalt laboratory to a height of 170 mm and a diameter of 150 mm. For the purpose of a relatively uniform distribution of air void and smooth surface, the specimens were then cored and cut to attain a dimension of 150 mm in height and 100 mm in diameter for the dynamic modulus test.

The dynamic modulus test was conducted in the load-controlled compression mode using the Asphalt Mixture Performance Tester (AMPT) in accordance with AASHTO T 378 [12]. In the test, each specimen was subjected to a frequency sweep loading at 25, 10, 5, 1, 0.5, and 0.1 Hz under multiple temperatures of 4.4° , 25° , and 37.8°C , given the focus on the intermediate-temperature cracking resistance. Axial deformation was measured using three linear variable differential transducers (LVDTs) that were mounted over the middle 70 mm of the specimen at 120° intervals. The on-specimen strain level for each loading condition was maintained at 50-75 microstrain such that the material was in the linear viscoelastic region without induced damage. For reducing the end friction, Teflon sheets were inserted between the specimen ends and loading plates. For each mixture, three replicates were used to assess variability in the test results.

The isotherms of dynamic modulus from different temperatures were shifted, utilizing the time-temperature superposition principle with a reference temperature of 21.1°C . The amount of shift for each temperature is termed the shift factor. The dynamic modulus master curve is commonly fitted via a sigmoidal function:

$$\log|E^*| = \delta + \frac{\kappa}{1 + \exp[\beta + \gamma \log(f \times a_T)]} \quad (1)$$

$$\log a_T = a_1 (T - T_R)^2 + a_2 (T - T_R) \quad (2)$$

where, $|E^*|$ is dynamic modulus, f is loading frequency, a_T is time-temperature shift factor, T is temperature, T_R is reference temperature (21.1°C), and δ , κ , β , γ , a_1 , and a_2 are fitting coefficients.

S-VECD Test

The S-VECD fatigue characterization approach is based on uniaxial loading of cylindrical specimens, thereby rendering a uniformed and clearly defined stress and strain distributions that can readily be used in mechanistic modelling. In addition, the S-VECD framework is built upon rigorous viscoelasticity and continuum damage theories. Therefore, in addition to the material level assessment, its finite element implementation is made possible for structural response and performance evaluation. The viscoelastic continuum damage (VECD) theory was initially developed for constitutive modelling of asphalt materials under monotonic loading conditions. In theory, it is assumed that the nonlinearity in the stress-strain relation is exclusively attributed to material's intrinsic viscoelasticity and microcrack damage. Later, some simplifying assumptions based on experimental observations and theoretical hypotheses were applied to the theory and its numerical algorithms to arrive at the S-VECD framework that is tailored for the analysis of cyclic fatigue data [13, 14, 15]. The capability and efficiency of the S-VECD modelling scheme have been demonstrated in predicting the fatigue cracking of full-scale test pavements [15, 16]. The material characterization results have also been shown to be sensitive to mixture compositions, such as asphalt content, PG, and modification of the binder, NMAS, and RAP and RAS content [17, 18, 19]. In most cases, inclusion of recycled asphalt would compromise the fatigue resistance of WMA and HMA while use of warm-mix technologies would benefit materials containing RAP and/or RAS [19, 20]. Nevertheless, a study also suggested that assessment using the existing S-VECD methodology, like all other evaluation approaches, be conducted on a case-by-case basis, as for certain mixtures even high RAP content may not bring noticeable detriment to materials' fatigue characteristics [19].

Samples used for the S-VECD direct tension cyclic fatigue test was compacted to 180 mm in height and 150 mm in diameter, and then were trimmed down to 130 mm in height

and 100 mm in diameter. This test was performed in the actuator-displacement controlled tension mode using AMPT according to AASHTO TP 107 [21]. Steel end plates were glued to the specimen using Devcon Plastic Steel Putty 10110, and a curing period of 16 hours was applied prior to testing. During testing, the apparent dynamic modulus and phase angle were calculated as is done in the dynamic modulus test, and were monitored for each cycle. The cycle number to failure, N_f , was determined as the cycle number at which the phase angle began to drop. Generally, two or three strain levels are required to characterize a mixture with the target N_f greater than 500 in accordance with AASHTO TP 107. In this study, the test temperature was 18°C and the loading frequency was 10 Hz. Axial deformation was measured using three LVDTs that were mounted over the middle 70 mm of the specimen at 120° intervals. For each mixture, three replicate samples with different initial strain levels were tested.

Analysis of the direct tension cyclic fatigue test was based on the VECD theory to yield damage characteristic relationship. The detailed analysis steps have been described in AASHTO TP 107. The following outlines the key concepts and equations used in analysis, which also provides the necessary background for the proposed evaluation parameters.

The S-VECD characterization essentially produces the damage characteristic relation between C , the secant pseudo stiffness indicating material integrity, and S , the internal state variable quantifying the load-induced damage. For a balance of theoretical rigor and practical feasibility in the model implementation, the calculation of C and S using the fatigue test data is divided into two steps, i.e., transient analysis for the first half cycle, and cyclic analysis for subsequent cycles. The transient analysis is necessitated because a significant amount of damage can be induced in the material due to the first loading cycle. The ascending load in the first half cycle can be treated as monotonic loading, and as such, the rigorous VECD algorithm should be adopted. Both C and S are determined for each time step in the transient analysis according to Equations (3-5). For subsequent cyclic analysis, due to the involvement of unloading and reloading, the simplified VECD algorithm is applied such that for each cycle, a pair of representative C and S values is obtained. The key functions for the cyclic analysis are summarized in Equations (6-8). It is noted that for the cyclic analysis, damage is assumed to develop only during the tensile loading portion in each cycle. The C and S values from the last time step in the transient analysis serve as the initial condition for the cyclic analysis.

$$\varepsilon^R = \frac{1}{E_R} \int_{0^-}^{\xi} E(\xi - \tau) \frac{d\varepsilon(\tau)}{d\tau} d\tau \quad (3)$$

$$C = \frac{\sigma}{\varepsilon^R \times DMR} \quad (4)$$

$$\Delta S_i = \left[-\frac{DMR}{2} (\varepsilon_i^R)^2 (C_i - C_{i-1}) \right]^{1+\alpha} (\xi_i - \xi_{i-1})^{\frac{1}{1+\alpha}} \quad (5)$$

where, ε^R is pseudo strain; E_R is reference modulus, usually taken as unity; ξ denotes reduced time; τ is the integration variable for time; ε denotes strain time history; DMR is dynamic modulus ratio, Equation (9); C is secant pseudo modulus; S is internal state variable for damage; i is the i -th time step in the transient analysis; and α is damage evolution rate.

$$C = \frac{\sigma_{pp}}{\varepsilon_{pp}^R \times DMR} \quad \text{with} \quad \varepsilon_{pp}^R = \frac{1}{E_R} (\varepsilon_{pp} \times |E^*|_{LVE}) \quad (6)$$

$$\Delta S_j = \left[-\frac{DMR}{2} \left(\frac{\varepsilon_{pp,j}^R}{2} \right)^2 (C_j - C_{j-1}) \right]^{1+\alpha} \cdot R_j^{\frac{1}{1+\alpha}} \quad (7)$$

$$R_j \equiv \int_{\xi_{b,j}}^{\xi_{e,j}} (\beta_j - \cos(\omega_r \xi))^{2\alpha} d\xi \quad (8)$$

where, σ_{pp} is stress amplitude in each cycle for the cyclic analysis; ε_{pp} is strain amplitude; $|E^*|_{LVE}$ is the representative dynamic modulus of the material under the fatigue loading condition, Equation (10); ε_{pp}^R is pseudo strain amplitude; j is the j -th cycle in the cyclic analysis; ω_r is reduced angular frequency, Equation (11); β_j is form factor measuring the portion of tensile loading in the j -th cycle, Equation (12); and $\xi_{b,j}$ and $\xi_{e,j}$ denote the beginning and ending of the reduced time of damage development in the j -th cycle, Equations (13) and (14), respectively.

DMR is used to eliminate the effect of test variability among replicates that may be attributed to discrepancies in specimen properties and test setup. Prior to each cyclic fatigue loading, a 50-cycle load controlled dynamic modulus test with zero-mean stress is

performed at the same frequency and temperature with the fatigue loading. The on-specimen deformation is maintained at a peak-to-peak magnitude of 50 to 75 microstrain ensuring that no damage is induced in the material. The measured dynamic modulus value is denoted as $|E^*|_{\text{fingerprint}}$ and is employed to calculate DMR as presented in Equation (9):

$$DMR = \frac{|E^*|_{\text{fingerprint}}}{|E^*|_{LVE}} \quad (9)$$

$$|E^*|_{LVE} = \sqrt{\left(E_\infty + \sum_{m=1}^M \frac{E_m \rho_m^2 \omega_r^2}{\rho_m^2 \omega_r^2 + 1}\right)^2 + \left(\sum_{m=1}^M \frac{E_m \rho_m \omega_r}{\rho_m^2 \omega_r^2 + 1}\right)^2} \quad (10)$$

$$\omega_r = 2\pi f a_T \quad (11)$$

where, f is the physical loading frequency, and E_∞ , E_m , and ρ_m are the Prony series coefficients determined based on the dynamic modulus test results.

$$\beta_j = \frac{\sigma_{\text{peak},j} + \sigma_{\text{valley},j}}{|\sigma_{\text{peak},j}| + |\sigma_{\text{valley},j}|} \quad (12)$$

where, $\sigma_{\text{peak},j}$ is the peak and valley tensile stress values in the j -th cycle, respectively.

$$\xi_{b,j} = \frac{\cos^{-1} \beta_j}{\omega_r} \quad (13)$$

$$\xi_{e,j} = \frac{2\pi}{\omega_r} - \frac{\cos^{-1} \beta_j}{\omega_r} \quad (14)$$

The damage evolution rate, α , has been related to material's linear viscoelastic time dependence in theoretical explorations [22]. Experimental investigations revealed that the maximum absolute value of the log-log slope of the linear viscoelastic relaxation modulus, n , could be used to represent the material's overall time dependence in the condition of microcracking damage, and the following relations produced consistent results, i.e., $\alpha = 1/n + 1$ for actuator-displacement controlled fatigue test and $\alpha = 1/n$ for load controlled test [14].

With the C and S data obtained from the transient and cyclic analyses, choices can then be made to use either the exponential function in Equation (15), or the power function in Equation (16) to fit the damage characteristic curve:

$$C(S) = e^{aS^b} \quad (15)$$

$$C(S) = 1 - C_1 S^{C_2} \quad (16)$$

where, a , b , C_1 , and C_2 are the fitting coefficients.

Development of Material Fatigue Sensitivity. The damage characteristic curve is a constitutive relation describing the path along which the microcrack damage in a viscoelastic material should follow. The $C(S)$ relation is yet not suited for ranking or correlating with the material's fatigue resistance because it is complicated by the role of (pseudo) stiffness. It would be straightforward to assess the fatigue resistance if fatigue life can be obtained based on the $C(S)$ relation. However, it is important to realize that the S-VECD theory is established based on the continuum assumption, which would be violated once microcracks start to coalesce and cause damage localization. The theory itself does not provide a definition for the applicable region. In other words, the portion of the $C(S)$ curve (starting from $C = 1$) that is applicable for the mixture of interest under the given loading condition is not specified. Hence, a separate failure criterion is required to complete the S-VECD framework. The failure criterion defines the point beyond which material is dominated by macrocracks (indicating fatigue failure), and is thus needed for the prediction of fatigue life N_f .

Sabouri and Kim developed a unified failure characterization approach based on the energy dissipation concept [23], and its validity has been verified on a variety of mixtures [17, 19, 24]. However, this unified failure criterion entails cyclic fatigue test with middle failure (fracture located within the LVDT mounting targets). Tests with end failure (fracture located beyond the LVDT range) can be used to construct the $C(S)$ curve but not to identify the failure criterion. It should be acknowledged that, even though the required test specimen height has been reduced to 130 mm for an improved possibility of middle failure in the test [25], achieving middle failure may still be an appreciable challenge especially for specimens with relatively large air void or aging gradient towards the two ends. Moreover, in order for an accurate characterization of the unified failure criterion, it is required that specimens in the test fail at a wide range of cycle numbers. Ideally, three valid tests are needed with the cycle numbers to failure on the order of magnitude of

1,000, 10,000, and 100,000, which is expected to be achieved by properly choosing the actuator-displacement amplitude [23]. This requirement poses another challenge to researchers and practitioners especially for the cases with limited material and time allocation.

In light of the above discussion and practical needs, a new material parameter named Material Fatigue Sensitivity (MFS) is developed [26] and is aimed to represent asphalt mixture's intrinsic resistance to fatigue cracking. Its calculation only needs the damage characteristic curve without experimental requirements on specimen failure location and the range of number of cycles to failure in the test. This advantage was greatly enjoyed in this study as in the S-VECD test. Almost half of the samples failed beyond the LVDT measurement range, presumably due to the high RAP/RAS incorporation and aging gradient. The following outlines the equations used for determining MFS.

The VECD theory originated from Schapery's work-potential theory [27] and the pseudo strain based correspondence principle [28], combined into

$$W^R = \frac{1}{2} C(S) (\varepsilon^R)^2 \quad (17)$$

and the damage evolution law [29]:

$$\frac{dS}{d\xi} = \left(-\frac{\partial W^R}{\partial S} \right)^\alpha \quad (18)$$

Substitution of (17) into (18) yields

$$\frac{dS}{d\xi} = \left(-\frac{1}{2} (\varepsilon^R)^2 \frac{dC}{dS} \right)^\alpha \quad (19)$$

For the experimentally determined damage characteristic curves, the exponential form was found to provide much better fitting than the power form. Using the exponential representation in Equation (15), the above expression reduces to

$$\frac{dS}{d\xi} = \left(-\frac{1}{2} (\varepsilon^R)^2 abS^{b-1} e^{aS^b} \right)^\alpha \quad (20)$$

which is then rearranged into

$$\left(-abS^{b-1}e^{aS^b}\right)^{-\alpha} dS = \left(\frac{1}{2}(\varepsilon^R)^2\right)^\alpha d\xi \quad (21)$$

For each individual cycle, the time history of pseudo strain can be expressed as

$$\varepsilon^R(\xi) = \frac{\varepsilon_{pp}^R}{2} [\beta - \cos(\omega_r \xi)] \quad (22)$$

Substituting Equation (22) into (21) and integrating from the initial loading to N_f , we obtain

$$\left[\frac{1}{8}(\varepsilon_{pp}^R)^2\right]^{-\alpha} \int_0^{S_f} \left(-abS^{b-1}e^{aS^b}\right)^{-\alpha} dS = \sum_{j=1}^{N_f} \int_{\xi_{b,j}}^{\xi_{e,j}} (\beta_j - \cos(\omega_r \xi))^{2\alpha} d\xi \quad (23)$$

where, S_f denotes the amount of damage at material failure. Note that in the above equation, the pseudo strain amplitude ε_{pp}^R is treated practically as a constant for all cycles, as without any induced damage asphalt concrete is able to reach the steady state fairly quickly. The form factor β in the strain-based simulation is evaluated via

$$\beta_j = \frac{\varepsilon_{peak,j}^R + \varepsilon_{valley,j}^R}{\varepsilon_{pp}^R} \quad (24)$$

where, $\varepsilon_{peak,j}^R$ and $\varepsilon_{valley,j}^R$ denote the peak and valley pseudo strain values in the j -th cycle, respectively.

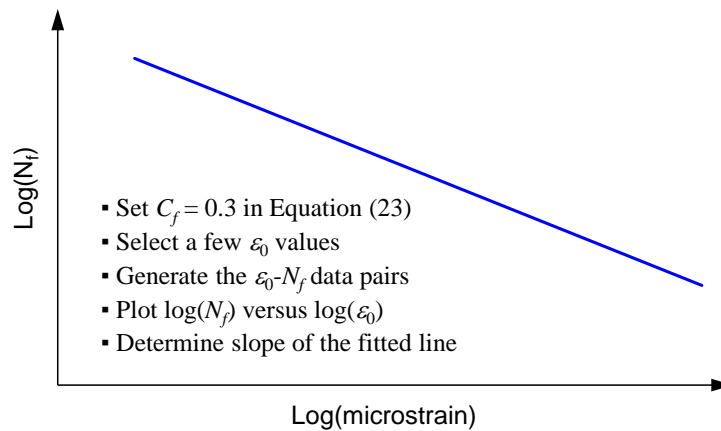
For the integration at the left hand side of Equation (23), it was found that a total of 1,000 intervals using the trapezoidal rule was adequate for evaluation. Therefore, the left hand side of Equation (23) can be conveniently evaluated for a given C_f (or S_f) value. Even though a closed-form solution for N_f is not available due to variation in the form factor β , the fatigue life N_f can still be easily obtained using the above-described numerical strategy.

For each mixture, using Equation (23), a series of failure envelopes (relations between N_f and ε_i) were constructed for multiple C_f values (i.e., 0.2, 0.3, 0.4, and 0.5) covering the range of C_f that is normally observed in the cyclic fatigue test. In this process, the strain-based fatigue simulation was carried out using the pavement temperature (20°C), and the loading frequency obtained from the finite element structural analysis (to be presented

later). The resulting relations between N_f and ε_f can be adequately represented using power functions, and are illustrated by straight lines in the double-logarithmic scales. The MFS parameter is defined as the magnitude of slope of the failure envelopes.

Figure 3 presents the calculation procedure for MFS. It is worth pointing out that, as a material constant, the MFS parameter is independent of the simulation conditions of temperature and frequency, and thus in practice the S-VECD test condition (e.g., 18°C, 10 Hz) can be utilized in place of the temperature and frequency within the pavement.

Figure 3. Illustration of MFS calculation procedure



Since MFS is independent of C_f that is directly associated with material's stiffness, the role of stiffness is excluded from fatigue evaluation. Hence, MFS could serve as a material parameter to indicate mixture's resistance to fatigue cracking. For higher MFS values, material's fatigue performance is more sensitive to variations in the loading condition. Therefore, MFS can be interpreted as an indicator to measure mixture's susceptibility to fatigue loading. Low MFS values are desirable for fatigue resistant mixtures.

Texas Overlay Test

The Texas overlay test was developed at the Texas Transportation Institute in late 1970s to ascertain material's resistance to reflective cracking in asphalt overlays [30]. This test has also been employed to evaluate the use of geosynthetics in asphalt layers in mitigating reflective cracking [31]. The test is performed on an overlay tester (OT) that uses a beam specimen in the early versions. The OT was later modified to use oval brick

specimens that can be trimmed from SGC samples and field cores [32]. During testing, the displacement is cycled so that the tensile and compressive stresses are induced and alternated in the specimen to simulate the crack closure and opening.

The Texas overlay test can be employed to obtain fracture and healing properties of asphalt mixture based on fracture mechanics theories and the concept of dissipated pseudo-strain energy [30, 31, 33]. However, these advanced analysis approaches should be used with caution because of the practical difficulties in measuring the crack propagation length during testing and the non-uniform distribution of stress and strain in the cross section of the specimen. Given this, the number of cycles to failure, denoted as $N_{f,OT}$, has been adopted to represent material's crack resistance, for which failure is defined as 93% reduction in the maximum tensile load [34]. Recently, Garcia et al. [35] developed a new analysis approach involving two parameters: critical fracture energy (CFE) and crack progression rate (CPR). CFE measures material's resistance to crack initiation and is an indicator of toughness. CPR is the rate of crack propagation under cyclic loading after the crack is initiated and is an indicator of material's flexibility [35].

In this study, sample fabrication and test procedures were performed in accordance with TxDOT Tex-248-F [36]. For each mixture, five SGC samples were compacted to 150 mm in diameter and 115 mm in height. Each sample was then trimmed down to obtain one 38-mm thick and 76-mm wide oval brick for testing. The test was conducted at 25°C under the displacement control mode using a triangular tensile waveform at a frequency of 0.1 Hz. The maximum displacement was 0.6 mm.

Existing Evaluation Parameters. As aforementioned, the existing evaluation parameters for the Texas overlay test consist of fatigue life, CFE, and CPR. Fatigue life, denoted by $N_{f,OT}$, was determined as the average from three replicates, which were selected out of the five to yield the minimum coefficient of variation (CoV) as suggested by Walubita et al. [37]. The CPR was determined as the magnitude of the exponent of the power-law fit to the curve of maximum tensile load versus cycle number. The CFE was calculated as

$$G_c = \frac{W_c}{B} \quad (25)$$

where, G_c is critical fracture energy (kJ/m^2), W_c is the area ($\text{kN}\cdot\text{m}$) under the curve of load-displacement in the first cycle up to peak load, and B is the cross-sectional area (m^2) of the test specimen.

Development of Corrected Crack Progression Rate. Derivation of the CPR parameter was based on the assumption that reduction in the maximum tensile load per cycle is exclusively attributed to fatigue damage in terms of cracking. However, it should be noted that viscoelastic relaxation of asphalt mixtures also contributed to the load reduction due to the continuous loading, and thus should have been accounted for in the analysis. Given this consideration, a new analysis approach was developed based on the CPR parameter by incorporating the viscoelastic relaxation effects. Without presence of damage, the linear viscoelastic stress response can be expressed as a convolution integral of the strain history:

$$\sigma_{LVE} = \int_0^t E(t-\tau) \frac{d\varepsilon}{d\tau} d\tau \quad (26)$$

where, σ_{LVE} denotes linear viscoelastic (LVE) stress, $E(t)$ is relaxation modulus that can be obtained through interconversion from the dynamic modulus master curve, ε is strain history, t is time, and τ is the integration variable for time. Equation (26) can be rewritten to obtain the relation between the LVE load and displacement:

$$\frac{F_{LVE}}{B} = \int_0^t E(t-\tau) \frac{d}{d\tau} \left(\frac{\Delta(\tau)}{L} \right) d\tau \quad (27)$$

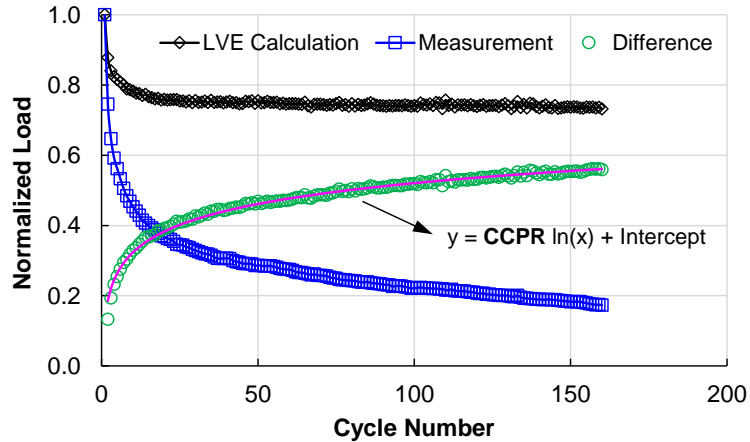
where, F_{LVE} denotes the linear viscoelastic load, B is the cross-sectional area, Δ is the applied displacement, and L is the effective gauge length (constant). Equation (27) is then rearranged to yield:

$$F_{LVE} = \frac{B}{L} \int_0^t E(t-\tau) \frac{d\Delta(\tau)}{d\tau} d\tau \quad (28)$$

Considering the variability in specimen dimension and setup among replicate testing, the linear viscoelastic load per cycle was normalized by F_{LVE} from the first cycle. Similarly, the maximum tensile load per cycle measured from the test was also normalized by that from the first cycle. The normalized LVE load decreases with cycle at a lower rate than the normalized maximum load from test since the latter is due to combined effects of viscous dissipation and cracking, as illustrated in Figure 4. To separate the effects of cracking damage, the difference between the two normalized loads was obtained and plotted against the cycle number. A logarithmic function was found to adequately describe the obtained relationship and the slope of the curve is proposed as the new parameter, corrected crack progression rate (CCPR), Figure 4. The CCPR parameter is

expected to represent the true crack propagation rate and low CCPR values are desired for crack resistant mixtures.

Figure 4. Development of the CCPR parameter



Beam Fatigue Test

The conventional approach for fatigue crack evaluation uses the four-point bending beam fatigue (BF) test, from which the well-known stress/strain versus fatigue life relationship (also referred to as failure envelope) is obtained. This relationship can be used to approach the classic concept of fatigue endurance limit [38] and has been adopted in some mechanistic-empirical pavement design algorithms including the AASHTOWare Pavement ME Design software.

The beam fatigue test was performed to evaluate the fatigue performance of asphalt mixtures in accordance with ASTM D7460 [39]. An asphalt roller compactor was used to compact the slabs with dimensions of 50 mm (height) by 300 mm (width) by 400 mm (length). Each slab was then trimmed to obtain four beams with 50 ± 2 mm in height, 63 ± 2 mm in width, and 380 ± 6 mm in length. Depending on the material availability, a minimum of four beam specimens were prepared for each mixture with air voids of $7.0 \pm 1.0\%$. The test was performed in strain-controlled mode, in which a beam specimen was subjected to a 10 Hz repeated sinusoidal deflection waveform and the resulting load was monitored throughout the test period. A minimum of two initial strain levels (peak-to-peak deflection) were applied to obtain the number of cycles to failure N_f on the order of 10^4 and 10^6 . Variability of duplicate test results was found to be much lower than the ASTM D7460 recommended acceptable repeatability level (i.e., difference in N_f less than

0.787 on the double logarithmic scale). The test results were then compiled to establish the failure envelopes that allowed for fatigue resistance evaluation and comparison. Note that two different definitions for fatigue failure in the bending beam test have been available: 50% reduction in flexural stiffness [40] and the peak of the normalized product of flexural stiffness and cycle number [41]. The latter definition yields a more convenient identification of fatigue life and was believed to be indicative of localization of cracking [42].

SCB Test

The SCB test configuration was first developed by Chong and Kuruppu [43] to obtain the stress intensity factor and fracture toughness for rock, concrete, and ceramic materials. Noting the drawbacks of the traditionally employed notched beam setup, Mull et al. [44] introduced the use of SCB configuration in asphalt concrete to obtain the critical strain energy release rate, J_c . The J_c parameter is based on fracture mechanics principles considering the nonlinear nature of constitutive behaviors of asphalt concrete. J_c measures the strain energy required to form a unit area of new surface that is fractured in a medium. A large J_c value represents high toughness, and thus is desired for crack resistant mixtures. The SCB test and the validity of J_c as an indicator for crack resistance has been widely investigated and verified in numerical analysis [45], laboratory experiments [46], and field evaluation [47]. This test has been favored by many researchers and practitioners due to the ease of sample preparation and simple testing procedure.

The SCB test was conducted at 25°C in accordance with ASTM D8044 [48]. Six SGC specimens were compacted to 57 mm in height and 150 mm in diameter. Each disk was then sliced along the diameter yielding two semi-circular halves. Subsequent to the oven aging, every four semi-circular specimens were notched at each of the three depths: 25.4 mm, 31.8 mm, and 38.1 mm. During testing, the specimen was loaded monotonically with an actuator-displacement rate of 0.5 mm/min until fracture in a three-point bending configuration. The collected load and displacement data were used to compute the J_c parameter via

$$J_c = -\frac{1}{w} \frac{dU}{dh} \quad (29)$$

where, J_c is the critical strain energy release rate (kJ/m²), w is specimen thickness (m), h is notch depth (m), and U is strain energy up to failure (kJ).

IDT Test

The IDT test was first introduced independently in Brazil and Japan in the 1940s. The test method and analysis approach were then further developed during the Strategic Highway Research Program [49, 50]. The IDT configuration was initially employed to acquire material properties such as resilient modulus, creep compliance, and Poisson's ratio. Later, it transitioned to an experimental tool for investigating the cracking behavior of asphalt mixtures in strength and fracture tests [51, 52]. This test employs a thin disk specimen that can be easily obtained from the Superpave gyratory compactor and field cores. Hence, it is appropriate for investigating existing pavements in forensic studies in addition to laboratory evaluations [53]. Besides, the IDT configuration also enjoys a unique advantage over other test methods due to the biaxial stress state it creates within the specimen. At the bottom of the asphalt layer in a pavement structure, materials are subject to tension and compression in horizontal and vertical directions, respectively, which makes it theoretically more suitable to select the IDT test from the perspective of fatigue evaluation [54]. The dissipated creep strain energy (DCSE) as a material parameter was proposed as the threshold defining the development of (non-healable) macrocracks [52]. Using this threshold concept, the HMA Fracture Mechanics model was developed [52], which accounted for the effect of pavement structure and provided the basis for the energy ratio (ER) parameter [55]. Based on a comprehensive evaluation of 22 field pavements that were in service for 10 years throughout the state of Florida, Roque et al. [55] recommended two criteria based on DCSE and ER to control the top-down cracking.

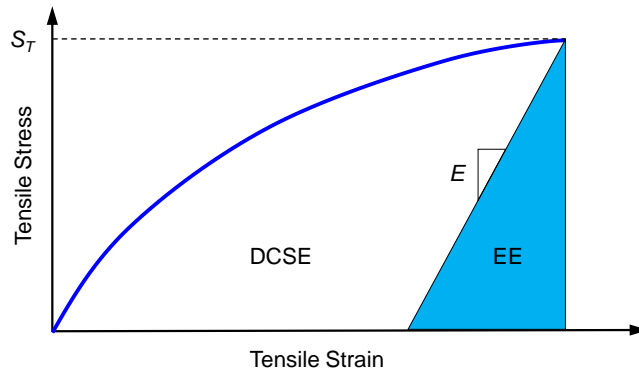
The IDT test includes three consecutive steps: dynamic modulus test, creep, and strength tests. In this study, all test steps were performed at 10°C on the same specimen with a minimum of 5-min interval. For each mixture, two SGC samples were compacted to 150 mm in diameter and 115 mm in height. Each sample was then trimmed to obtain two test specimens with 38-mm thickness. During testing, two sets of extensometers were mounted on both faces of the specimen for the measurement of horizontal and vertical deformations. The dynamic modulus test was conducted at a frequency of 10 Hz; the load level was adjusted to yield a nominal strain in the horizontal direction within 50 ± 5 microstrain. The creep load was carefully selected such that at the end of loading (i.e., 1000 s) the horizontal nominal strain was between 150 and 300 microstrain. The strength test was controlled in a monotonic mode with an actuator-displacement rate of 50 mm/min.

The DCSE has been found as independent of mode of loading (monotonic or cyclic), and can be easily obtained from the IDT strength test:

$$DCSE = FE - \frac{1}{2} \frac{S_T^2}{E} \quad (30)$$

where, FE is fracture energy (kJ/m^3) obtained as the area under the curve of tensile stress versus tensile strain at the specimen center up to the peak stress, S_T is tensile strength (kPa), and E denotes the dynamic modulus (kPa) obtained from the first step. Figure 5 presents the illustration for the calculation.

Figure 5. Illustration of calculation of DCSE



ER is defined as the ratio of $DCSE$ to the minimum dissipated creep strain energy $DCSE_{\min}$ that is required to preclude top-down cracking in the pavement:

$$ER = \frac{DCSE}{DCSE_{\min}} \quad \text{with} \quad DCSE_{\min} = m^{2.98} \cdot D_1 / A \quad (31)$$

where, m and D_1 (in GPa^{-1}) are the power-law regression coefficients of the creep compliance, $D(t) = D_0 + D_1 t^m$ in which D_0 is another regression constant and t denotes time; A (in MPa^{-2}) is obtained via $A = 8.64 \times 10^{-4} (6.36 - S_T) / \sigma^{3.1} + 3.57 \times 10^{-3}$, which was derived from the HMA fracture mechanics model [52]. Note that for calculating A , the strength S_T from the IDT test and tensile stress σ that is obtained from pavement structural analysis should be reported in MPa.

It is deemed necessary to briefly review the derivation of $DCSE_{\min}$ here for facilitating subsequent discussion. Using the HMA Fracture Mechanics model [52], Rogue et al. [55]

predicted the number of cycles to initiate and propagate a crack to a length of 50.8 mm for a total of 14 field pavement sections in the state of Florida. It was found that the value of 6000 cycles was able to distinguish the sections that cracked from those that did not, and that this value corresponded to $DCSE_{min}$ that is expressed in terms of material constants (m , D_1 , and S_T) and tensile stress (σ) of pavements, as shown in Equation (31). Therefore, both $DCSE_{min}$ and ER involve a pavement structure, and are no longer mere evaluation parameters for asphalt mixtures. Further, it should be borne in mind that the coefficients present in the expressions for $DCSE_{min}$ and A are specific for the threshold value of 6000 cycles that was applicable to the 14 Florida pavements. In general, this threshold would not apply to pavements in other regions with different material sources and traffic and environmental characteristics. Once the threshold value changes, the expressions for $DCSE_{min}$ and A will differ accordingly. The above investigation invalidates the general use of $DCSE_{min}$ and ER as indicators for the cracking resistance of asphalt mixtures. Besides, during application of the ER parameter, the authors observed the irrational trend that mixtures containing higher RAP contents tended to yield higher ER values. Hence, it was decided only the DCSE parameter was utilized for the IDT test in this study.

As suggested in Equation (30), dynamic modulus is required to quantify the amount of energy used to deform the material (i.e., elastic energy). This energy should be excluded from the fracture energy to obtain DCSE that is associated with the fatigue damage mechanism. The dynamic modulus was obtained following the viscoelastic solutions under the plane stress assumption [53]:

$$E = \frac{4P_a}{\pi w d} \cdot \frac{MG + NF}{|V_y^*|(F + G) - |U_x^*|(M - N)} \quad (32)$$

Where, E denotes dynamic modulus from the first IDT test step; P_a is the amplitude (i.e., half of peak-to-peak magnitude) of the harmonic load; w is the width of the loading strip; d is the specimen thickness; $|U_x^*|$ and $|V_y^*|$ are the amplitudes (both positive) of the displacements between the gauge points in the horizontal and vertical directions, respectively; ν denotes Poisson's ratio; and F , G , M , and N are geometry constants defined as

$$F = \int_{-l}^l f(x) dx \quad \text{with} \quad f(x) = \frac{(1 - x^2 / r^2) \sin 2\theta}{1 + 2x^2 / r^2 \cos 2\theta + x^4 / r^4} \quad (33)$$

$$G = \int_{-l}^l g(x)dx \quad \text{with} \quad g(x) = \tan^{-1} \left(\frac{1 - x^2 / r^2}{1 + x^2 / r^2} \tan \theta \right) \quad (34)$$

$$M = \int_{-l}^l m(y)dy \quad \text{with} \quad m(y) = \frac{(1 - y^2 / r^2) \sin 2\theta}{1 - 2y^2 / r^2 \cos 2\theta + y^4 / r^4} \quad (35)$$

$$N = \int_{-l}^l n(y)dy \quad \text{with} \quad n(y) = \tan^{-1} \left(\frac{1 + y^2 / r^2}{1 - y^2 / r^2} \tan \theta \right) \quad (36)$$

Where, r is specimen radius, θ is the radial angle formed by half the loading strip, and l denotes half the gauge length.

I-FIT Test

The Illinois flexibility index test (I-FIT) was recently developed by Al-Qadi et al. [56] using the semi-circular bend geometry via an investigation involving various temperatures and loading rates. The resulting flexibility index (FI) parameter is used to represent mixture's crack resistance. Materials with higher FI values are expected to exhibit higher resistance to cracking. To date, limited studies have been conducted with respect to this test. In some studies, the obtained FI was found to yield reasonable correlations with field performance of pavements [56]. Others provided both positive and negative conclusions regarding the capability of this test in discriminating mixtures by compositional and volumetric factors [57, 58]. In a more recent study, FI was found to be highly variable and was not sensitive to the presence and type of polymer modifiers [59].

The I-FIT test was conducted in accordance with AASHTO TP124 [60]. For each mixture, two SGC samples were compacted to 150 mm in diameter and 160 mm in height. Each sample was then cut to obtain two 50-mm thick disks, which were then sliced to yield a total of four semi-circular specimens. Prior to aging, each specimen was notched to a depth of 15 ± 1 mm and width of 1.5 ± 0.1 mm. Loading was performed monotonically with a displacement rate of 50 mm/min at 25°C. The flexibility index (FI) was calculated as:

$$FI = \frac{G_f}{n} \times \phi \quad \text{with} \quad G_f = \frac{W_f}{A_{lig}} \quad (37)$$

where, G_f is fracture energy (J/m^2); W_f is work of fracture (J) obtained as the area under the load versus displacement curve up to the post-peak cut-off load of 0.1 kN; A_{lig} is the

ligament area (m^2); n is the absolute value of slope (kN/mm) at the post-peak inflection point; and ϕ is a scaling factor set at 0.01.

In order to obtain the slope, a portion of the post-peak load versus displacement curve containing the inflection point was fitted using the generalized logistic function:

$$F(\delta) = \kappa + \frac{\mu - \kappa}{\left[\chi + \gamma e^{-\phi(\delta - \tau)} \right]^{1/\eta}} \quad (38)$$

where, F is load (kN), δ is displacement (mm), and κ , μ , χ , γ , ϕ , τ , and η are fitting coefficients. For all tests, the resulting R^2 -values of fitting were above 99.0%. The slope n was then numerically determined as the absolute value of minimum of the first derivative of $F(\delta)$ in Equation (38).

Asphalt Binder Testing and Data Analysis Methods

Asphalt Binder Extraction and Recovery

Asphalt binders were extracted and recovered from the long-term aged specimens according to AASHTO TP 164 [61] and AASHTO R 59 [62], respectively. Recovered asphalt binders were characterized for their rheological and chemical properties. Rheological characterization included Superpave performance grading, frequency sweep test, and linear amplitude sweep (LAS) test. Chemical characterization consisted of saturate, aromatic, resin, and asphaltene (SARA) analysis, gel permeation chromatography (GPC) test, and Fourier-transform infrared spectroscopy (FTIR) test.

Superpave Performance Grading

The Superpave performance grading consisted of the high-temperature grading using a dynamic shear rheometer (DSR) following AASHTO R 29 [63], and low-temperature grading using a bending beam rheometer (BBR) following AASHTO T 313 [64]. In general situations for liquid asphalts, prior to grading, they should be first treated following the standard aging procedures through the rolling thin-film oven (RTFO) test according to AASHTO T 240 [65] and pressurized aging vessel (PAV) according to AASHTO R 28 [66]. In the present study, the asphalts to be graded were recovered from compacted mixture samples that had already been long-term aged. For this reason, they were treated as RTFO aged samples for the high-temperature grading and as PAV aged

for low-temperature grading; that is, no further aging treatment was applied to the recovered binders prior to performance grading. The performance grading results were then determined in accordance with AASHTO M 320 [67].

A rheological parameter that can be determined from the Superpave performance grading test is critical temperature difference denoted as ΔT_c , which is defined as:

$$\Delta T_c = T_S - T_m \quad (39)$$

where, T_S is the critical temperature at which the flexural stiffness (S) of the beam equals 300 MPa, and T_m is the critical temperature at which the slope (m) of stiffness versus time in the log-log scale equals 0.300. Note that both T_S and T_m were evaluated at a creep loading time of 60 seconds. Using the BBR test data, T_S and T_m can be obtained from interpolation following the practice specified in ASTM D7643 [68].

ΔT_c was established upon its correlation observed with the viscosity function for unmodified asphalt binders, $G'/(\eta' / G')$, where G' is storage modulus and η' denotes dynamic viscosity [69, 70]. Glover et al. found that $G'/(\eta' / G')$ was well correlated with the ductility measured at 15°C and 1 cm/min for conventional asphalts [69], while in the meantime the ductility had been concluded as an adequate indicator of pavement cracking [71]. Rowe pointed out that $G'/(\eta' / G')$ can be represented in terms of dynamic shear modulus and phase angle, an expression that has now been commonly referred to as the Glover-Rowe (G-R) parameter [72]. In sum, the ΔT_c , $G'/(\eta' / G')$, and G-R parameters are all correlated with ductility and have been used as potential indicators of asphalt binder cracking resistance. In the present study, ΔT_c was selected as it was readily available from the PG testing.

Frequency Sweep Test

The frequency sweep test was performed at multiple temperatures using an Anton Paar MCR 302 DSR equipment to ascertain the linear viscoelastic properties of the asphalt binders. The parallel testing geometry with 8-mm diameter and 2-mm gap was employed. This test was conducted from 100 rad/s to 0.1 rad/s at three temperatures of 35°, 20°, and 5°C. The strain level was controlled at 0.1% to ensure that the material response was within the linear viscoelastic region. Two replicates were used for each asphalt binder considering the small variability typically observed in this test.

The isotherms of dynamic shear modulus were shifted to construct the modulus master curve with respect to a reference temperature of 20°C. The master curve was then fitted using the Christensen-Anderson (CA) model [73]:

$$|G^*(\omega_r)| = G_g \left[1 + \left(\frac{\omega_c}{\omega_r} \right)^{(\log 2)/R} \right]^{-R/\log 2} \quad (40)$$

where, $|G^*(\omega_r)|$ is dynamic shear modulus; G_g is glassy modulus taken as 1 GPa; ω_c is crossover angular frequency; R is a dimensionless shape parameter referred to as the rheological index; and ω_r is reduced angular frequency, $\omega_r = \omega a_T$, where ω is physical angular frequency, and a_T is time-temperature shift factor fitted via the second-order polynomial function as already shown in Equation (2) for the dynamic modulus master curves of asphalt mixtures.

The frequency sweep test result is needed in the VECD analysis of the LAS data. Apart from that, this test also provides the rheological index R , which has been utilized to gain insights into the fatigue cracking performance of asphalt binders. It has been reported that R is proportional to the width of the relaxation spectrum of asphalt binders and is also related to the degree of skewness in the spectrum [74]. Moutier et al. [75] identified a strong correlation between the fatigue resistance of asphalt mixtures and the width of the relaxation spectrum of the asphalt binders. By plotting R -values of short-term aged binder versus mixture bending beam fatigue test results, Christensen et al. [74] obtained a very high correlation between R -value and fatigue performance. Studies have also found that R increases during oxidative aging and decreases during effective rejuvenation [76, 77], and higher R -values appear to be associated with increasing molecular weight [75, 78]. In this study, R determined from the frequency sweep test was utilized as a rheological parameter to investigate the crack resistance of asphalt binders and to correlate with the chemical properties.

Linear Amplitude Sweep Test

The LAS test was conducted at an intermediate temperature of 18°C in accordance with AASHTO TP 101 [79] to ascertain the fatigue resistance of asphalt binders. The parallel-plate geometry with 8-mm diameter and 2-mm gap was used. This test procedure consisted of frequency sweep followed by the amplitude sweep with a 1-min. interval for stress relaxation. The frequency sweep was performed at 0.1% strain over a frequency range of 0.1 to 30 Hz to obtain material properties at the intact state of the LAS test

condition. The amplitude sweep had a constant frequency of 10 Hz and began with 100 cycles of sinusoidal oscillation at 0.1% strain. Each successive loading step comprised 100 cycles at strain amplitude linearly increasing from 1% to 30% at a rate of 1% per step.

The LAS data analysis was based on the viscoelastic continuum damage theory [80, 81, 82]. The analysis approach described in AASHTO TP 101 was critically reviewed and the formulation revised. A parameter denoted as A_{LAS} was developed and proposed as the indicator of asphalt binder fatigue resistance [83]. The following is devoted to the development of the formulation and the A_{LAS} parameter.

Analogous to the S-VECD model applied to asphalt mixture fatigue characterization, the structural integrity of asphalt binder is represented by the normalized dynamic shear modulus:

$$C = \frac{|G^*|}{DMR \cdot |G^*|_{LVE}} \quad (41)$$

where, $|G^*|$ is the apparent dynamic shear modulus in the amplitude sweep calculated as the ratio of stress amplitude to strain amplitude for each cycle, $|G^*|_{LVE}$ is the linear viscoelastic dynamic modulus corresponding to the LAS test temperature and frequency and can be interpolated from the dynamic shear modulus master curve, Equation (40), and DMR for asphalt binder is calculated as

$$DMR = \frac{|G^*|_{0.1\%}}{|G^*|_{LVE}} \quad (42)$$

where, $|G^*|_{0.1\%}$ is the dynamic modulus value obtained from the frequency sweep of the LAS test with 0.1% strain which serves as the fingerprint of the sample.

The pseudo strain energy for asphalt binder is given by

$$W^R = \frac{1}{2} DMR \cdot C(S) \cdot (\gamma^R(\xi))^2 \quad (43)$$

where, $\gamma^R(\xi)$ is the pseudo-shear strain time history given by

$$\gamma^R(\xi) = \gamma \cdot |G^*|_{LVE} \cdot \sin(\omega_r \xi) \quad (44)$$

where, γ denotes shear strain amplitude.

Combining Equations (18), (43), and (44), making appropriate substitutions, and integrating over a cycle, the damage increment per cycle is

$$\Delta S_i = \left[\frac{1}{2} DMR \cdot (\gamma_i \cdot |G^*|_{LVE})^2 (C_{i-1} - C_i) \right]^{1+\alpha} \cdot Q^{\frac{1}{1+\alpha}} \quad \text{with} \quad Q = \int_0^{2\pi/\omega_r} (\sin(\omega_r \xi))^{2\alpha} d\xi \quad (45)$$

where, α is determined according to AASHTO TP 101 as the exponent of the power-law fit to $|G^*|$ versus ω_r obtained from the frequency sweep step in the LAS test.

It is worth noting that in modeling fatigue of asphalt mixtures under uniaxial cyclic loading, damage is assumed to develop only during tensile loading, hence the need of the form factor as in Equation (12). Damage development in modeling asphalt binder, however, is assumed to occur all the time as the material is subjected to oscillatory distortion. Therefore, in the VECD formulation for binder, the form factor is not present.

The obtained C - S data pairs are then cross-plotted and fitted using the power-law form as shown in Equation (16). The substitution of Equation (16) into Equation (18) and following a derivation procedure similar to that for Equation (23), following relation can be used for fatigue simulation:

$$N_f = \left[\frac{1}{2} C_1 C_2 \cdot (|G^*|_{LVE})^2 \right]^{-\alpha} \cdot (\kappa Q)^{-1} \cdot (S_f)^\kappa \cdot \gamma_0^{-2\alpha} \quad (46)$$

where, $\kappa = 1 + \alpha - \alpha C_2$, and γ_0 is the strain amplitude for simulation. Note that the effect of loading condition (temperature and frequency) is incorporated in Q as can be seen from its definition in Equation (45).

Equation (46) presents a power-law relationship between fatigue life N_f and strain input γ_0 , which are related through a coefficient herein denoted as A_{LAS} :

$$A_{LAS} = \left[\frac{1}{2} C_1 C_2 \cdot (|G^*|_{LVE})^2 \right]^{-\alpha} \cdot (\kappa Q)^{-1} \cdot (S_f)^\kappa \quad (47)$$

The A_{LAS} parameter is then proposed as an indicator of asphalt binder fatigue resistance. A higher A_{LAS} value is desired for fatigue resistance asphalt binders, as can be seen from Equation (46).

SARA Analysis

The SARA analysis determines the chemical composition of asphalt binder by fractionating it into saturates, aromatics, resins, and asphaltenes. Asphaltenes are defined operationally as the pentane- or heptane-insoluble component of asphalt binder, while maltenes are the soluble component that can be further separated into the other three fractions. Asphaltenes consist of extremely complex, highly polar molecules; they exhibit a very high tendency to associate into molecular clusters, and play a significant role as viscosity builders in the rheology of asphalt binder [84]. During the oxidative aging process, ketones are formed, which significantly changes the polarity and thus the solubility of the associated aromatic components leading to their agglomeration to form the asphaltene component [85]. The resulting increase in the asphaltene fraction then becomes the primary reason for the increase in the asphalt viscosity due to aging [86]. Hence, in this study the asphaltenes fraction determined from the SARA analysis was used in investigation with respect to the asphalt binder composition and cracking performance.

Based on the SARA results, an additional parameter, referred to as the colloidal index, can be obtained as the ratio of the sum of the saturates and asphaltenes contents to that of the resins and aromatics contents. This parameter was developed considering asphalt binder as a colloidal structure [87, 88]. A small colloidal index indicates a well-dispersed system (i.e., the resins keep the highly associated asphaltenes dispersed in the light oily phase), more sol-like and homogeneous. A high colloidal index suggests a more gel-like system that is less dispersed and more heterogeneous. Asphalt binders with low colloidal indices are thus expected to exhibit better resistance to cracking due to its homogeneity and the free moving of the asphalt micelles [89]. The colloidal index was therefore utilized as another evaluation parameter from the SARA analysis.

Each recovered asphalt binder was first deasphalted in accordance with ASTM D3279 [90] to yield asphaltenes (insoluble) and maltenes (soluble). The maltenes component was further fractionated on an Iatroscan TH-10 Hydrocarbon Analyzer to obtain the components of saturates, aromatics, and resins. The n-pentane was used to elute the saturates, and a 90/10 toluene/chloroform mixture was used to elute the aromatics. The resins were not eluted and remained at the origin.

GPC Test

The gel permeation chromatography (GPC) presents an alternative technique for component fractionation of asphalt binder according to the sizes (hydrodynamic volumes) of different molecules. The separation process is analogous to the aggregate sieving process in which the largest molecules elute first, followed successively by smaller ones. The size-separated molecules are detected, typically by a differential refractive index detector or an ultraviolet detector, and recorded according to their concentration. Through calibration with molecules of known molecular weight (MW), hydrodynamic volume is then converted to MW; consequently, the MW distribution of an asphalt binder sample can be determined [84]. Compared to SARA analysis that is based on the complex property of solubility, GPC's ability to fractionate asphalt by molecular size is one of the great advantages of this technique [84].

The chromatogram obtained from GPC characterization is typically divided into three slices defined as large molecular size (LMS), medium molecular size (MMS), and small molecular size (SMS). It has been reported that aging increases the LMS region while decreasing the SMS region by agglomerating the small molecules to produce large ones [91]. In addition, asphalt mixtures with higher content of large molecules were found to exhibit lower tensile strength and thus presumably lower crack resistance in the field [91]. Correlations between large molecules and pavement cracking have been identified, which suggested that excessive amount of large molecules in asphalt binder would cause cracking in field pavements [92, 93]. Hence, in this study, the high molecular weight (HMW) fraction was used as the chemical parameter determined from the GPC test.

The gel permeation chromatography (GPC) characterization was performed using an EcoSEC high performance GPC system (HLC-8320GPC) of Tosoh Corporation, equipped with a differential refractive index detector and an ultraviolet detector. A set of four microstyragel columns of pore sizes 200 Å, 75 Å (2 columns), and 30 Å from Tosoh Bioscience was used for the analysis. Tetrahydrofuran (THF) was used as the solvent at a flow rate of 0.35 mL/min. The columns were calibrated using polystyrene standard mixtures PStQuick B (MW= 5480000, 706000, 96400, 10200, and 1000 Daltons), PStQuick E (MW= 355000, 37900, 5970, and 1000 Daltons), and PStQuick F (MW= 190000, 18100, 2500, and 500 Daltons) from Tosoh Bioscience. Each recovered asphalt binder was dissolved in the THF solvent at a concentration of 0.5%, and the solution was filtered using 0.45-micron Teflon filters.

FTIR Test

The Fourier transform infrared spectroscopy (FTIR) technique has been utilized for identification and quantification of functional groups present in asphalt binders. This approach is developed by exploiting the fact that molecules absorb light of the so-called resonant frequencies that are characteristics of the covalent bonds in the molecules. By analyzing the position, shape, and intensity of peaks in the obtained infrared spectrum, details on the molecular structure of the asphalt can be revealed. However, it is almost impossible to exactly identify all the functional groups present in such a chemically complex substance as asphalt binder. In this study, one of the few relatively well-established functional groups, the carbonyl (C=O, a carbon atom double-bonded to an oxygen atom), was evaluated in relation to aging and crack resistance. The underlying rationale is that highly polar and strongly interacting oxygen-containing functional groups, including carbonyl, are formed during the oxidative aging process. When the concentration of such polar functional groups becomes sufficiently high to cause molecular immobilization through increased intermolecular interaction forces, cracking will occur [86].

It is noted that carbonyl species are also present in virgin asphalt binder, yet with a very small concentration. Therefore, the relative degree of oxidative aging in an asphalt binder sample can be quantified by comparing the intensity of the carbonyl region (centered on the wave number of 1700 cm^{-1}) to the region associated with the saturated C-C vibrations [94]. The obtained parameter is referred to as the Carbonyl index, which was employed as the chemical parameter determined from the FTIR test to evaluate the impact of oxidized asphalt binders introduced from RAP/RAS.

The FTIR spectra for the asphalt samples were obtained using a Bruker Alpha FTIR spectrometer (Alpha), which uses a diamond single reflection attenuated total reflectance (ATR). An OPUS 7.2 data collection program was used for data analysis. The following settings were used for data collection: 16 scans per sample, spectral resolution 4 cm^{-1} , and wave number range $4000\text{-}500\text{ cm}^{-1}$. Each recovered asphalt binder was dissolved in carbon disulfide (CS_2) at a concentration of approximately 1% and the solution was filtered using a 0.2-micron filter. A few drops of the solution were kept on the diamond crystal and allowed to evaporate the solvent. Spectrum was collected after the complete evaporation of the solvent. The OPUS spectroscopy software provided with the Bruker FTIR instrument was used to calculate the band areas measured from valley to valley and determine the Carbonyl index via [95]:

$$\text{Carbonyl index (\%)} = \frac{\text{Area of carbonyl centered around } 1700 \text{ cm}^{-1}}{\sum \text{Area of spectra bands between } 1490 \text{ and } 1320 \text{ cm}^{-1}} \quad (48)$$

Discussion of Results

This chapter is divided into four subsections dealing with asphalt mixture test results, asphalt binder test results, correlation between the performance evaluation results of asphalt binders and mixtures, and correlation between laboratory and field fatigue performance. Within the first two subsections, given the variety of test methods employed, correlations among the obtained parameters were also examined.

Asphalt Mixture Testing

Dynamic Modulus Test

The dynamic modulus master curves were constructed using the time-temperature superposition principle. In this study, a reference temperature of 21.1°C was used. Figure 6 presents the dynamic modulus master curves for the ten ALF mixtures. It is noted that the three HMA mixtures incorporating 20% RAS or 40% RAP by RBR (i.e., L3, L5, and L7) exhibited higher stiffness than all other materials over the majority range of the reduced frequency. Conversely, the control mixture from L1 containing no recycled materials was relatively softer, but it tended to be stiffer than other mixtures at high reduced frequencies which physically represent low temperatures and/or high loading frequencies. Incorporation of recycled asphalt materials was seen to distort the dynamic modulus master curve shape by flattening the curves.

Figure 6. Dynamic modulus master curves for the ALF mixtures

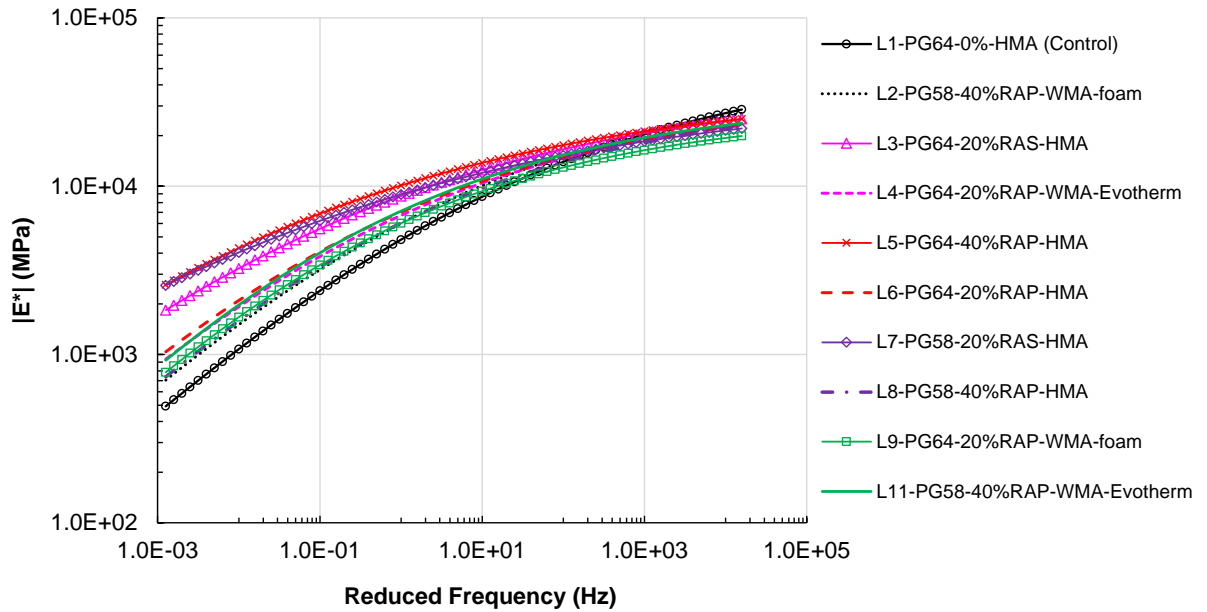
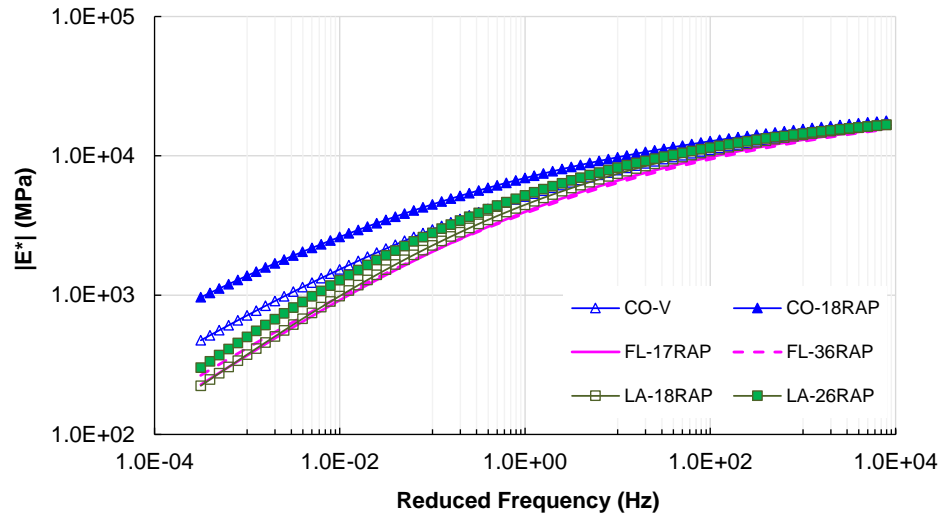


Figure 7 presents the dynamic modulus test results for the CO, FL, and LA mixtures. Within the CO mixtures, despite the difference in the base binder grade, use of 18% RAP considerably enhanced the stiffness over the entire reduced frequency range evaluated. Conversely, within the FL mixture group, use of 17% and 36% RAP provided very similar master curves, which may be partly attributed to the softer base binder used with the higher RAP percentage. Within the LA mixtures, use of 26% RAP yielded slightly higher stiffness towards the high temperature/low frequency region, which may be due to the small difference in the RAP content.

Figure 7. Dynamic modulus master curves for the CO, FL, and LA mixtures



S-VECD Test

The damage characteristic curve was identified by subjecting specimens to the direct tension cyclic fatigue test until the specimen was pulled apart. It was found that an initial on-specimen strain level of 250 microstrain as opposed to 300 microstrain as suggested in AASHTO TP107 was more suitable for the first replicate (targeting $N_f > 500$), potentially because all specimens underwent the long-term oven aging process. It was also observed that the exponential function in Equation (15) was able to provide a better fitting quality for the damage characteristic curves in all cases than the power-law form.

The fitted damage characteristic curves for the ALF mixtures are presented in Figure 8. Note that in actual testing, the failure location on a specimen may be beyond the LVDT gage points (i.e., end failure, in contrast to middle failure which occurs within the gage points). While experimental evidences have shown that both middle and end failures yield the same $C(S)$ curve, middle failure usually results in lower C_f values because the whole macroscopic response of microcrack initiation and localization can be captured by the LVDT measurements. In Figure 8, each curve is plotted to the minimum C_f value of the replicates for the corresponding mixture. It is noted that a number of mixtures failed at relatively high C_f values, which is attributed to the combined effects of end failures, the increased material brittleness due to the oven-aging process, and the incorporation of recycled materials. Another noticeable trend is that stiffer mixtures (such as those from L3, L5, and L7) usually produced higher $C(S)$ curves, which also has been reported in the literature [24]. Figure 9 provides the results for the CO, FL, and LA mixtures, for which

the same trend was noted that those with higher RAP contents produced curves that are situated higher in the C - S space. It is seen that the two FL mixtures provided similar $C(S)$ curves, presumably due to their similar stiffness properties as shown in Figure 7.

The above observation revealed that the damage characteristic relationship is complicated by the stiffness property, and that therefore the $C(S)$ curves cannot be directly used to compare materials' fatigue resistance. As can be seen in Equations (4)-(7), computation of S depends on the pseudo stiffness C . In fact, the variable C is essentially the apparent dynamic modulus normalized by the initial modulus value when the material is intact, but apparently the initial stiffness varies with mixtures. Hence, when the $C(S)$ curves for different mixtures are plotted together, as in Figure 8, the S values are not comparable even for the same C value. For example, for a given C value, mixtures having higher S values do not necessarily mean that they have undergone more damage as they may have higher stiffness.

The MFS parameter suited the purpose as an indicator of fatigue resistance without the complication of deformation resistance (i.e., stiffness). The MFS parameter was developed as an indicator for fatigue resistance of asphalt mixtures. This parameter was obtained by performing fatigue simulation following the procedure outlined in Figure 3. Figure 10 provides the MFS results for all the asphalt mixtures. Recall that lower MFS values indicate higher fatigue resistance. Within each mixture group, the results are presented in the sequence of decreasing resistance to fatigue cracking. It is seen that for the ALF materials, the three HMA mixtures from L3, L5, and L7 containing 40% RAP or 20% RAS yielded the lowest fatigue resistance. The L1 control HMA and the L2 foamed WMA containing 40% RAP and soft base binder exhibited the highest fatigue performance. Similarly, for the remaining three material sources, incorporation of higher RAP percentage in the mixtures resulted in reduced fatigue resistance as evidenced by the increased MFS values. Since MFS was obtained from fatigue simulation, not from testing with replicates, no further statistical analysis was performed on the results.

Figure 8. Damage characteristic curves of the ALF mixtures

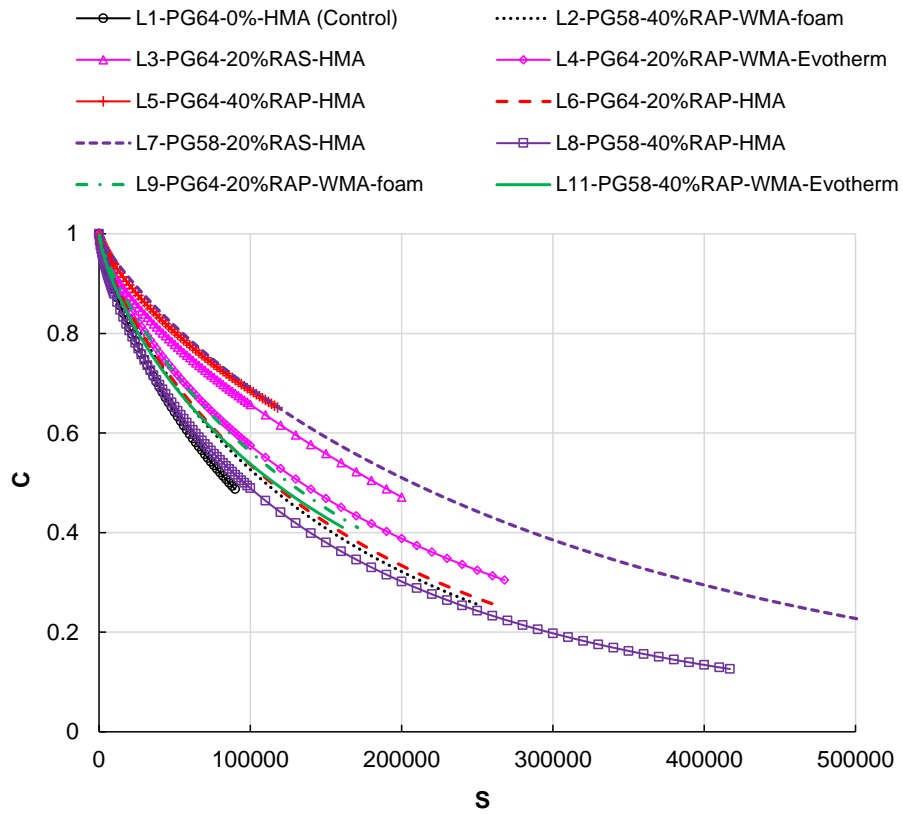


Figure 9. Damage characteristic curves of the CO, FL, and LA mixtures

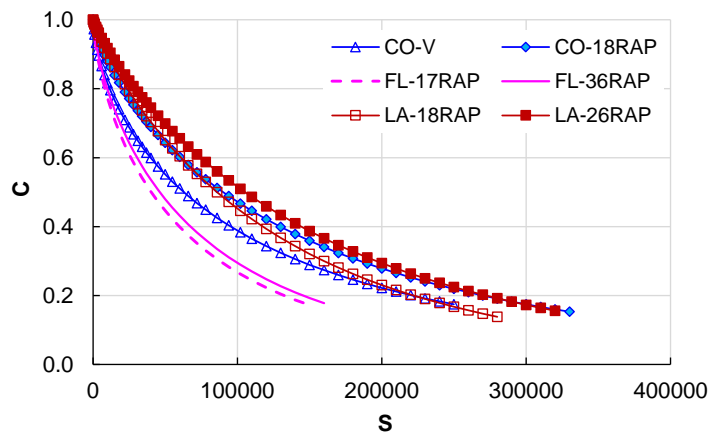
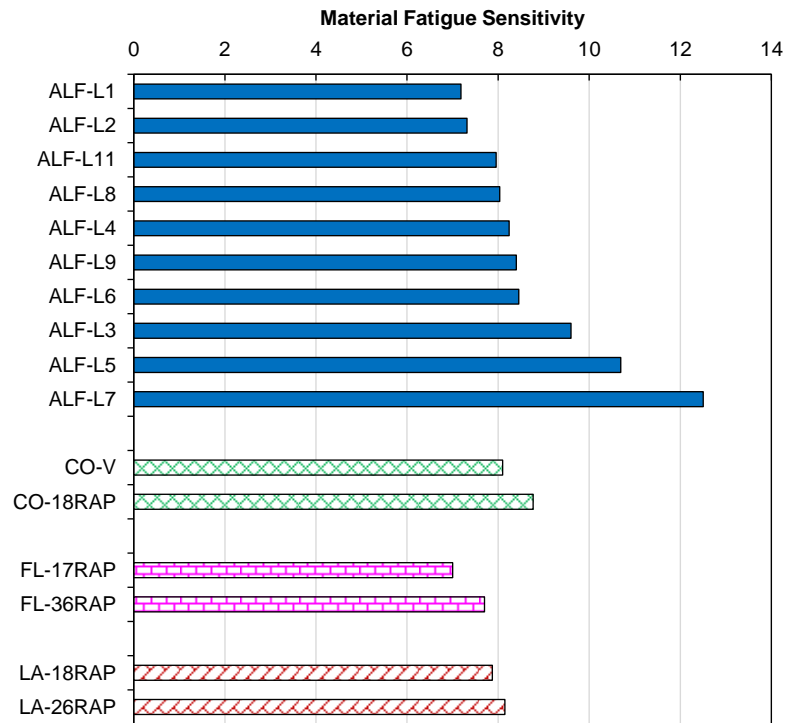


Figure 10. The MFS parameter from the S-VECD test for all the asphalt mixtures



Texas Overlay Test

Figure 11 gives the fatigue life results from the Texas overlay test for all the asphalt mixtures. The CoV of $N_{f,OT}$ varied between 7% and 42% with an overall average of 24%. The analysis of variance (ANOVA) using Fisher's Least Significant Difference (LSD) method were used to compare the mean $N_{f,OT}$ values at a 5% error rate. The obtained statistical grouping results are indicated by the letters A, B, etc., representing statistically distinct crack resistance from best to lowest. Despite the relatively high variability, the $N_{f,OT}$ parameter exhibited a wide range for the ten ALF mixtures and presented five statistical groups. According to $N_{f,OT}$, the HMA mixtures from L3, L5, and L7 containing 40% RAP or 20% RAS demonstrated the lowest performance; the L9 foamed WMA with 20% RAP exhibited the highest fatigue resistance, followed by the L1 control mixtures. For the other three material sources, use of higher RAP percentages yielded significantly lower fatigue performance within each mixture group.

Figure 11. Fatigue life results of the Texas overlay test for all the asphalt mixtures

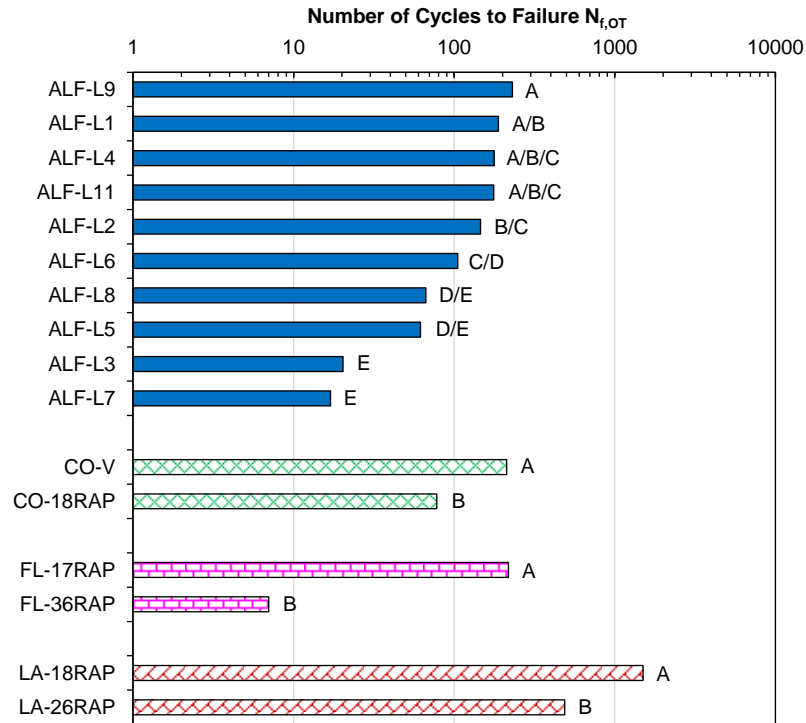
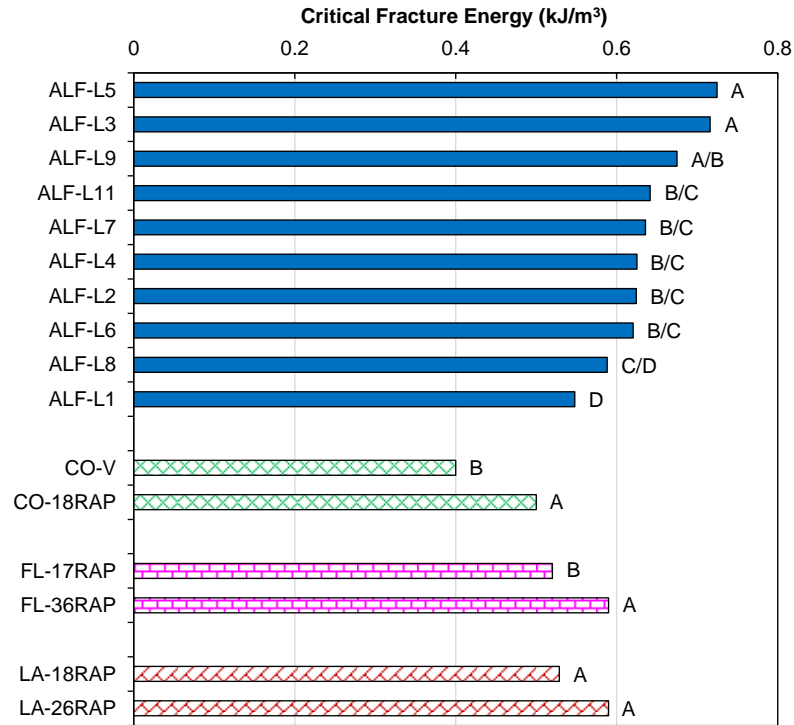


Figure 12 presents the critical fracture energy results for all the asphalt mixtures. The CoV of CFE ranged from 3% to 19% with an overall average of 6% for all the mixtures. This parameter provided four statistical groups for the ALF mixtures according to the ANOVA analysis. It is noted that the L1 control mixture had the lowest CFE value, whereas the L5 and L3 mixtures containing 40% RAP and 20% RAS, respectively, presented the highest CFE values. The results from the other material sources also exhibited a similar trend that incorporation of higher RAP produced higher CFE values. This trend is expected since it has been recognized that CFE is strongly positively related with mixtures' stiffness [35]. As such, Garcia et al. [35] proposed lower and upper limits for CFE based on the field fatigue performance in Texas, such that the stiffness properties are within a reasonable range so as not to compromise the cracking performance. In other words, higher or lower CFE values do not necessarily represent higher or lower crack resistance, respectively. Given the poor correlation between CFE and the crack resistance as implied based on the material composition in this study, this parameter is dropped in subsequent investigations.

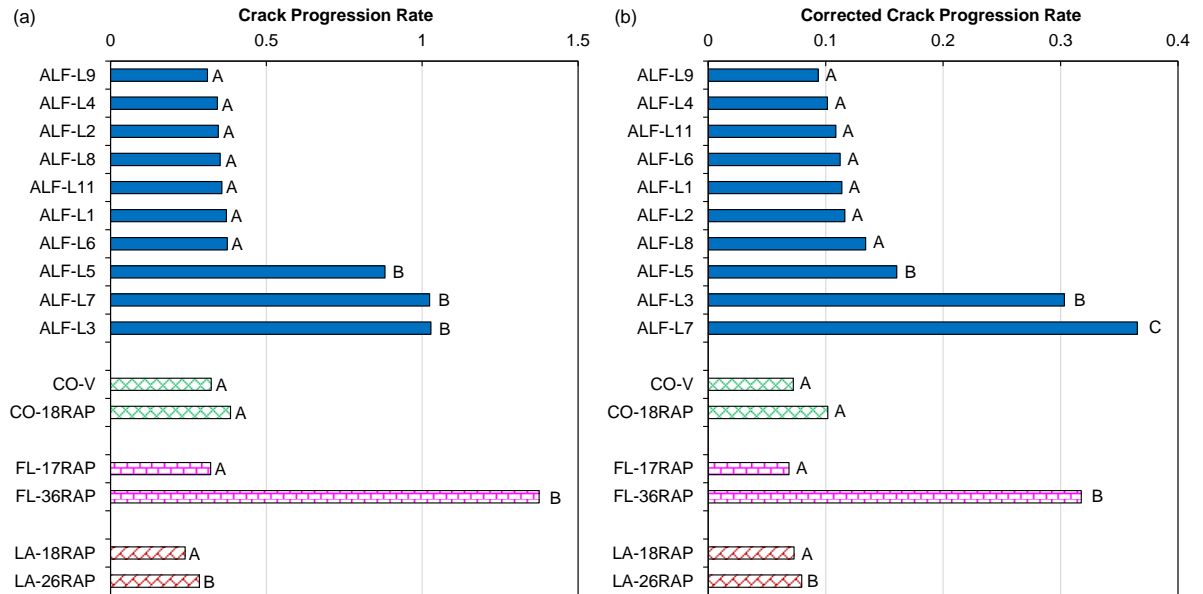
Figure 12. Critical fracture energy results for all the asphalt mixtures



The results of crack progression rate and corrected crack progression rate are illustrated in Figure 13 for all the asphalt mixtures. For the ALF mixtures, the CoV of CPR varied between 7% and 25% with an overall average of 12%, and this parameter yielded only two statistical groups. It is seen that the three HMA mixtures from L3, L5, and L7 containing 40% RAP or 20% RAS yielded significantly higher CPR results than the other mixtures within the ALF group. Comparatively, the CCPR parameter provided three statistical groups for the ALF mixtures. The CoV of CCPR ranged from 9% to 26% with an overall average of 13%, comparable to that of CPR. Accordingly, the L7 HMA containing 20% RAS presented the lowest crack resistance, followed by the HMAs from L3 and L5.

For the other three material sources, the two parameters of CPR and CCPR exhibited very similar CoV values, ranging from 2% to 16% with an overall average of 10%. Use of higher RAP contents consistently yielded lower resistance to crack propagation; the two parameters were able to distinguish the FL and LA mixtures but not between the CO mixtures.

Figure 13. Crack progression rates and corrected crack progression rates for all the asphalt mixtures



Beam Fatigue Test

As previously mentioned, fatigue failure in the beam fatigue test has been defined at 50% drop in flexural stiffness or, alternatively, at the peak of normalized product of flexural stiffness and cycle. Both definitions were explored during the course of the study. Yet, a number of tests did not present a clearly defined peak based on the latter definition even though the beam stiffness had dropped below 40% of the initial value, which were set as one of the test stopping criteria [96]. The other stopping criterion was set at 1.5 million loading cycles. Given this, the conventional 50% drop in stiffness criterion was employed to define fatigue failure.

The obtained fatigue envelopes in terms of power-law relationships between fatigue life and strain amplitude are given in Figure 14 for all the ALF mixtures and in Figure 15 for the remaining materials. In all cases, the test variability among replicates as measured by the difference of the fatigue lives in the logarithmic scale was between 0.03 and 0.72 with an overall average of 0.24, and was within the threshold of 0.787 as specified in ASTM D7460 [39]. It is noted that the failure lines were generally not parallel but intersected within the strain range evaluated. Within the ALF mixtures, the L9 foamed WMA mixture containing 20% RAP yielded considerably better fatigue performance than all other materials in the low strain region, whereas the L11 mixture (WMA Evotherm, 40% RAP) was the best performer in the high strain region; the L1 control mixture performed

moderately as seen in Figure 14. Evaluation of the mixtures from the other sources provided relatively more consistent results given the simpler material factorials involved; use of higher RAP percentages resulted in lower failure lines for the majority of the strain range.

Figure 14. Relationship of fatigue life $N_{f,BF}$ versus strain level for the ALF mixtures

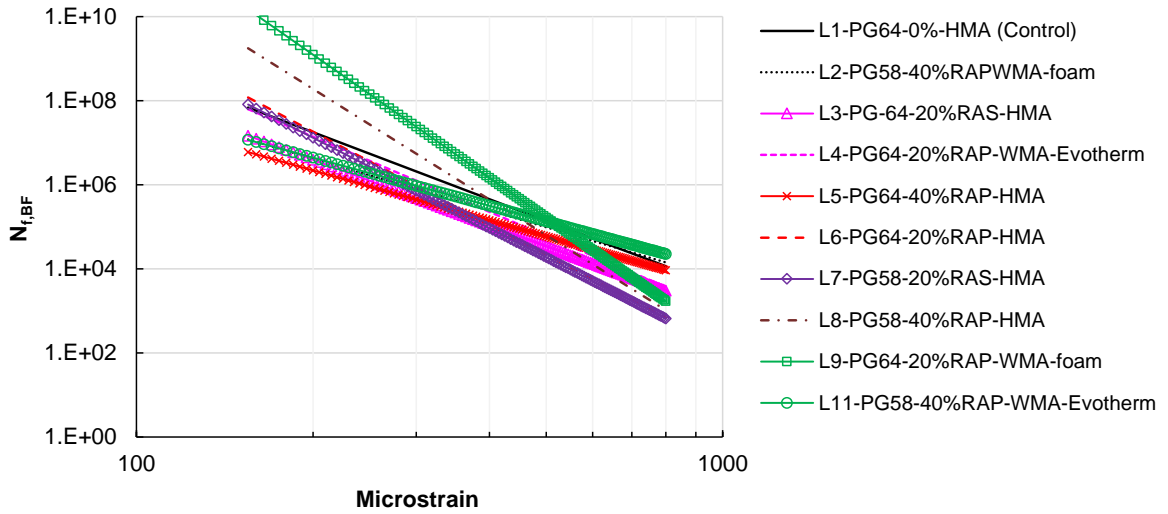
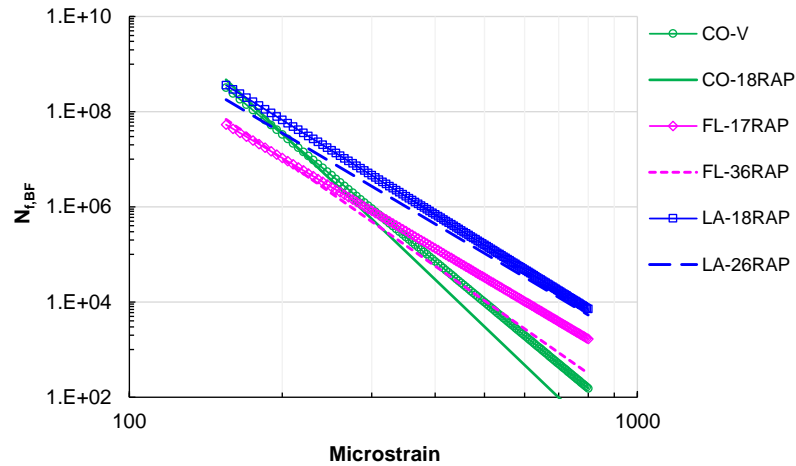


Figure 15. Relationship of fatigue life $N_{f,BF}$ versus strain level for the CO, FL, and LA mixtures

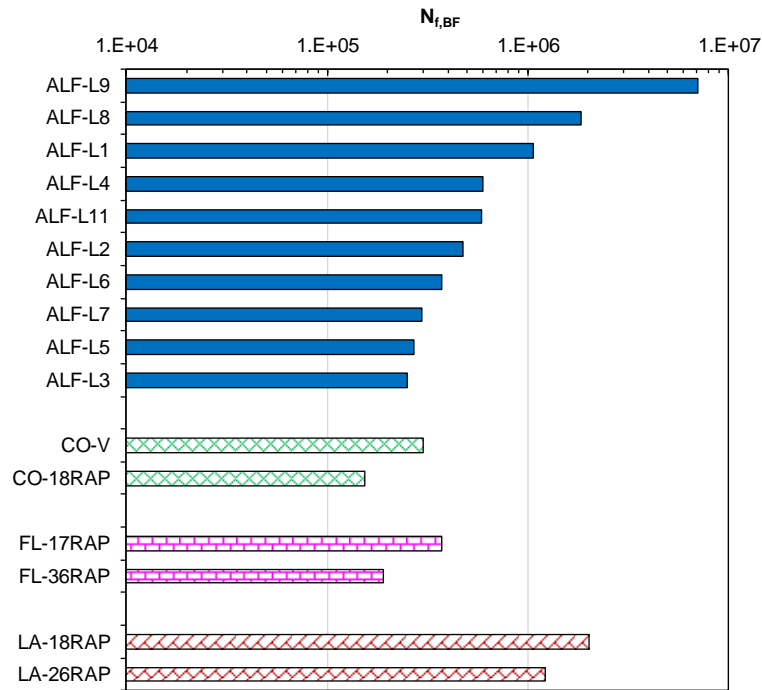


Given the unparallel failure lines and the need for a parameter for indicating the fatigue resistance, the fatigue life corresponding to 340 microstrain was interpolated for each mixture and was denoted as $N_{f,BF}$. This strain level was the average of the strains at the bottom of the ALF lanes obtained using the finite element analysis; see Table 6 in a later

section (detailed analysis will be given subsequently). The other mixtures, despite the different sources, were from field projects of thin pavements for low traffic volumes having similar structural layout with the ALF lanes. Given this and the fact that the material properties of the unbound layers were not available, the same averaged strain of 340 microstrain was applied also to the CO, FL, and LA mixtures.

Figure 16 presents the $N_{f,BF}$ parameter for all the asphalt mixtures, given in the logarithmic scale. According to $N_{f,BF}$, within the ALF mixtures, the L9 foamed WMA with 20% RAP exhibited the highest fatigue resistance, while the L1 control mixture was ranked in the third place following L8 (HMA, PG 58-28, 40% RAP). The three HMAs from L3, L5, and L7 containing 20% RAS or 40% RAP yielded the lowest performance. For the other material groups, the trend is consistent that use of higher RAP percentages resulted in lower fatigue lives. Note that since $N_{f,BF}$ was calculated from the N_f -strain relationships, the statistical analysis was not available for this parameter.

Figure 16. Fatigue life $N_{f,BF}$ results at 340 microstrain for all the asphalt mixtures

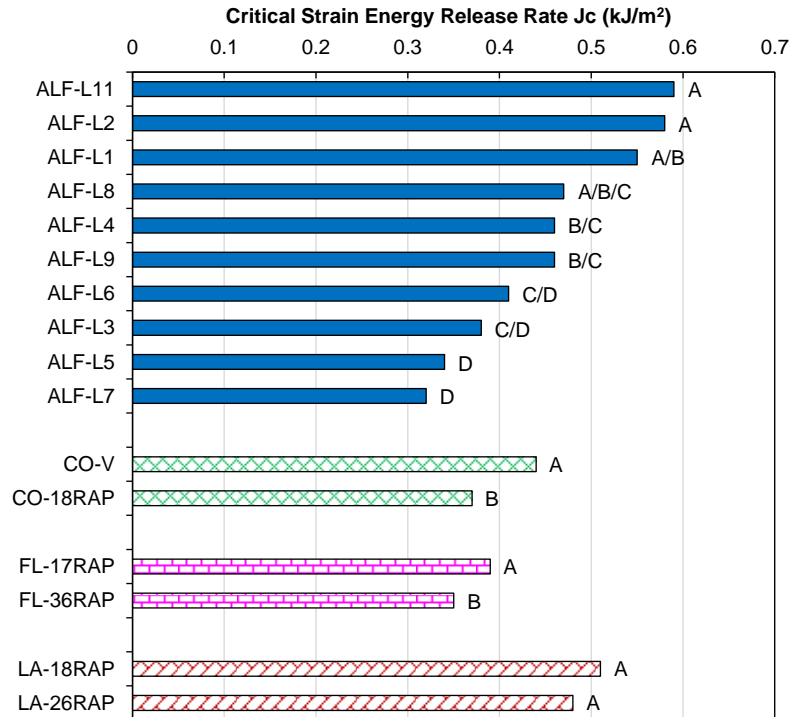


SCB Test

Figure 17 presents the critical strain energy release rates for all the mixtures evaluated. The averaged CoV for the strain energy (per unit thickness) ranged from 3% to 25% with

an overall average of 13% for all the mixtures, which indicated a satisfactory repeatability. For the ALF mixtures, four statistical groups were identified according to the ANOVA analysis. It was observed that mixtures containing RAS and high RAP content in general exhibited relatively high test variability. As shown in Figure 17, the HMA mixtures containing 20% RAS or 40% RAP (L3, L5, L7) exhibited the lowest resistance to cracking, whereas the L1 control mixture and the two WMA mixtures from L2 and L11 containing the soft base binder (PG 58-28) yielded the highest J_c values. Within the CO and FL groups, the SCB J_c parameter was able to distinguish the two mixtures as per the RAP content. However, the two LA mixtures were considered statistically similar in terms of cracking resistance, which may be attributed to the small difference in the RAP percentages used.

Figure 17. The J_c parameter from the SCB test for all the asphalt mixtures

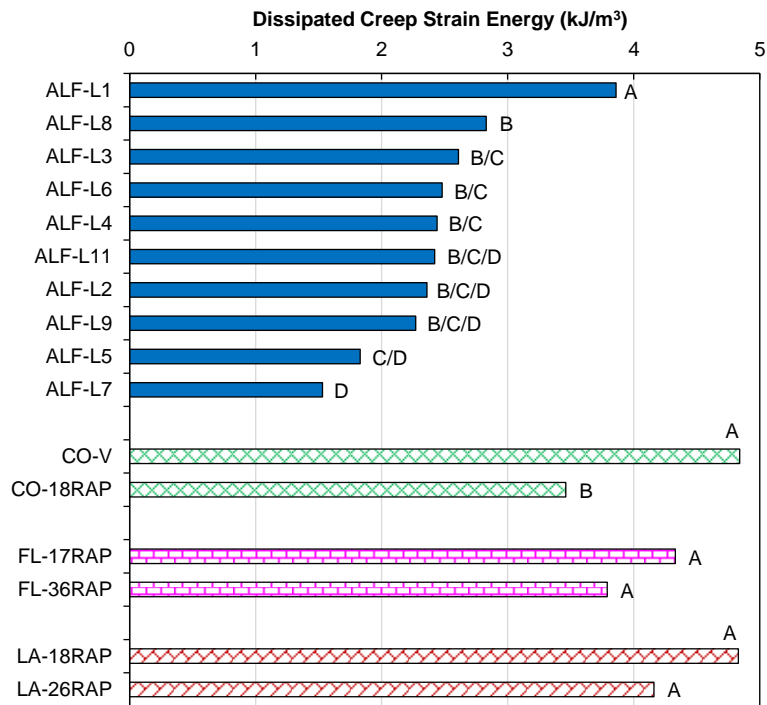


IDT Test

For the IDT test, data analysis was performed to yield the DCSE parameter. Figure 18 presents the results for all the asphalt mixtures. The CoV for all the mixtures ranged between 4.3% and 34.2% with an overall average of 18.2%. For the ALF mixtures, four statistical groups were identified according to the ANOVA analysis, and the L1 control

mixture was ranked the best performer whereas L5 and L7 were among the lowest. The L9 water foamed WMA with 20% RAP was ranked next to the lowest two mixtures, but recall that this mixture was considered to have moderate to best cracking resistance according to the S-VECD, Texas overlay, beam fatigue, and SCB tests. Additionally, note that the L3 HMA with 20% RAS was ranked the third best according to DCSE, but it was among the lowest three performers based on the above-mentioned tests. For the CO, FL, and LA mixtures, higher RAP percentages yielded lower DCSE values. Based on the statistical comparison, this parameter was able to differentiate the two CO mixtures, but considered the mixtures within the FL and LA groups were statistically similar in terms of cracking resistance.

Figure 18. Dissipated creep strain energy results for all the asphalt mixtures

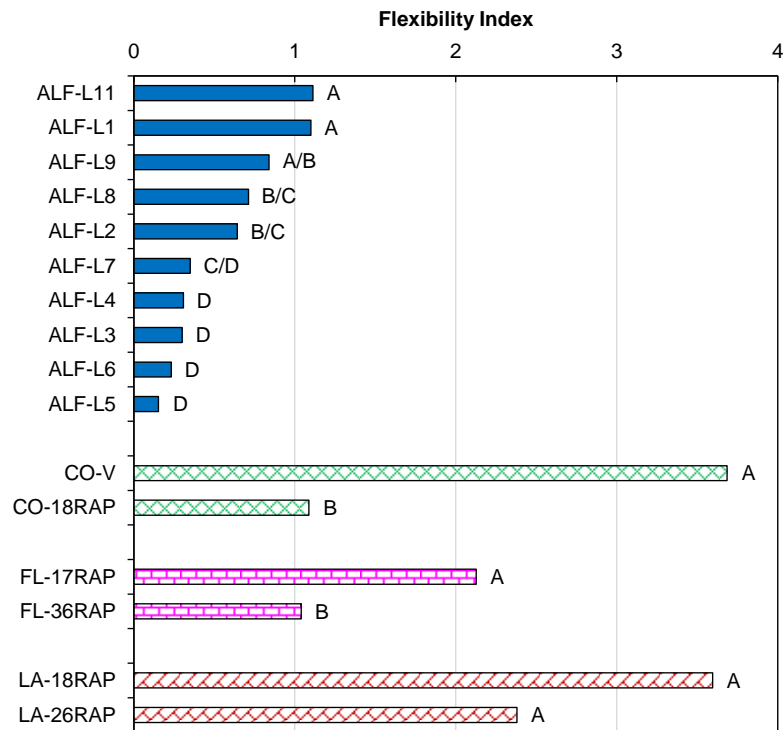


I-FIT Test

Figure 19 presents the FI results for all the mixtures obtained from the I-FIT test. The CoV of FI was between 10% and 48% with an overall average of 25% for all the mixtures. The relatively high test variability associated with FI has been also noted in the literature [59]. This parameter yielded four statistical groups for the ALF materials according to the ANOVA analysis. The high test variability was believed to be associated

with the high stiffness of these materials. It is noted that in order to accommodate the high stiffness and the resulting high brittleness, the data acquisition rate was increased to 500 Hz. It is seen in Figure 19 that the L1 control mixture and L11 (WMA Evotherm, 40% RAP, PG 58-28 base binder) yielded the highest FI values, whereas L5 HMA mixture containing 40% RAP and PG 64-22 base binder exhibited the lowest fracture resistance. Within each of the other three groups, use of higher RAP percentage consistently resulted in lower FI values. This parameter was able to statistically discriminate the CO and FL mixtures, but ranked the two LA materials similar due to the higher CoV with LA-26RAP and the similar RAP dosages between the two.

Figure 19. Flexibility index results for all the asphalt mixtures



Discussion in Relation to Material Composition

This section presents the discussion on each of the fatigue/fracture parameters evaluated for the asphalt mixtures with respect to material composition, i.e., RAP/RAS content, and use of warm-mix technology and base binder. The parameters used in comparison are MFS from the S-VECD test, $N_{f,OT}$, CPR, and CCPR from the Texas overlay test, $N_{f,BF}$ from the beam fatigue test, J_e from the SCB test, DCSE from the IDT test, and FI from

the I-FIT test. For facilitating the inspection, all parameters were normalized using the values of the respective control mixtures (HMA with the lowest RAP/RAS content) in each material group. Since higher fatigue/fracture resistance is represented by smaller MFS, CPR, and CCPR values but larger values of all the other parameters, in the normalization process, the reciprocal was used for MFS, CPR, and CCPR. In addition, considering the wide range of $N_{f,BF}$ covering several orders of magnitude as compared to the other parameters, its normalization used the logarithmic value.

Effect of RAP/RAS. Within the ALF group, the effect of incorporation of recycled materials on mixtures' resistance to fatigue/fracture can be observed by comparing the normalized parameters for mixtures from L1, L3, L5, and L6, all being HMA mixtures with base binder PG 64-22. Figure 20 presents the normalized parameters for the four ALF mixtures. It is noted that the S-VECD MFS and the SCB J_c parameters consistently ranked the cracking resistance as L1 (control) > L6 (20% RAP) > L5 (40% RAP) > L3 (20% RAS). The L6 mixture was expected to be a better performer than L3 as both contained 20% recycled materials by RBR but L6 had the contribution from RAP which was less oxidatively aged than RAS in L3. Between these two mixtures, only the parameters of MFS, $N_{f,OT}$, CPR, CCPR, $N_{f,BF}$, and J_c provided the reasonable ranking. Comparison between L3 (20% RAS) and L5 (40% RAP) was not conclusive, as the two tests of Texas overlay ($N_{f,OT}$, CPR, CCPR) and beam fatigue ($N_{f,BF}$) ranked L5 better, whereas according to the remaining four parameters from other test methods, L3 outperformed L5.

The effect of RAP on the CO, FL, and LA mixtures was illustrated in Figure 21. In general, within each mixture group a higher RAP content yielded lower fatigue/fracture resistance according to all the parameters evaluated.

Figure 20. Normalized parameters for evaluating the effect of RAP/RAS on the ALF mixtures (HMA with PG 64-22 base binder)

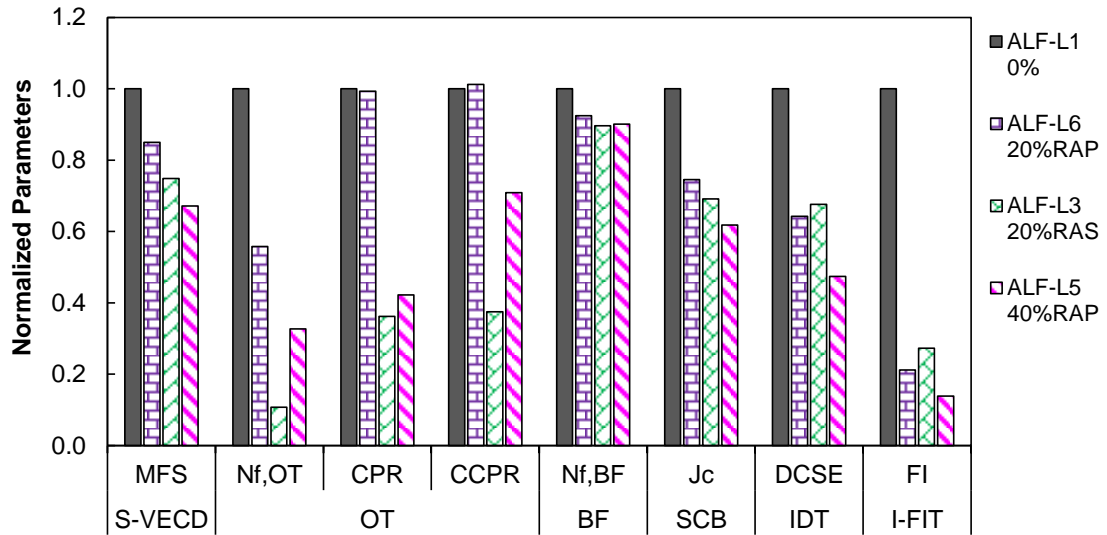
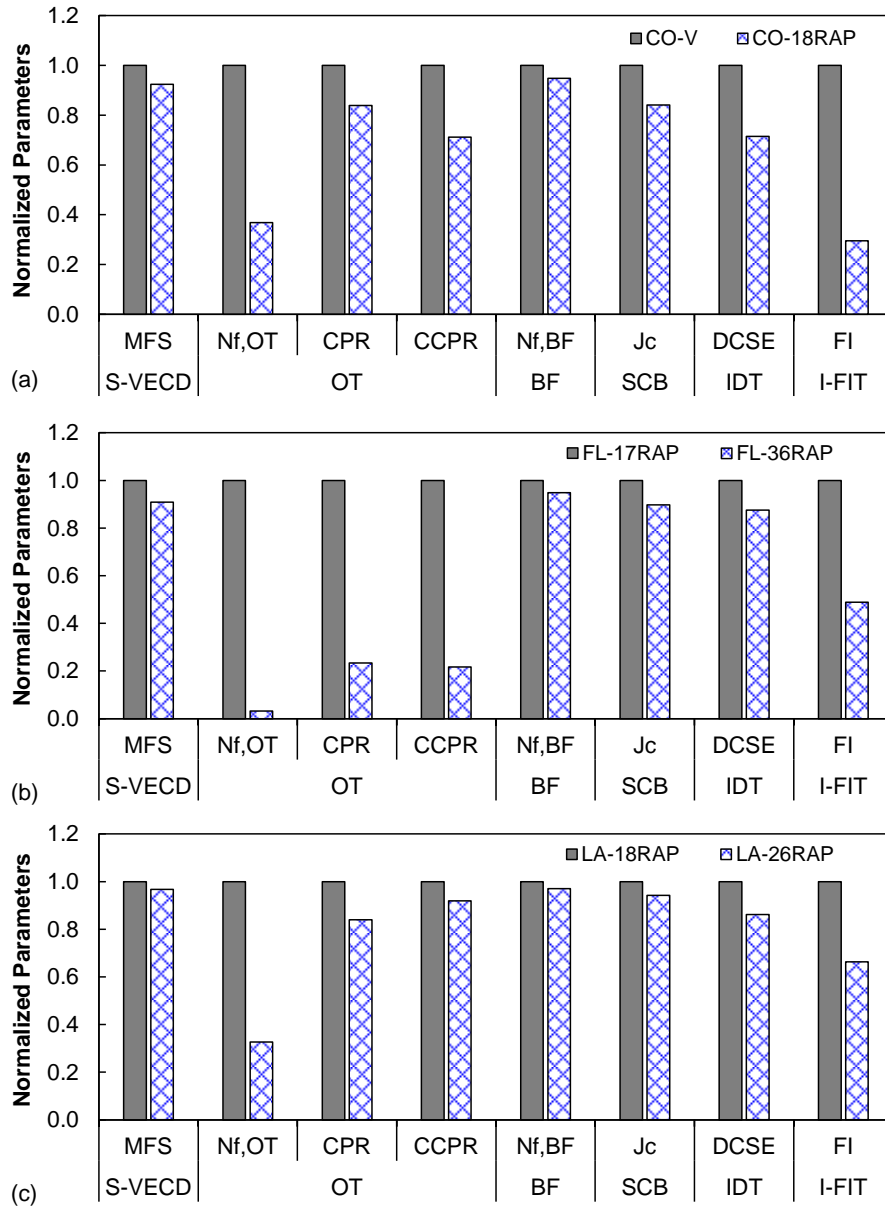


Figure 21. Normalized parameters for evaluating the effect of RAP on the CO, FL, and LA mixtures

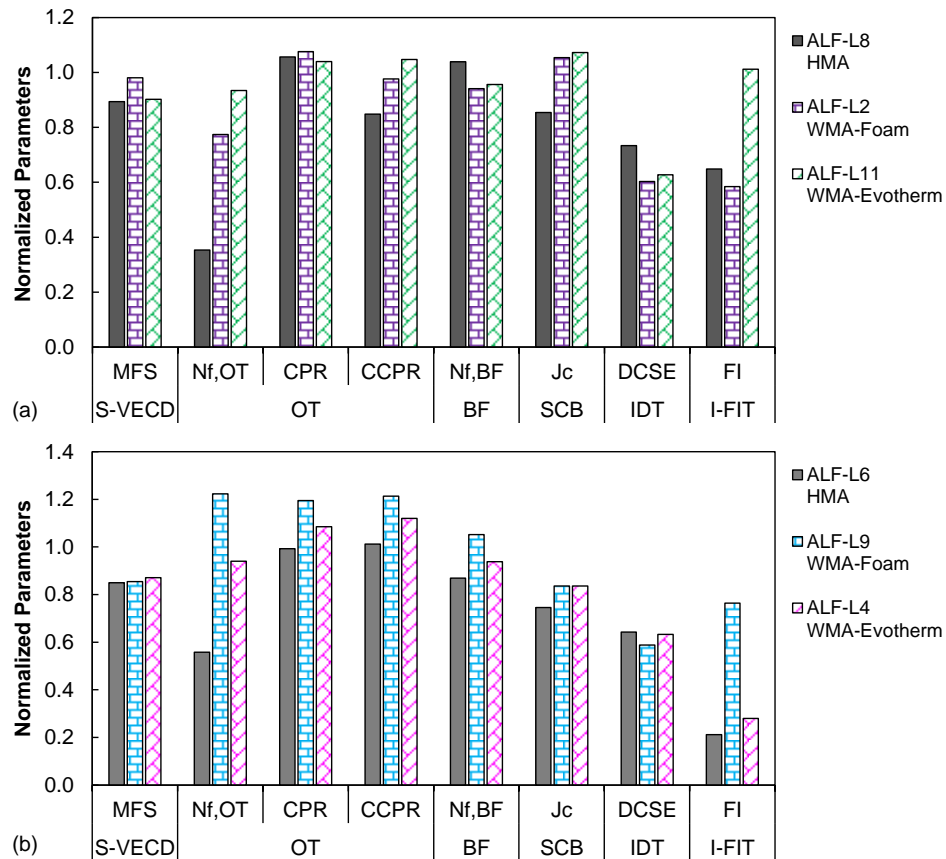


Effect of Warm-mix Technologies. The effect of WMA technology can be examined through two sets of comparisons from the ALF mixture group. The first set includes L2, L8, and L11, all containing 40% RAP with base binder PG 58-28, Figure 22(a). The L8 HMA mixture was considered similar to the two WMA mixtures based on MFS, and CPR, and slightly better according to DCSE and $N_{f,BF}$, but lower based on $N_{f,OT}$, CCPR, and J_c . The FI parameter ranked L8 HMA similar to the L2 foamed WMA, but considerably lower than the L11 WMA-Evotherm. Between the two WMA processes,

water foaming versus Evotherm, they were seen to generally exhibit similar performance by all the test methods, except that $N_{f,OT}$ and FI ranked the foaming process (L2) lower than Evotherm (L11).

The second set consists of L4, L6, and L9, all containing 20% RAP with base binder PG 64-22, Figure 22(b). The L6 HMA mixture exhibited comparable performance with the two WMA mixtures according to MFS, J_c , and DCSE, but was ranked (slightly) lower based on the Texas overlay, beam fatigue, and I-FIT tests. Between the two WMA mixtures, similar performance was observed according to MFS, J_c , and DCSE. However, L9 (water foaming) outperformed L4 (Evotherm) according to the Texas overlay, beam fatigue, and I-FIT tests.

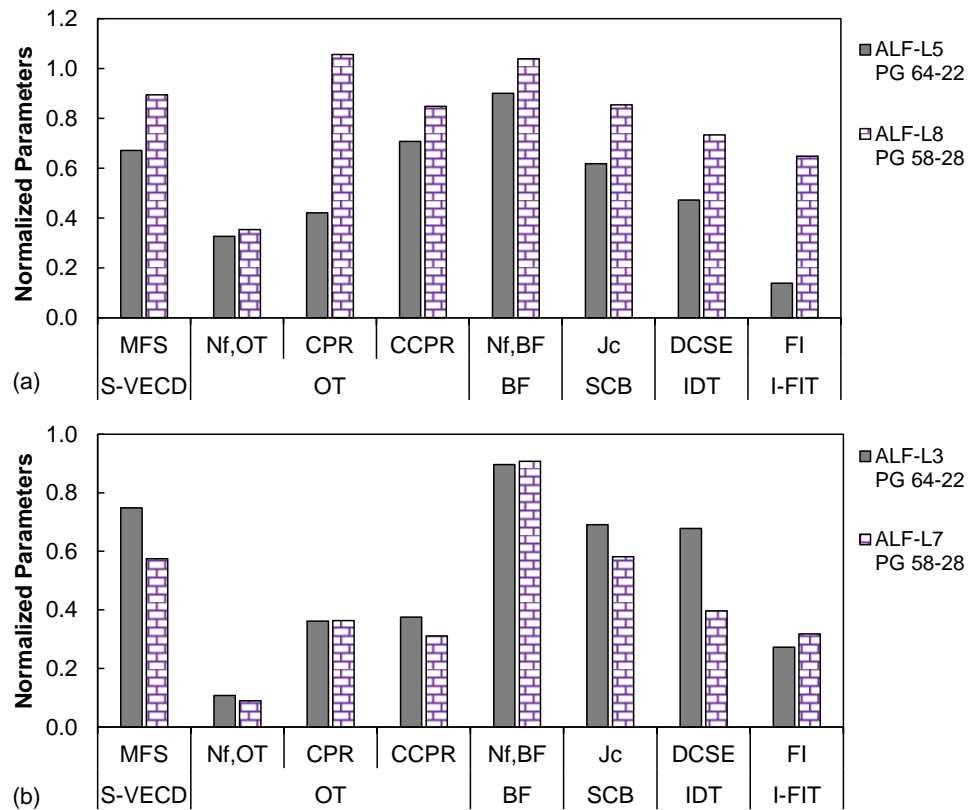
Figure 22. Normalized parameters for evaluating the effect of WMA technologies on the ALF mixtures containing: (a) 40% RAP with PG 58-28 base binder, and (b) 20% RAP with PG 64-22 base binder



In summary, the above observations based on all parameters from the different test methods led to an inconclusive comparison between the two WMA technologies, water foaming and Evotherm. It can be conservatively stated that the two warm-mix processes provided comparable fatigue/fracture performance with reference to the conventional hot-mix asphalt mixtures.

Effect of Soft Base Binder. The effect of soft binder can be evaluated using the ALF data by comparing L5 with L8, and L3 with L7, all being HMA mixtures with the first group containing 40% RAP and the latter 20% RAS. It is seen that all parameters provided consistent ranking results that with 40% RAP use of the soft base binder PG 58-28 yielded improved fatigue/fracture resistance, Figure 23(a). According to CPR, $N_{f,BF}$, and FI, use of the soft base binder PG 58-28 with 20% RAS yielded similar or slightly better cracking resistance as shown in Figure 23(b), but the trend was opposite based on all the other parameters. It is clearly demonstrated that use of the soft base binder was more effective in accommodating oxidatively aged binder from RAP than from RAS.

Figure 23. Normalized parameters for evaluating the effect of soft base binder on the ALF mixtures containing: (a) 40% RAP, and (b) 20% RAS



Correlation among the Asphalt Mixture Test Results

Relationships among the obtained parameters indicating the cracking resistance of asphalt mixtures were investigated using the results for the ALF mixtures. Table 4 presents the best fit using simple functional relationships for paired parameters and the corresponding R^2 value.

It is noted from the table that the S-VECD MFS parameter and the Texas overlay CPR parameter exhibited overall the best correlations with the remaining parameters, followed by $N_{f,OT}$ and SCB J_c . Also note that for the Texas overlay test, three parameters were used and among them high correlations existed. Hence, compared to the other tests, more weight was placed on the Texas overlay in arriving at the above observation. The $N_{f,BF}$ from the beam fatigue test presented overall the lowest correlation with the other parameters, presumably due to the high variability in this test. Based on the degree of mutual correlation from strongest to weakest, the ranking of these evaluation parameters is: MFS, CPR, $N_{f,OT}$, J_c , CCPR, FI, DCSE, and $N_{f,BF}$.

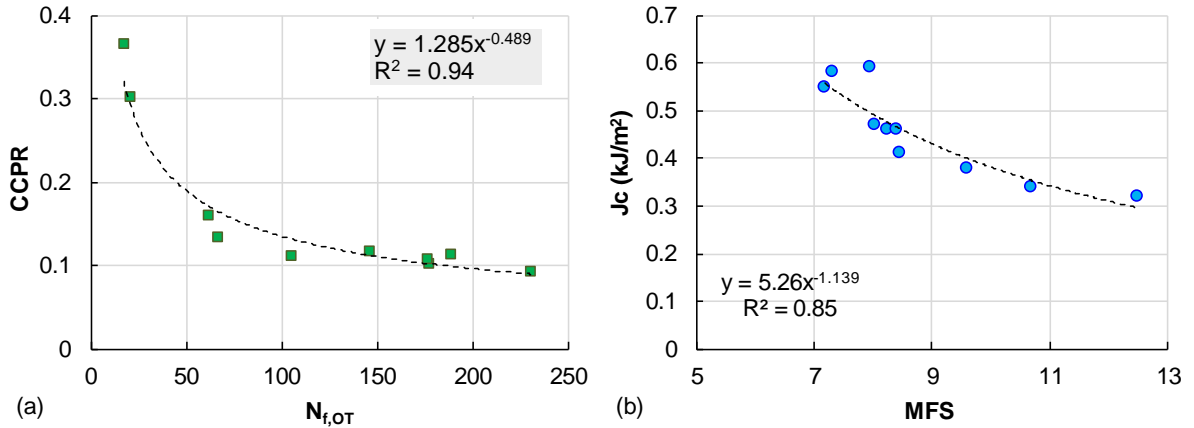
Out of the 28 interrelationships evaluated, the one between $N_{f,OT}$ and CCPR was the strongest with an R^2 value of 0.94 as shown in Figure 24(a); note that these two parameters were from the same test. Among the parameters from different tests, the SCB J_c and S-VECD MFS provided the highest correlation with R^2 of 0.85, as shown in Figure 24(b).

Table 4. Relationships between parameters indicating asphalt mixture cracking resistance

Independent Variable	Dependent Variable	Functional Relationship	R^2
MFS	$N_{f,OT}$	$y = 4820.5\exp(-0.452x)$	0.64
MFS	CPR	$y = 1.54\ln(x) - 2.79$	0.76
MFS	CCPR	$y = 0.047x - 0.253$	0.68
MFS	J_c	$y = 5.26x^{-1.139}$	0.85
MFS	$N_{f,BF}$	$y = 8.54E6\exp(-0.288x)$	0.21
MFS	DCSE	$y = 7.012\exp(-0.121x)$	0.67
MFS	FI	$y = 117.21x^{-2.548}$	0.41

Independent Variable	Dependent Variable	Functional Relationship	R²
$N_{f,OT}$	CPR	$y = -0.297\ln(x) + 1.87$	0.82
$N_{f,OT}$	CCPR	$y = 1.285x^{-0.489}$	0.94
$N_{f,OT}$	J_c	$y = 0.202x^{0.177}$	0.60
$N_{f,OT}$	$N_{f,BF}$	$y = 2.29E5\exp(8.98E-3x)$	0.42
$N_{f,OT}$	DCSE	$y = 1.358x^{0.127}$	0.23
$N_{f,OT}$	FI	$y = 3.03E-3x + 0.214$	0.41
CPR	CCPR	$y = 0.066\exp(1.43x)$	0.87
CPR	J_c	$y = 0.345x^{-0.348}$	0.66
CPR	$N_{f,BF}$	$y = 2.45E5x^{-1.351x}$	0.42
CPR	DCSE	$y = 3.046\exp(-0.445x)$	0.31
CPR	FI	$y = 0.253x^{-0.841}$	0.37
CCPR	J_c	$y = 0.237x^{-0.327}$	0.51
CCPR	$N_{f,BF}$	$y = 5.90E4x^{1.25}$	0.32
CCPR	DCSE	$y = 2.962\exp(-1.315x)$	0.26
CCPR	FI	$y = 0.350\ln(x) - 0.105$	0.21
J_c	$N_{f,BF}$	$y = 3.28E6x^{1.98}$	0.17
J_c	DCSE	$y = 4.407x^{0.756}$	0.44
J_c	FI	$y = 3.015x - 0.800$	0.65
$N_{f,BF}$	DCSE	$y = 0.827x^{0.079}$	0.11
$N_{f,BF}$	FI	$y = 1.61E-3x^{0.424}$	0.41
DCSE	FI	$y = 0.332x - 0.243$	0.33

Figure 24. The highest correlations among the parameters: (a) CCPR versus $N_{f,OT}$, and (b) J_c versus MFS



Asphalt Binder Testing

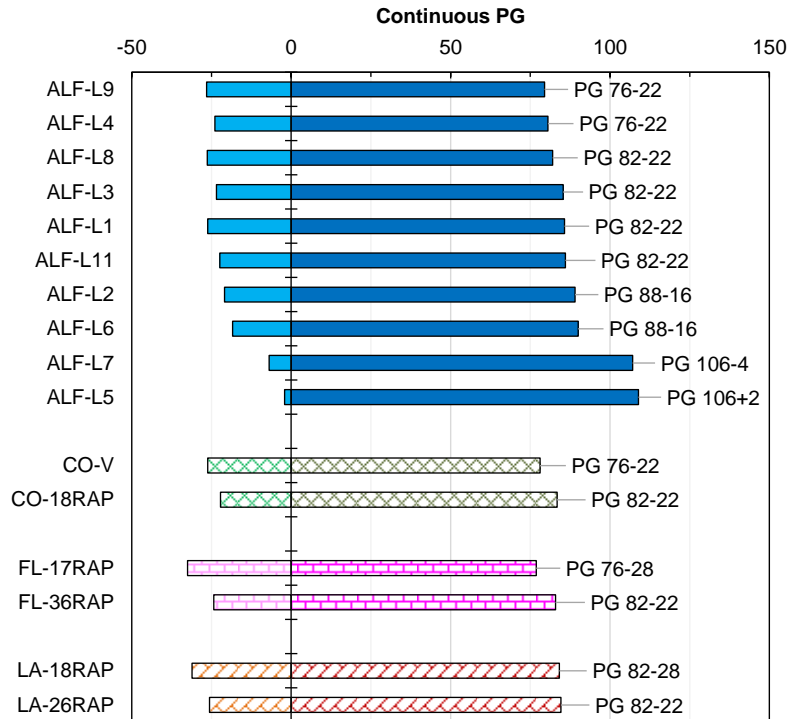
This section presents the asphalt binder testing results, including both rheological and chemical characterizations. Rheological testing included the Superpave performance grading, frequency sweep, and linear amplitude sweep tests. Chemical evaluation was based on SARA fractionation, GPC, and FTIR tests. All testing was performed on the asphalt binders extracted from the compacted asphalt mixture samples that were long-term aged following AASHTO R30 [11].

Superpave Performance Grading

The continuous PG results were determined in accordance with ASTM D7643 [68] and are shown in the sequence of increasing continuous high-temperature PG in Figure 25 along with the PG values for all the extracted binders. Within the ALF group, it is seen that the low-temperature PG was either the same or bumped up by one or more grades compared to the base binder. For the high-temperature PG, it was bumped up by a minimum of two grades up to eight grades. The asphalt binders extracted from L7 (with 20% RAS) and L5 (with 40% RAP) exhibited the greatest changes in both ends. In particular, note that the L7 extracted binder was considerably stiffer than that of L3, which helped in explaining the higher fatigue/fracture resistance of L3 as ranked by the mixture parameters shown in Figure 23(b). For the asphalt binders extracted from the CO and FL mixtures, it was consistently seen that use of higher RAP contents produced increased continuous PG values at both ends.

For the asphalt binders extracted from the LA mixtures, use of higher RAP content did not affect the high end but only increased the lower end. It was confirmed through the contractor that the same RAP source (fractionated) was utilized in both LA mixtures, but the RAP was milled from different milling depths. As the RAP source materials were also provided for this LA project (which was not the case for all the other mixtures), asphalt binders were extracted from them and the Superpave performance grading was performed. The continuous high-temperature PG for the extracted binder from RAP used in LA-18RAP was 90.9°C, whereas it was 87.8°C for that in LA-26RAP. Therefore, the LA-26RAP mixture had more incorporation of slightly softer recycled asphalt contributing from the RAP, which resulted in similar high-temperature PG results as compared to LA-18RAP.

Figure 25. Superpave PG results of all the extracted asphalt binders

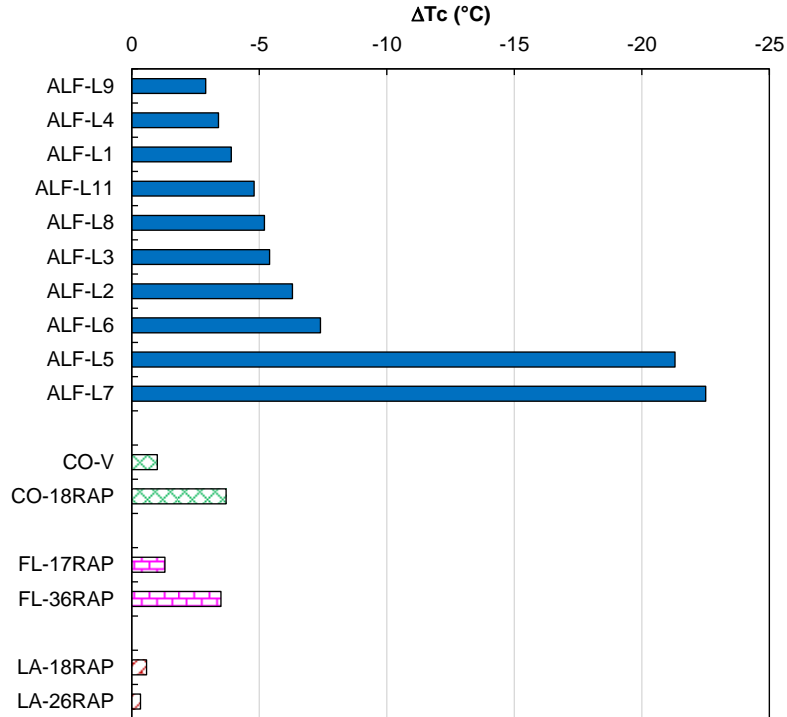


Another thing that is worth noting is that in certain cases such as FL-17RAP, the low-temperature PG of the extracted binder was -28°C, which was even one grade lower than that of the base binder used in this mixture (-22°C). In this study, all asphalt binders were extracted from compacted SCB samples that had been aged at 85°C for 5 days. These recovered asphalt binders were directly subjected to the BBR testing for the low-

temperature PG without any further aging treatment. However, for the base binders they had to be first aged through RTFO and PAV tests before they were evaluated for the low-temperature PG. It is suggested that for some material cases, the aging intensity in asphalts as enforced by the laboratory long-term aging protocol of AASHTO R30 on compacted mixtures was less severe than that by the RTFO and PAV procedures directly on asphalt binders.

Figure 26 presents the obtained ΔT_c results for all the extracted asphalt binders. It is shown that all the ΔT_c values are negative, indicating that all the asphalt binders were *m*-controlled ($T_m > T_s$). Existing studies reported that with increase in the aging intensity, ΔT_c would become more negative, which suggests a loss of relaxation capability [70]. Within the ALF binders, those recovered from L5 (40% RAP, PG 64-22 base binder) and L7 (20% RAS, PG 58-28 base binder) HMA mixtures yielded ΔT_c values that were considerably higher than the others in magnitude. The asphalt binders recovered from L4 (Evotherm) and L9 (water foaming) WMA mixtures, both containing 20% RAP with PG 64-22 base binder, and from L1 control mixture (HMA) provided the lowest ΔT_c in magnitude. As ΔT_c suggests ductility and stress relaxation capability, the binders recovered from L5 and L7 mixtures exhibited the least ductility and lowest potential to relax stresses under loading, hence the most susceptible to cracking. Conversely, the asphalt binders from L1, L4, and L9 are expected to demonstrate the best performance against cracking. For the asphalt binders extracted from the CO and FL mixtures, it is clearly shown in Figure 26 that higher RAP percentages yielded more negative ΔT_c values, indicating reduced cracking resistance. For the asphalt binder extracted from the LA mixtures, however, the trend was reversed; incorporation of higher RAP content provided slightly better cracking resistance; this complexity should be attributed to the close RAP percentages and also due to the softer binder contributed by RAP in LA-26RAP. It is noted that all the asphalt mixture testing methods ranked the LA-26RAP as a lower performer than LA-18RAP, Figure 21(c).

Figure 26. The ΔT_c parameter for all the extracted binders



Frequency Sweep Test

The isotherms of dynamic shear modulus obtained from the multi-temperature frequency sweep test were shifted based on the time-temperature superposition principle to construct the dynamic shear modulus master curve. Figure 27 presents the modulus master curves fitted using the CA model for the ALF extracted binders [73]. In the region of low reduced frequency, the binder extracted from the L5 HMA mixture with 40% RAP and PG 64-22 base binder was considerably stiffer than the other asphalts, followed by the binder extracted from L7 (HMA with 20% RAS and PG 58-28). Recall from the mixtures dynamic modulus master curves as shown in Figure 6 that these two mixtures also exhibited the highest stiffness within the low reduced frequency region. The extracted binder from L1, which incorporated no recycled binder, exhibited moderate modulus at low reduced frequencies but was among the stiffest at high reduced frequencies. The corresponding mixture exhibited the lowest stiffness in the low reduced frequency region and also provided the highest stiffness in the high frequency region, Figure 6. The dynamic shear modulus master curve for the CO, FL, and LA extracted binders are given in Figure 28. Within each group, use of higher RAP percentage had a

pronounced effect in improving the stiffness of the asphalt binders; this trend in stiffness is consistent with the corresponding asphalt mixtures as shown in Figure 7.

Figure 27. Dynamic shear modulus master curves for the ALF extracted binders

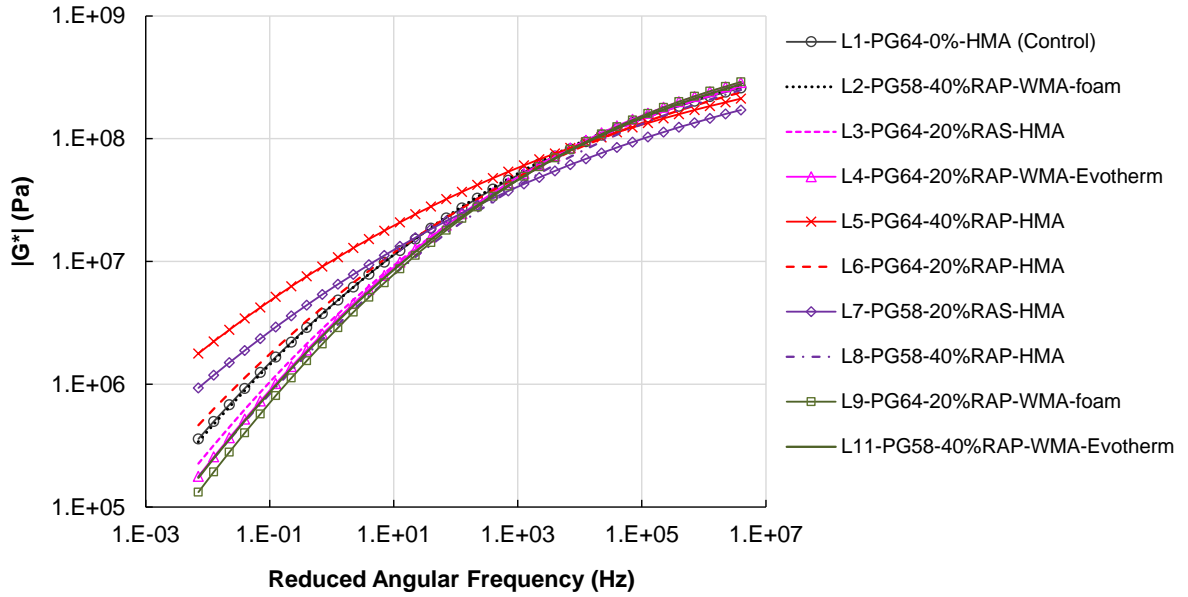
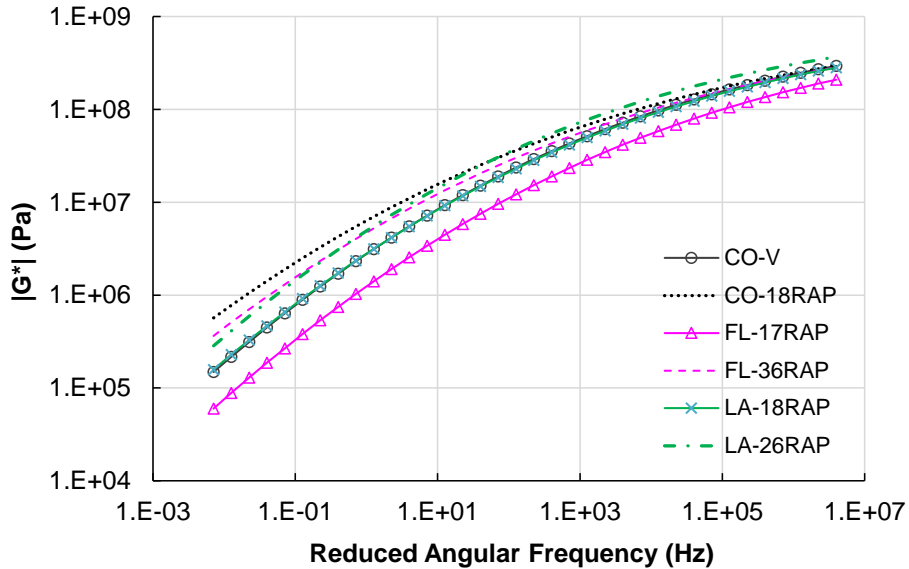
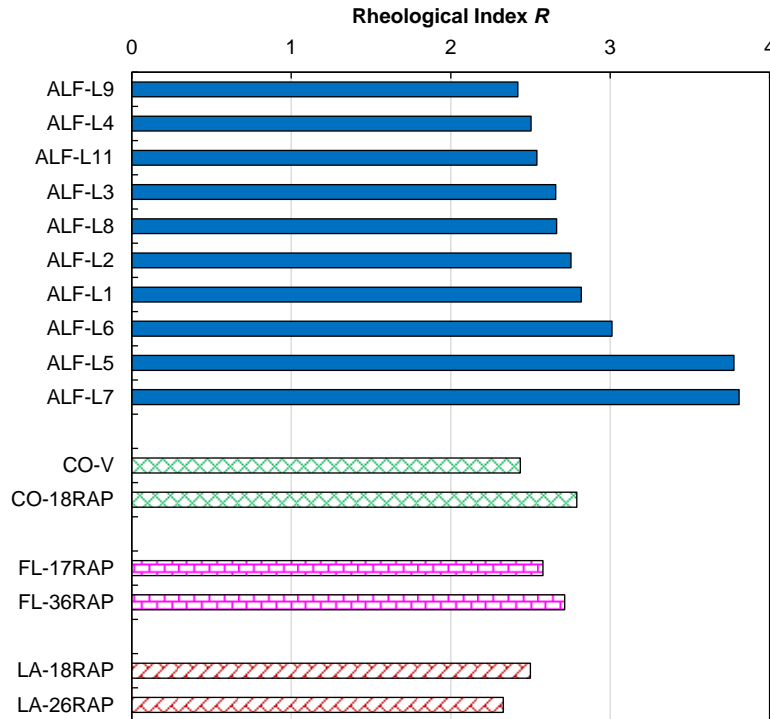


Figure 28. Dynamic shear modulus master curves for the CO, FL, and LA extracted binders



By fitting the $|G^*|$ master curves using the CA model, the rheological index R parameter was determined, and the results are shown in Figure 29 for all the extracted binders. As stated earlier, asphalt binders containing more recycled asphalt that has been oxidized tend to exhibit higher R -values. Within the ALF group, the asphalt binders recovered from L5 (40% RAP, PG 64-22 base binder) and L7 (20% RAS, PG 58-28) HMA mixtures yielded the highest R -values, which can be explained by the incorporation of high RAP content and RAS, respectively. Asphalt binders recovered from L4 (20% RAP, PG 64-22 base binder, Evotherm), L9 (20% RAP, PG 64-22, water foaming), and L11 (40% RAP, PG 58-28, Evotherm) WMA mixtures provided the lowest R -values. It is thus inferred that the asphalt binders from L5 and L7 are most susceptible to cracking, whereas those from L4, L9, and L11 are most crack resistant.

Figure 29. The R parameter for all the extracted asphalt binders



Inspection of the asphalt binders recovered from the CO and FL mixtures provided consistent observations that use of higher RAP percentages compromised the cracking resistance as inferred from the increased R -values. However, the LA extracted asphalt binders exhibited an opposite trend; use of higher RAP percentage yielded a slightly lower R , indicating better cracking resistance. Note that this trend is consistent with the

observation based on ΔT_c as shown in Figure 26, but does not agree with observations based on all the mixture tests as seen in Figure 21(c). Additionally, all asphalt binders exhibited R -values higher than the threshold value of approximately 1.92 [97], which suggests that they were all m -controlled. This conclusion is consistent with that based on ΔT_c (all negative) as given in Figure 26.

Linear Amplitude Sweep

The LAS test data were analyzed to yield the damage characteristic curves. In this process, the damage evolution rate was determined according to AASHTO TP 101 [79] using the data from the frequency sweep step. Fatigue failure was defined as the peak of pseudo-strain energy, Equation (43), which was derived from the unified failure criterion originally developed for asphalt mixtures [23, 82]. The underlying rationale is that pseudo-strain energy represents material's remaining capacity to store the applied energy (excluding the viscous dissipation) under the damage state characterized by C . Decline in this energy signals the material losing its energy-storing capacity under repeated loading, which serves a reasonable definition for fatigue failure. Figure 30 presents the obtained $C(S)$ relationships for the ALF extracted binders. Similar to mixtures, stiff binders (e.g., from L5 and L7) tended to have $C(S)$ curves lying above those for soft ones (e.g., from L8 and L9). Figure 31 provides the $C(S)$ relationships for the extracted binders from the CO, FL, and LA mixtures. Similarly, within each group, increase in the RAP percentage considerably elevated the $C(S)$ curve due to the increased stiffness as already shown in Figure 28.

Figure 30. Damage characteristic curves for the ALF extracted binders

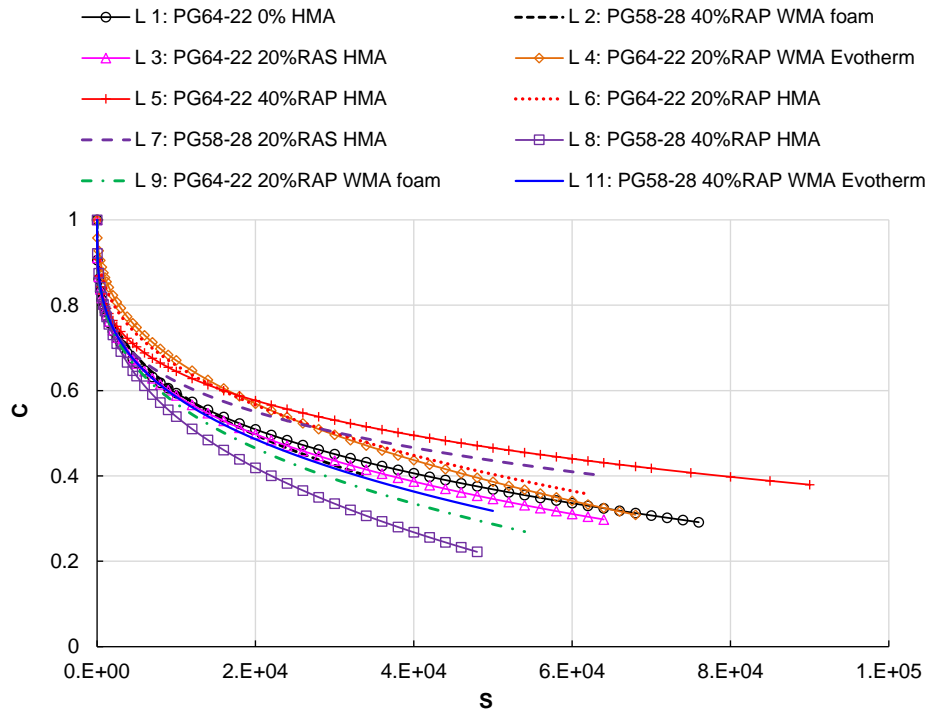


Figure 31. Damage characteristic curves for the CO, FL, and LA extracted binders

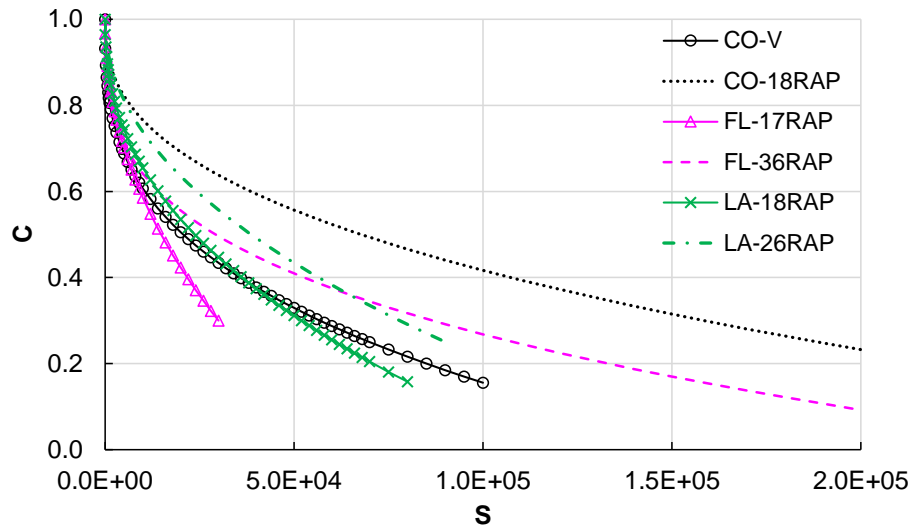
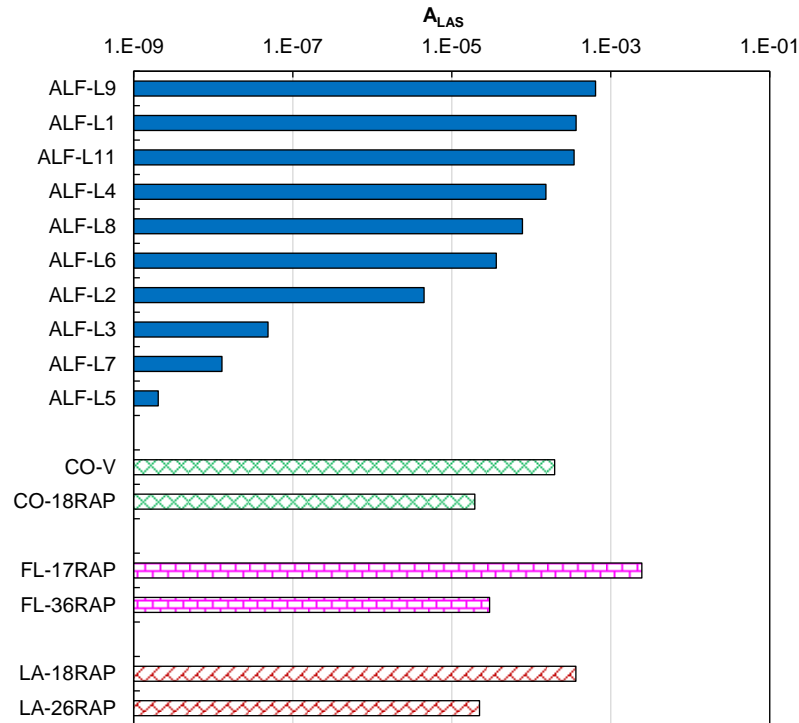


Figure 32 presents the obtained A_{LAS} parameter for all the recovered asphalt binders. Within the ALF group, the binders extracted from the L1 control, L9 (PG 64-22 20% RAP WMA foam), and L11 (PG 58-28 40% RAP WMA Evotherm) demonstrated the

highest fatigue resistance, whereas the binders extracted from the three HMA mixtures with 20% RAS or 40% RAP (i.e., L3, L5, L7) exhibited the lowest resistance. For the asphalt binders recovered from CO, FL, and LA mixtures, it is clearly shown that within each group, higher RAP percentages considerably reduced the fatigue resistance. Note that as stated earlier, the A_{LAS} parameter is derived from the LAS fatigue test and is a more immediate indicator of fatigue cracking resistance as compared to the other rheological parameters. Even though R and ΔT_c yielded unexpected trends with respect to the RAP content in the LA group, the A_{LAS} parameter provided a more reasonable ranking that was consistent with all the mixture testing results.

Figure 32. The A_{LAS} parameter for all the extracted asphalt binders

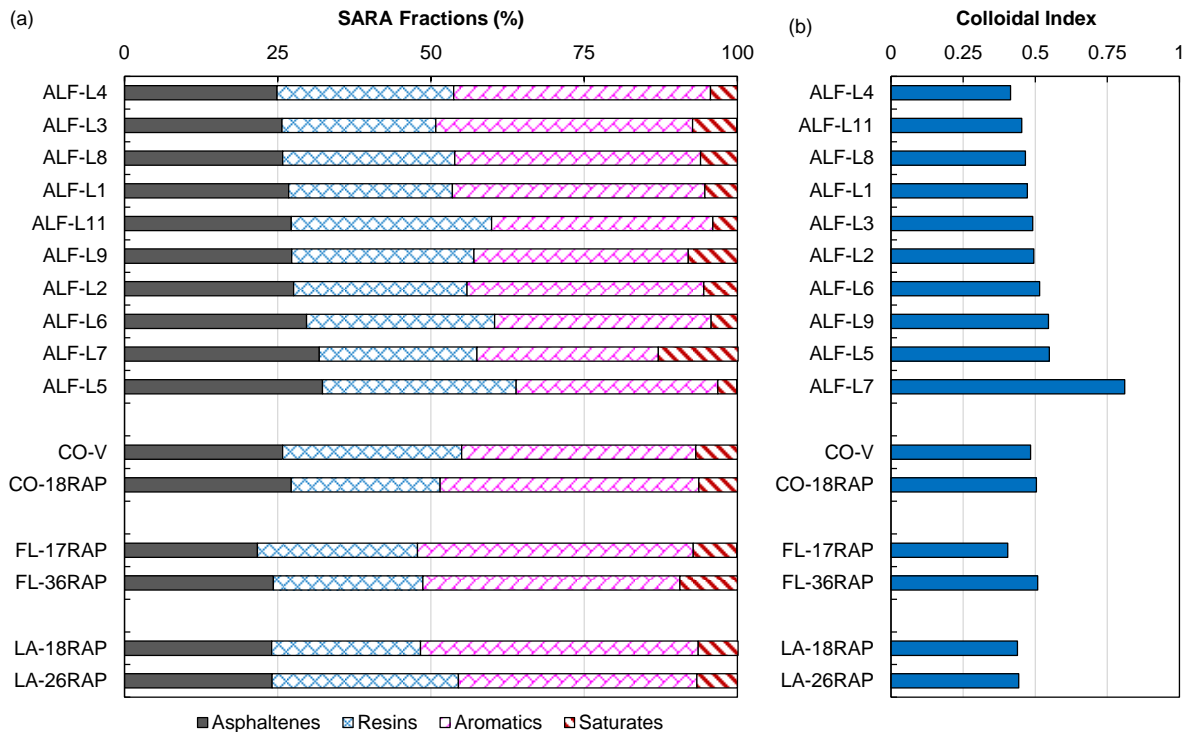


SARA Analysis

The extracted binders were fractionated into saturates, aromatics, resins, and asphaltenes (SARA), and the results are given in Figure 33(a). Note that within each group, the results are presented in the order of increasing percentage of asphaltenes. The asphalt binders extracted from L5 (HMA, 40% RAP, PG 64-22) and L7 (HMA, 20% RAS, PG 58-28) had the highest asphaltenes concentration. It is interesting to note that the

asphaltenes percentage in the asphalt binder extracted from L3 (HMA, 20% RAS, PG 64-22) was among the lowest despite the use of RAS. Overall, the asphaltenes percentage varied in a narrow range, from 24.9% (L4) to 31.8% (L5). For the asphalt binders recovered from the CO and FL mixtures, it is clearly observed that increase in the RAP percentage yielded higher asphaltenes concentrations. For the asphalt binders extracted from the LA mixtures, higher RAP incorporation did not affect the asphaltenes concentration, which may be due to the close RAP percentages and the softer binder contributed from the RAP used in LA-26RAP. Figure 33(b) shows the colloidal index presented in the sequence of increasing values within each group. It is observed that higher asphaltenes concentrations generally resulted in higher colloidal indices. Nevertheless, the L9 extracted binder yielded an unexpectedly high colloidal index, whereas the L3 binder had a moderate value. Use of higher RAP or RAS materials and high production temperatures generally yielded asphalt binders having a less dispersed microstructure that was expected to be more susceptible to cracking.

Figure 33. SARA fractionation results for all the extracted asphalt binders

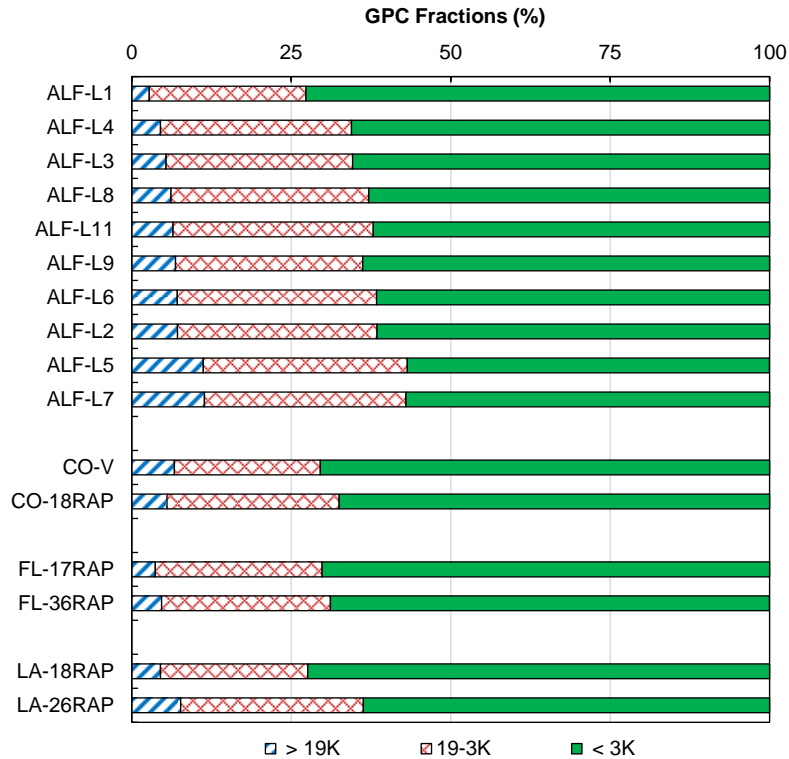


GPC Test

The GPC technique fractionates asphalt binder molecules based on the molecular sizes, which were then converted to molecular weight after calibration. Asphalt molecules are usually fractionated into three portions: high molecular weight (HMW) component (consisting of polymers and associated asphaltenes) with molecular weight greater than 19,000 Dalton (> 19K), asphaltenes component with molecular weight between 3,000 and 19,000 Dalton (19-3K), and maltenes component with molecular weight lower than 3,000 Dalton (< 3K). It should be acknowledged that the GPC and SARA techniques fractionate asphalt binders based on different properties (molecular size versus solubility) of the molecules and thus the obtained results such as asphaltenes and maltenes percentages are not necessarily comparable. Figure 34 gives the GPC fractionation results for all the extracted binders, presented in the sequence of increasing HMW percentages for the ALF group. It is noted that within the ALF materials the binders extracted from L5 (HMA, 40% RAP, PG 64-22) and L7 (HMA, 20% RAS, PG 58-28) contained the highest HMW percentages, while the binder extracted from the L1 control mixture yielded the lowest HMW percentage. Also, it is interesting to find that the HMW concentration of the extracted binder from L3 was among the lowest, despite the use of 20% RAS in the mixture. Interestingly, by comparing the ranking of the ALF extracted binders as shown in Figure 33 and Figure 34, the two separation approaches produced very similar ranking results.

For the binders recovered from the CO, FL, and LA mixtures, use of higher RAP did not produce consistent results in the HMW concentration, but resulted in lower percentages of maltenes (MW < 3,000 Dalton). For the CO materials, use of 18% RAP yielded a slightly reduced HMW concentration compared to the virgin. For the FL and LA groups, increase in the RAP percentage resulted in a slight increase in the HMW portion.

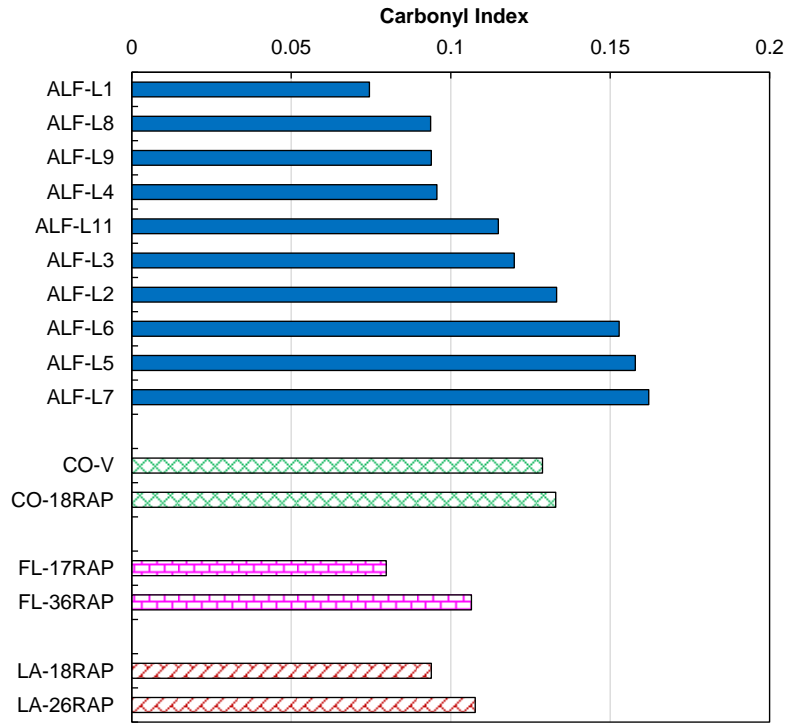
Figure 34. GPC fractionation results for all the extracted binders



FTIR Test

The Carbonyl index parameter was determined using the FTIR spectrum and the results are given in Figure 35 for all the extracted binders. As previously stated, the Carbonyl index would increase as asphalt binder ages. The asphalt binder recovered from the L1 control mixture yielded the lowest Carbonyl index as no RAP/RAS was incorporated. Meanwhile, the three asphalt binders recovered from the HMAs of L5, L6, and L7 containing 40% RAP, 20% RAP, and 20% RAS, respectively, exhibited the highest Carbonyl index values. For the asphalt binders recovered from the CO, FL, and LA mixtures, it is shown that use of higher RAP contents yielded higher Carbonyl indices. In general, the FTIR test reasonably detected the presence and dosages of RAP/RAS.

Figure 35. Carbonyl index results for all the extracted asphalt binders



Discussion in Relation to Material Composition

In order to facilitate discussion with respect to material composition, all asphalt binder indices were normalized using the values for the corresponding control (asphalts recovered from the virgin or low RAP mixtures) such that with increase in RAP/RAS percentage the parameters would generally decrease, suggesting a trend of decreasing cracking resistance. Note that for A_{LAS} , its logarithmic value was used given its wide spread covering several orders of magnitude.

Effect of RAP/RAS. Figure 36 presents the normalized parameters for the ALF extracted binders. With the RAP content increased from 0% to 40%, all normalized parameters saw a consistent reduction in the magnitude, suggesting reduced resistance to fatigue/fracture due to oxidative aging. Such observations agreed with the mixture parameters in Figure 20. The extracted binder from L3 containing 20% RAS exhibited higher values of normalized parameters than L6 (20% RAP) and L5 (40% RAP) and sometimes even higher than L1 control, except for the use of A_{LAS} . As previously stated with respect to mixture parameters, based on material composition the L3 (20% RAS), extracted binders

would have normalized parameters lower than those of L6 (20% RAP). Within the binder parameters evaluated, only the A_{LAS} parameter was able to properly rank the two binders.

Figure 36. Normalized parameters for evaluating the effect of RAP/RAS on the ALF extracted binders

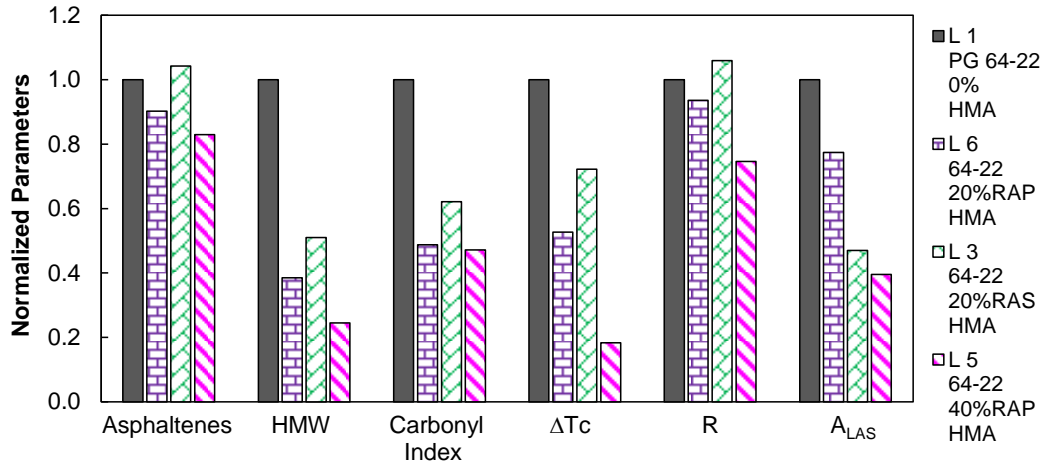
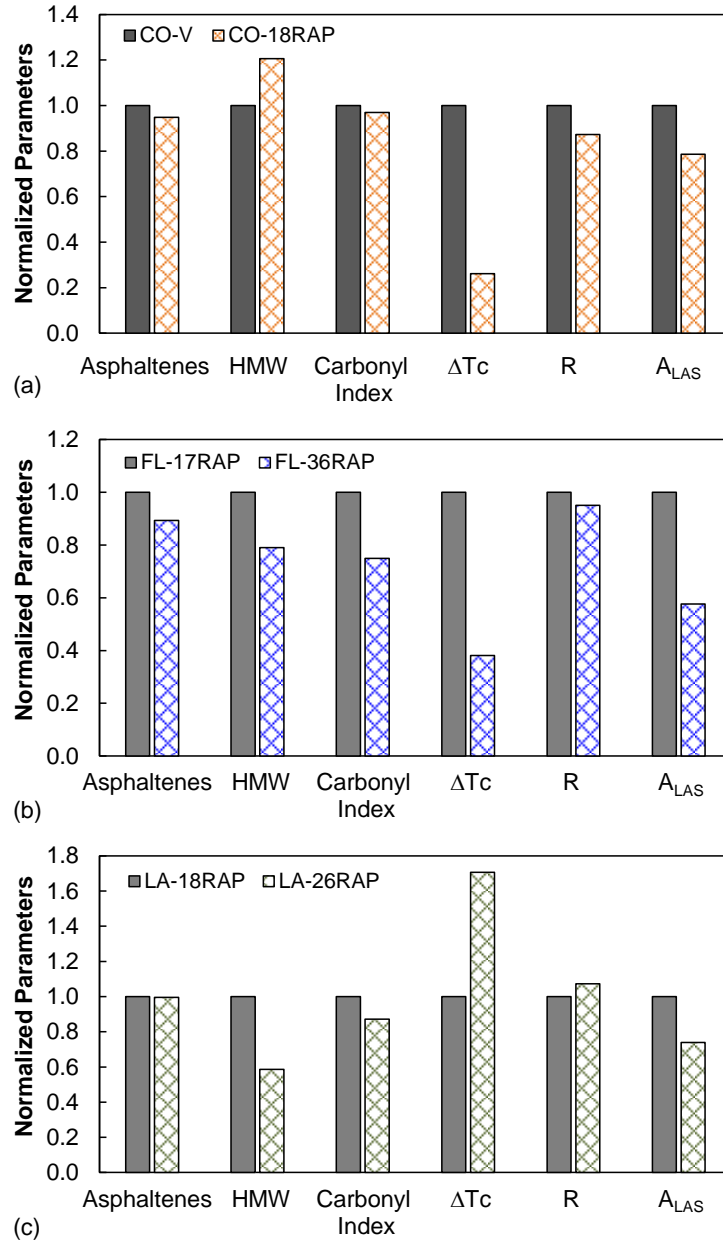


Figure 37 gives the normalized parameters for the CO, FL, and LA extracted binders. Within these material groups, the only variable was the RAP percentage. It is shown that for the CO and FL groups with increase in the RAP content, each parameter decreased, suggesting reduced cracking resistance, the only exception being the HMW parameter for the CO extracted binders. For the LA extracted binders, the HMW, Carbonyl index, and A_{LAS} parameters provided consistent ranking with the corresponding mixture testing results. According to the asphaltenes percentage, the two LA extracted binders were almost identical, whereas ΔT_c and R ranked the binder extracted from LA-26RAP slightly superior. These complications were attributed to the difference in the RAP binder property even though the same RAP source material was used in the two mixtures. Based on the results for the three material sources, within the three rheological parameters, the A_{LAS} parameter appeared to be the best indicator for cracking resistance.

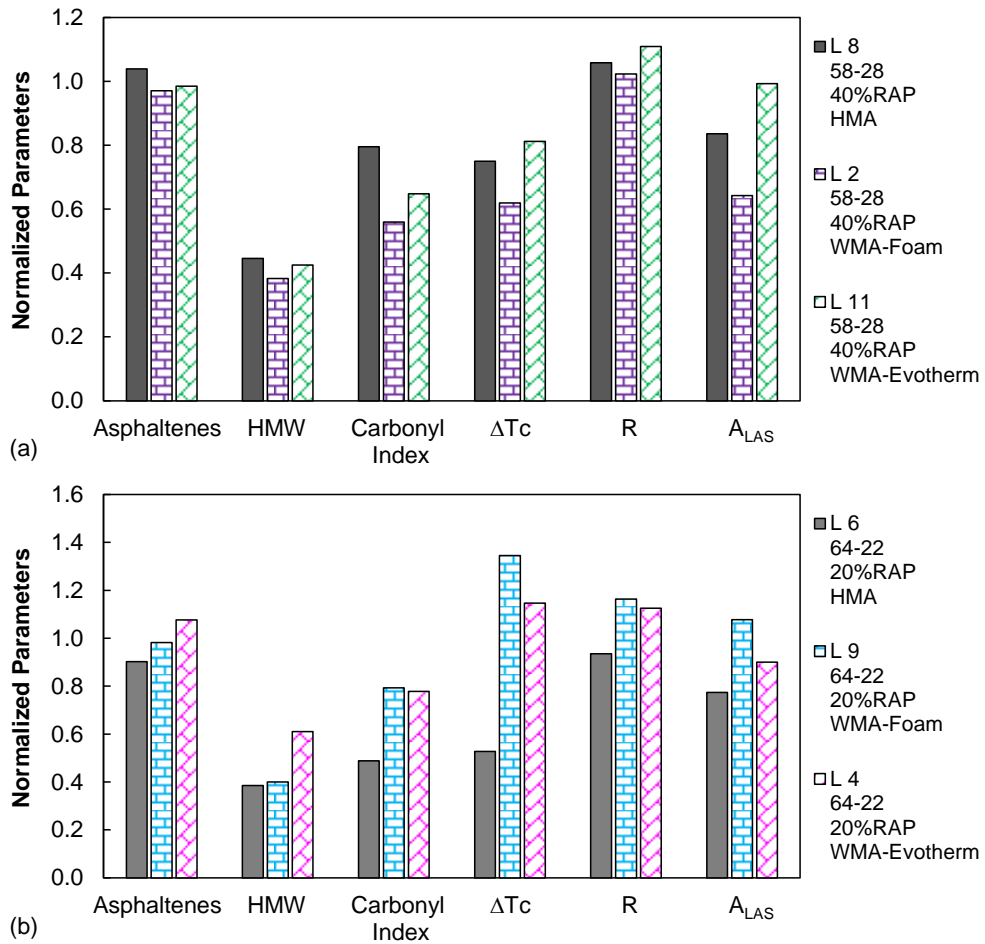
Figure 37. Normalized parameters for evaluating the effect of RAP/RAS on the CO, FL, and LA extracted binders



Effect of Warm-mix Technologies. The effect of WMA technologies was evaluated through two sets of comparisons. The first set consists of L8 (HMA), L2 (water foaming), and L11 (Evotherm), all containing 40% RAP with PG 58-28 base binder; see Figure 38(a). All the binder parameters ranked L2 foamed WMA similar or lower to the L11 WMA with Evotherm. Based on the asphaltenes fraction, HMW, ΔT_c , and R, the recovered binder from L8 HMA is expected to have a similar performance as compared

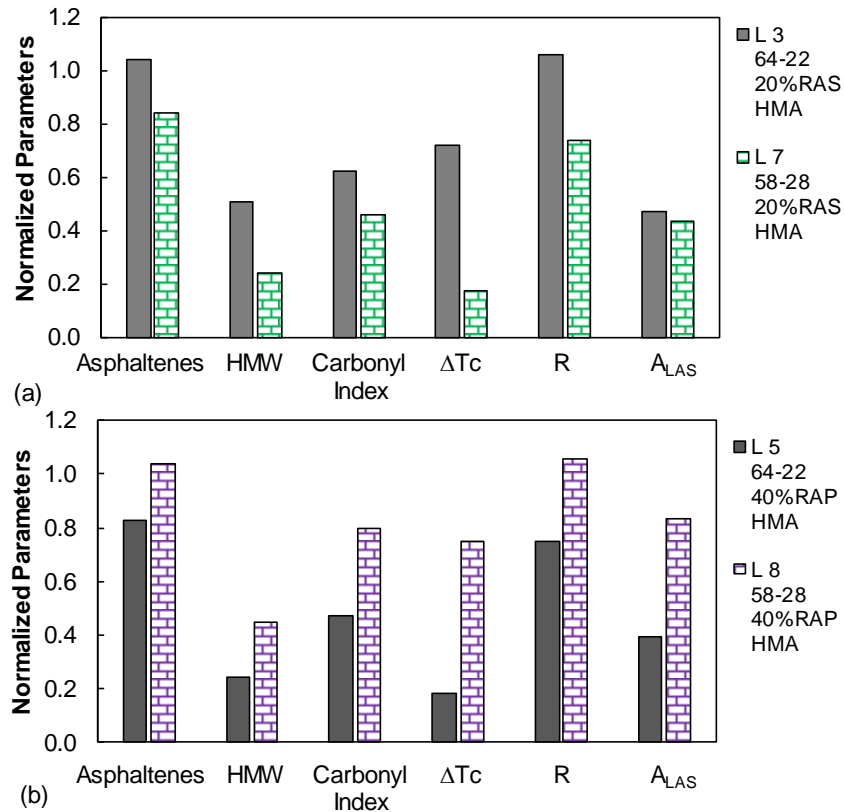
to L11 WMA with Evotherm. Meanwhile, the former was ranked slightly better according to the Carbonyl index, but lower according to A_{LAS} . The second set includes L6 (HMA), L9 (water foaming), and L4 (Evotherm), all containing 20% RAP with PG 64-22 base binder; see Figure 38(b). The asphalt binders from these lanes were considered similar according to asphaltenes fraction. The Carbonyl index, ΔT_c , R , and A_{LAS} parameters ranked the asphalt binder recovered from L9 foamed WMA better than the counterpart from L6 HMA, and better or similar as compared to the recovered binder from L4 WMA with Evotherm. Based on HMW, the recovered binder with the Evotherm technology is expected to be more crack resistant than the other two recovered binders.

Figure 38. Normalized parameters for evaluating the effect of WMA technologies on the extracted binders from the ALF mixtures containing: (a) 40% RAP with PG 58-28 base binder, and (b) 20% RAP with PG 64-22 base binder



Effect of Soft Base Binder. The effect of different base binders were examined by comparing the materials from L3 versus L7, and from L5 versus L8, all being HMA with the first group containing 20% RAS and the latter 40% RAP. As shown in Figure 39(a), all binder parameters consistently ranked the recovered asphalt binder from L3 with PG 64-22 base binder better than L7 with the soft base binder PG 58-28. On the contrary, use of the soft base binder with 40% RAP was seen to improve the cracking performance according to all the binder parameters as shown in Figure 39(b). The above observations were consistent with those based on the mixture performance tests as presented in Figure 23. It appears that the soft base binder was more effective in accommodating the aged binder from RAP than from the highly oxidized RAS.

Figure 39. Normalized parameters for evaluating the effect of soft base binder for the extracted binders from the ALF mixtures containing: (a) 40% RAP, and (b) 20% RAS



Correlation among the Asphalt Binder Test Results

A total of six parameters were selected and determined for the extracted asphalt binders: three chemical parameters including asphaltenes fraction, HMW, Carbonyl index, and

three rheological parameters namely ΔT_c , R , and A_{LAS} . Among these parameters, the three chemical parameters have all been used to relate to asphalt binder oxidative aging. Since aging would deteriorate the cracking resistance, it is expected within the scope of this study that these parameters should also present a correlation with the cracking resistance. The two rheological parameters ΔT_c and R are found to relate with cracking or fatigue performance of asphalt mixtures. The developed parameter A_{LAS} is an immediate indicator of fatigue resistance of asphalt binders. Evaluation of the correlations among the asphalt binder parameters was conducted on the ALF extracted binders. Table 5 presents the best functional fit for every paired parameters and the corresponding R^2 value.

Table 5. Relationships among the asphalt binder parameters

Independent Variable	Dependent Variable	Functional Relationship	R^2
Asphaltenes	HMW	$y = 0.924x - 18.89$	0.77
Asphaltenes	Carbonyl index	$y = 0.010x - 0.160$	0.69
Asphaltenes	ΔT_c	$y = -2.57x + 63.46$	0.80
Asphaltenes	R	$y = 0.180x - 2.133$	0.83
Asphaltenes	A_{LAS}	$y = 3.19E9\exp(-1.211x)$	0.43
HMW	Carbonyl index	$y = 4.22E-2x^{0.544}$	0.73
HMW	ΔT_c	$y = -2.42x + 8.45$	0.80
HMW	R	$y = 0.152x + 1.848$	0.66
HMW	A_{LAS}	$y = 0.0469\exp(-1.28x)$	0.53
Carbonyl index	ΔT_c	$y = -0.597\exp(19.79x)$	0.75
Carbonyl index	R	$y = 1.760\exp(4.052x)$	0.60
Carbonyl index	A_{LAS}	$y = 6.725\exp(-115.2x)$	0.56
ΔT_c	R	$y = -0.067x + 2.339$	0.95
ΔT_c	A_{LAS}	$y = 6.158E-4\exp(0.543x)$	0.70
R	A_{LAS}	$y = 2.158E4\exp(-7.557x)$	0.64

Among the three chemical parameters, relatively good correlations were observed with R^2 values ranging from 0.69 to 0.77. Nevertheless, it should be acknowledged that in general, the chemical parameters are not necessarily highly correlated with each other, as they are based on different properties of the asphalt molecules reacting to oxidative aging [84]. Meanwhile, among the three rheological parameters, good to strong relationships were identified with R^2 values varying between 0.64 and 0.95. Correlations between the chemical and rheological properties were also investigated. The asphaltenes fraction determined via the SARA analysis was found to provide in general the highest correlations with the three rheological parameters, followed by HMW and Carbonyl index. Recall that R and ΔT_c are highly correlated ($R^2 = 0.95$), both indicating the relaxation property of asphalt binders. Their strong correlations with the asphaltenes concentration suggest that the microstructural change in terms of increasing the asphaltenes fraction is the primary cause of the loss in the relaxation capability. This observation agrees with existing findings in that the formation of asphaltenes due to oxidative aging reduces the molecular mobility and capability to relax stresses under loading [85]. Among the three rheological parameters, ΔT_c exhibited the highest correlations with the three chemical parameters, followed by R and A_{LAS} .

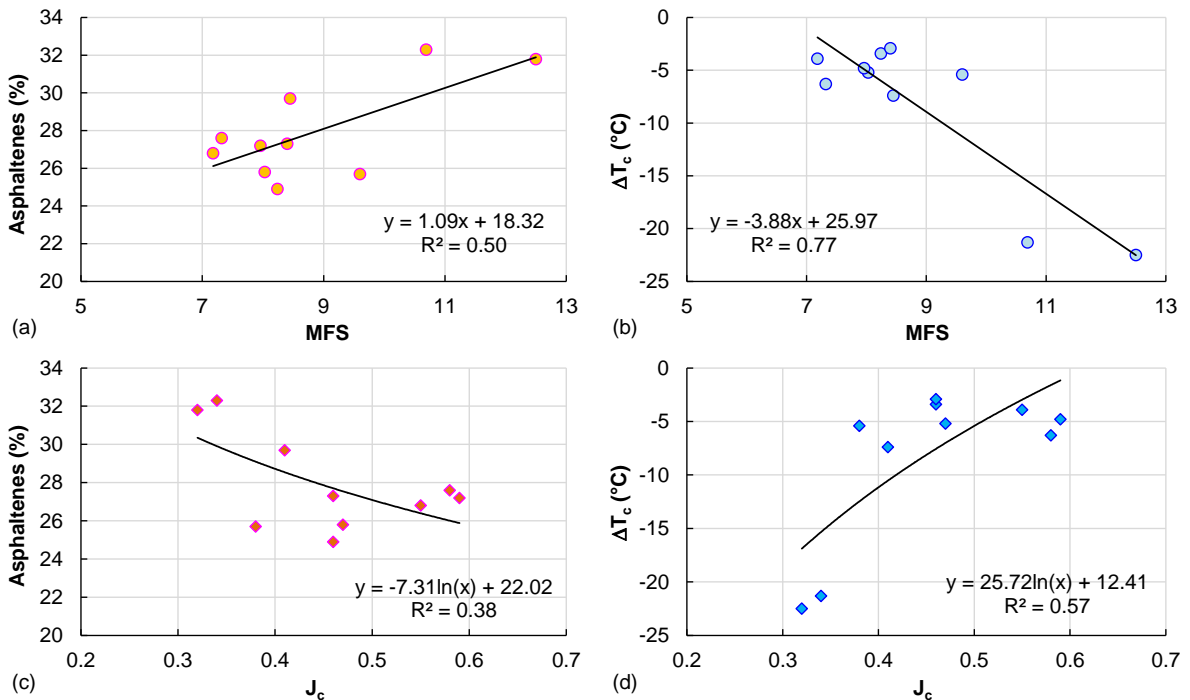
Correlation of Evaluation Parameters between Asphalt Binders and Mixtures

In this study, a total of eight index parameters were used to represent the fatigue/fracture resistance of asphalt mixtures. On the other hand, six parameters were determined as indicators of the fatigue/fracture resistance of the extracted asphalt binders. Investigation of the relationships between the parameters of asphalt binders and mixtures were conducted on the ten ALF mixtures as they form a relatively large data pool compared to other material groups, and also because the asphalt binder property is the primary design variable among these mixtures. In order to facilitate subsequent discussion, not all the evaluation parameters were involved. Only two parameters were selected for the asphalt mixtures, one from a cyclic test and one from a monotonic test. Also, two parameters were selected for the extracted binders, one for chemistry and one for rheology. The selection was based on the following criteria: 1) the selected parameters should reasonably reflect the effect of material composition, especially the RAP content; and 2) they should also present high correlations with the remaining asphalt binder or mixture parameters. Therefore, MFS (S-VECD, cyclic testing) and J_c (SCB, monotonic testing) were selected as the two mixture parameters, and asphaltenes fraction (SARA, chemistry)

and ΔT_c (Superpave performance grading, rheology) were selected as the two asphalt binder parameters for further discussion. All parameters provided the same comparison on the effect of different RAP percentages by reasonably ranking the asphalt mixtures and extracted binders from L1 (control), L6 (20% RAP), and L5 (40% RAP).

Figure 40 presents the correlations between the parameters of asphalt mixtures and extracted asphalt binders. It is seen that overall the MFS parameter determined from the S-VECD test exhibited stronger relationships with the asphalt binder parameters compared to the SCB J_c parameter. Within the two binder parameters, ΔT_c provided higher correlations with the two mixture parameters. In general, reasonable trends were noted for all the parameters; increase in the asphaltenes concentration or when ΔT_c became more negative for the extracted asphalt binders, the asphalt mixtures saw a deterioration in fatigue/fracture resistance as evidenced by the increase in MFS or reduction in J_c . However, a general lack of strong correlation was noted between the parameters of asphalt mixtures and the extracted asphalt binders, which may be attributed to the complicating role of aggregate structure in resisting deformation and cracking.

Figure 40. Correlations among the selected parameters for asphalt mixtures and extracted asphalt binders



Correlation between Laboratory and Field Fatigue Performance

Laboratory performance tests on asphalt mixtures are desired to predict or provide significant correlations with their field performance in pavement. The availability of the measured fatigue performance of the ALF full-scale test lanes provided a unique database that allowed for evaluating the validity of the six mixture test methods and their parameters, namely S-VECD (MFS), Texas overlay ($N_{f,OT}$, CPR, CCPR), beam fatigue ($N_{f,BF}$), SCB (J_c), IDT (DCSE), and I-FIT (FI). Asphalt pavement is a composite structure consisting of multiple layers with various bound and unbound materials, and is subject to complex traffic loading and environmental conditions. The stiffness and fatigue resistance of asphalt mixture are prevailing factors determining the fatigue performance of a pavement structure, but are not the only important ones. Within the scope of this study, the effect of ALF loading, test temperature, and difference among the lane structure layouts were considered through the tensile strain response at the bottom of the asphalt layer. This section presents the strain response calculation, the adjusted ALF fatigue performance based on the obtained strain responses, and the relationships between the laboratory mixture performance parameters and the adjusted ALF field performance.

Finite Element Analysis of Pavement Response

The horizontal tensile strain response is the key parameter to be identified in fatigue performance evaluation of asphalt pavement. For this purpose, the finite element package developed at North Carolina State University named FlexPAVE (previously known as LVECD) was employed [17, 24, 98]. In this program, asphalt concrete is treated as a linear viscoelastic continuum while the unbound base and subgrade materials are considered in the linear elastic domain. For asphalt layers, the dynamic modulus test results served as the input for the linear viscoelastic response computation. For the base and subgrade, the moduli were obtained from back calculation using falling weight deflectometer (FWD) measurements [10]; see Table 2. Adjacent layers are assumed to be fully bonded. Stress and strain responses in asphalt materials under the impact of moving wheel loading are obtained via fast Fourier transform techniques. The ALF wheel loading was configured in the software by its contact area (assumed to be rectangular), contact pressure (689 kPa), wheel load (63.2 kN), and speed (4.9 m/s). The tensile strain responses at the bottom of the asphalt layer under the ALF wheel loading were computed and presented in Table 6. The loading frequency was determined to be 2.5 Hz for the lanes.

Table 6. Tensile strain responses and fatigue performance of the ALF lanes

Lane	Tensile Strain ($\times 10^{-6}$)	Measured Fatigue Life	$ E^* $ of Asphalt Mixture (MPa)	Correction Factor	Adjusted Fatigue Life
L 1	360	368,254	6,726	1.00	368,254
L 2	333	123,035	8,103	0.89	109,809
L 3	289	42,399	10,768	0.47	19,808
L 4	360	88,740	8,675	1.47	130,192
L 5	289	36,946	12,092	1.59	58,773
L 6	344	122,363	8,983	0.86	105,080
L 7	302	23,005	10,620	0.81	18,622
L 8	383	47,679	7,944	2.01	95,939
L 9	368	270,058	7,785	0.96	260,131
L 11	375	74,544	9,190	2.08	155,142

FHWA-ALF Test Lane Fatigue Performance

Table 6 also provides the measured fatigue lives of the ALF lanes, which were determined as the number of load passes to the first appearance of surface cracking [10]. Note that even though the ALF lanes were designed to have the same structure with the only variable being the asphalt mixture, the as-constructed lanes varied in terms of asphalt layer thickness and properties of the base and subgrade; see Table 2. To accommodate such variations in correlating laboratory mixture results with field pavement performance, the measured ALF fatigue data would need to be adjusted. For this purpose, a similar strategy adopted by West et al. [99] using the Asphalt Institute fatigue equation [100] was employed:

$$N_f = A \times 0.00432 C \varepsilon_t^{-3.291} |E^*|^{-0.854} \quad (49)$$

$$C = 10^M \quad \text{with} \quad M = 4.84 \left(\frac{V_{be}}{V_a + V_{be}} - 0.69 \right) \quad (50)$$

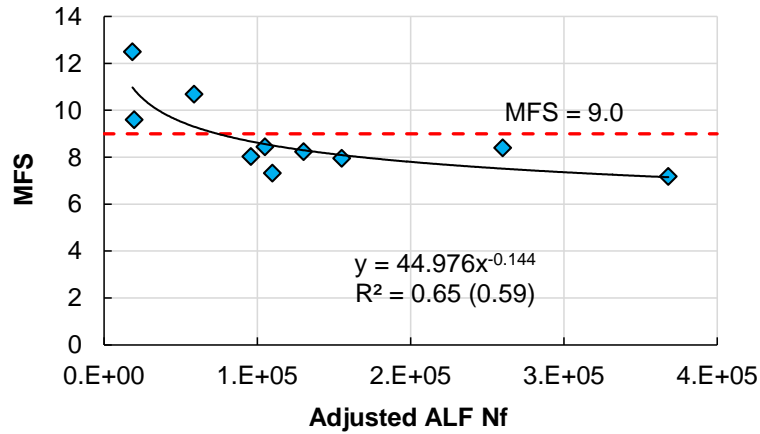
Where, N_f is the predicted fatigue life, $A = 18.4$ is the field shift factor, ε_t is tensile strain, $|E^*|$ is dynamic modulus (psi), V_{be} is the effective asphalt binder volume (%), and V_a is air void content (%).

To calculate N_f , $|E^*|$ in Equation (49) was interpolated using the dynamic modulus master curves at the ALF test temperature (20°C) and loading frequency (2.5 Hz); see Table 6. A correction factor for each lane was determined by normalizing the calculated N_f using the N_f -value of L1. The adjusted fatigue lives of the ALF lanes were then obtained by multiplying the observed performance by corresponding correction factors, and the results are presented in the last column of Table 6. According to both the measured and adjusted fatigue lives, L1 is the best performer while the three HMA lanes (L3, L5, and L7) incorporating 40% RAP or 20% RAS exhibited the lowest fatigue resistance. Both the measured and adjusted fatigue performance were to be used in correlating with the laboratory results for comparative purposes.

Correlation of Laboratory Mixture Parameters to the ALF Performance

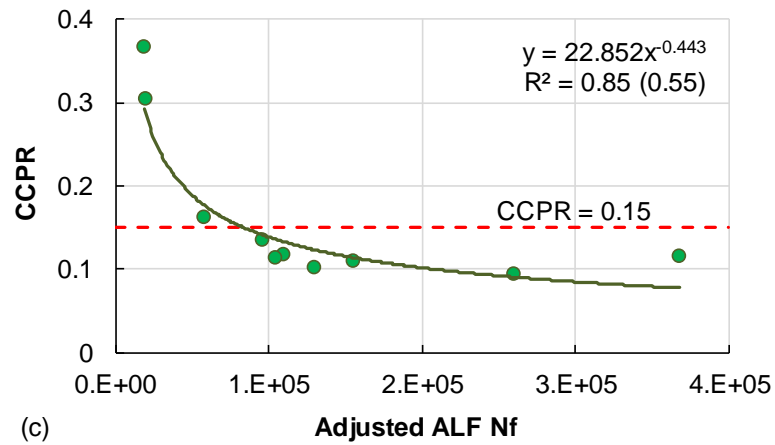
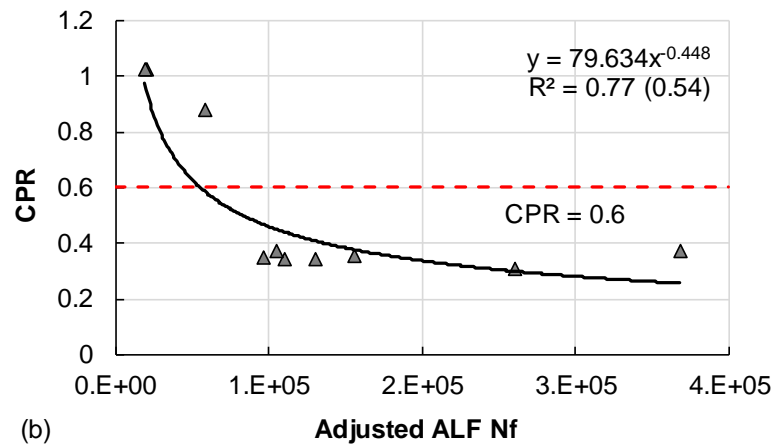
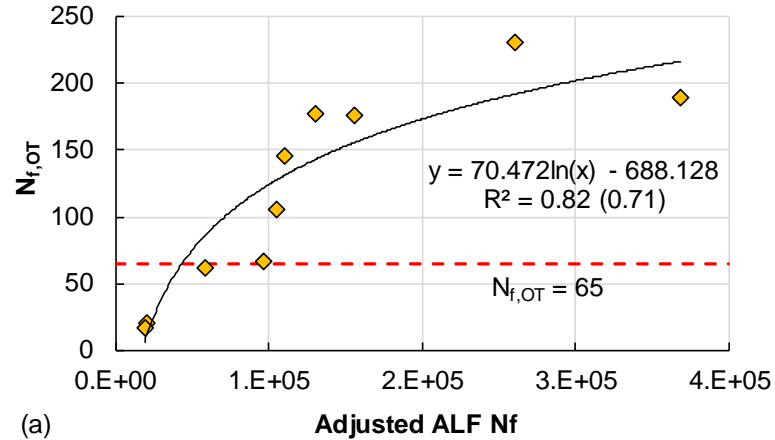
Correlation between S-VECD test and ALF performance. The relationship between the MFS parameter of the S-VECD test and the ALF performance is given in Figure 41. A power function was found to best describe the observed relationship. The R^2 value provided by the measured ALF fatigue life with MFS was 0.59, whereas a stronger correlation with $R^2 = 0.65$ was yielded when the adjusted fatigue life was used. For a clear presentation, hereinafter the data points and the trend line for the measured fatigue lives are not shown in the figure; only its R^2 value is indicated in the parenthesis. In general, a lower MFS value predicted a larger number of load passes that the lane sustained prior to surface cracking. An MFS value of 9.0 appeared to properly separate the lowest three ALF performers, i.e., L3, L5, and L7.

Figure 41. Relationship between MFS and the adjusted ALF performance.



Correlation between Texas overlay test and ALF performance. Figure 42(a) provides the relation between the $N_{f,OT}$ parameter from the Texas overlay test and the adjusted ALF performance, for which a logarithmic fit was found to be adequate. The R^2 value was improved from 0.71 to 0.82 when the measured ALF performance was adjusted. In general, a higher fatigue life determined from the test corresponded to better performance of the lanes. A threshold value of $N_{f,OT} = 65$ seemed to reasonably separate the lowest three lanes (i.e., L3, L5, and L7) from the others. Figure 42(b) presents the relationship between CPR and the adjusted ALF performance, which yielded an improved R^2 of 0.77 from 0.54. A lower CPR value corresponded to better performance of the lanes. A threshold value of $CPR = 0.6$ seemed to reasonably separate the lowest three lanes (i.e., L3, L5, and L7) from the others. Figure 42(c) presents the relationship between CCPR and the adjusted ALF performance, which provided the highest R^2 of 0.85. Use of the actual ALF performance without adjustment yielded R^2 of 0.55. Similar to CPR, a lower CCPR value corresponded to better performance of the lanes. A threshold value of $CCPR = 0.15$ seemed to reasonably separate the lowest three lanes (i.e., L3, L5, and L7) from the others.

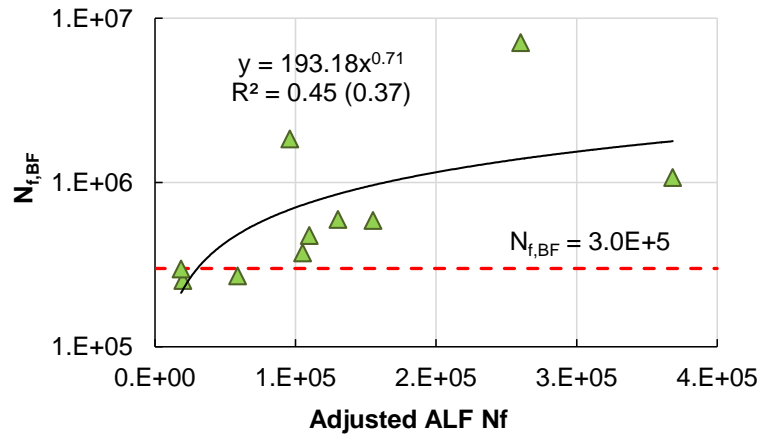
Figure 42. Relationships between the Texas overlay parameters and the adjusted ALF performance



Correlation between beam fatigue test and ALF performance. Figure 43 presents the relationship between the beam fatigue test parameter $N_{f,BF}$ and the ALF fatigue performance. The relationship was best described by a power-law function, which yielded R^2 of 0.45 and 0.37 for the adjusted and measured fatigue lives, respectively. In general,

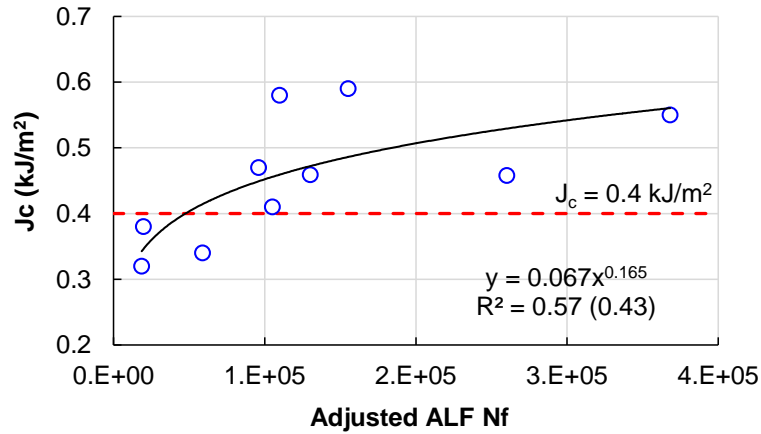
higher $N_{f,BF}$ corresponded to better field performance of the lanes. A threshold value of $N_{f,BF} = 3.0E+5$ (evaluated at $340 \mu\epsilon$) seemed to be able to separate the lowest three performers (i.e., L3, L5, and L7) from the rest.

Figure 43. Relationship between $N_{f,BF}$ and the adjusted ALF performance



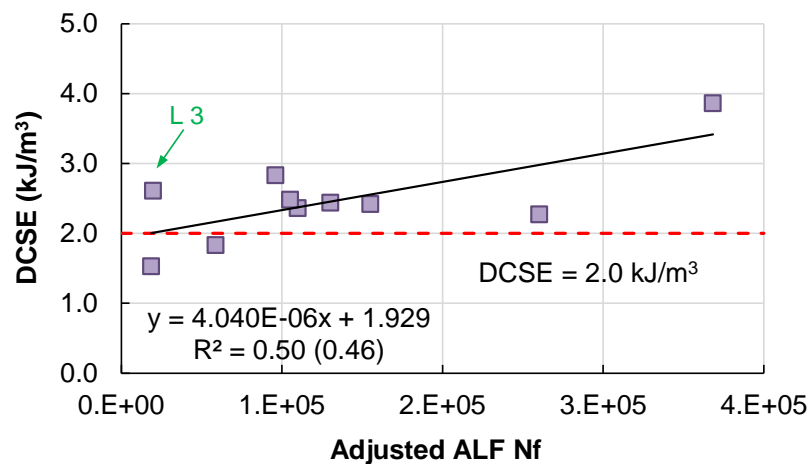
Correlation between SCB test and ALF performance. Figure 44 presents the correlation between the SCB J_c parameter and the adjusted ALF fatigue performance. A power function was found to best describe the observed relationship. The R^2 value provided by the measured ALF fatigue life with J_c was 0.43, whereas a stronger correlation with $R^2 = 0.57$ was yielded when the adjusted fatigue life was used. In general, a higher J_c value corresponded to a large number of load passes before the pavement failed. A threshold value of $J_c = 0.4 \text{ kJ/m}^2$ appeared to properly separate the lowest three ALF performers, i.e., L3, L5, and L7.

Figure 44. Relationship between J_c and the adjusted ALF performance.



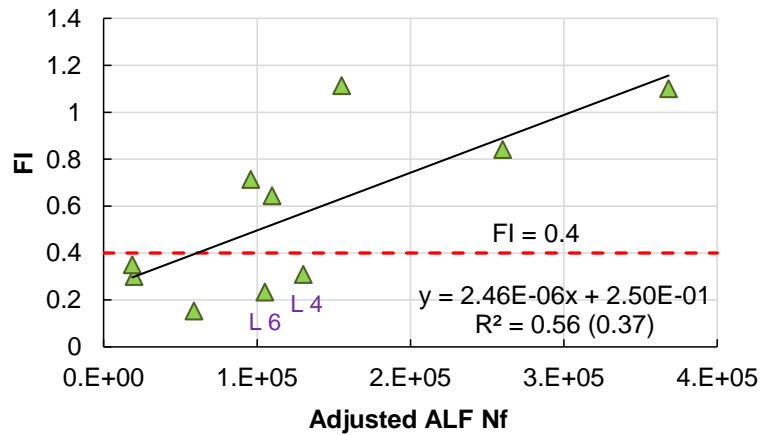
Correlation between IDT test and ALF performance. Figure 45 presents the relationship between the DCSE parameter and the adjusted ALF performance. In general, increase in DCSE corresponded to better fatigue performance observed on the ALF lanes; the relationship was fairly described by a linear function, with R^2 values of 0.50 for the adjusted ALF performance and 0.46 for the measured ALF performance. A threshold value of $DCSE = 2.0 \text{ kJ/m}^3$ was able to only identify the two lowest performers: L5 and L7. According to this parameter, the L3 mixture exhibited better fracture resistance than many other mixtures that performed at the relatively medium to good level in the ALF lanes. However, the L3 structure was actually among the lowest three performers in the ALF experiment.

Figure 45. Relationship between DCSE and the adjusted ALF performance



Correlation between I-FIT test and ALF performance. Figure 46 presents the relationship between the FI parameter and ALF performance. A linear function was found to best describe the observed relationship and use of the adjusted ALF performance, which improved the R^2 value from 0.37 to 0.56. A threshold value of $FI = 0.4$ seemed to be able to separate the lowest three ALF performers (L3, L5, L7), but this criterion would also rank the mixtures from L4 and L6, which performed moderately well in the ALF experiment, among the lowest.

Figure 46. Relationships between FI and the adjusted ALF performance



Rank Correlation. In addition to the numerical relationships between the ALF fatigue performance and different mixture test parameters, it would be also of interest to examine the rank correlation. For this purpose, the ten ALF mixtures were ranked from best to lowest using numbers of 1 to 10, and the results are given in Table 7. It is noted that the parameters from the S-VECD and IDT tests ranked the L1 control mixture the most cracking resistant, as consistent with the adjusted ALF performance. All parameters ranked the L3, L5, and L7 among the lowest performers, except the DCSE parameter that ranked the L3 mixture the third most resistant to cracking and FI that considered the L7 mixture a moderate performer.

With the ranking results provided in Table 7, the degree of agreement between each of the laboratory test parameters and the adjusted ALF fatigue performance was investigated, and this was done by computing the Kendall's τ coefficient [101]. The Kendall's τ coefficient served as a numerical indicator that measures the degree of agreement in ranking results, and is defined as:

$$\tau = \frac{N_{con} - N_{dis}}{N(N-1)/2} \quad (51)$$

where, N_{con} denotes number of concordant pairs; N_{dis} is the number of discordant pairs; and N is the total number of objects.

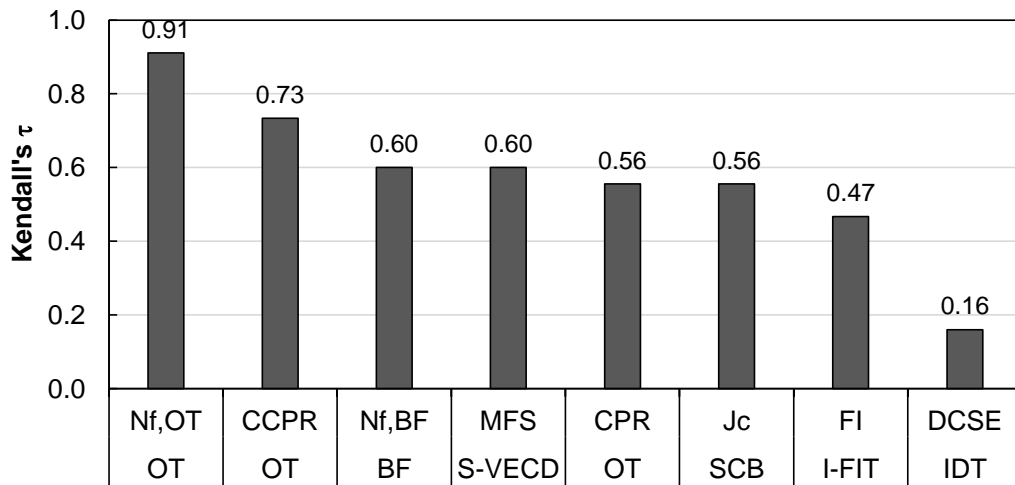
The Kendall's τ coefficient varies between -1 and 1, representing fully different (i.e., reversed) and identical rankings, respectively. Intuitively, higher τ coefficients correspond to more similar rankings between the laboratory test parameters and the reference (adjusted ALF fatigue performance). To calculate the Kendall's coefficient, all lanes were first arranged based on the lane number and then evaluated in a pairwise manner to calculate N_{con} and N_{dis} for all possible pairs. As an example, the pair of (L3, L11) is ranked as (9, 3) by the measured performance (adjusted). Given the inverse order, this pair was scored -1. Likewise, the same pair was scored -1 and +1 according to the SCB J_c and IDT DCSE parameters, respectively. Multiplying the scores by the measurement and each parameter, we obtain +1 and -1 for J_c and DCSE, respectively. Hence, the (L3, L11) pair should be considered as one concordant pair by the J_c parameter but a discordant pair by DCSE. In this case, the relative ranking between L3 and L11 is consistent between the adjusted ALF performance (reference) and the SCB test, but not consistent between the IDT test and the reference.

Table 7. Ranking results for the ALF mixtures

Lane	Adjusted ALF	MFS	$N_{f,OT}$	CPR	CCPR	$N_{f,BF}$	J_c	DCSE	FI
L1	1	1	2	6	5	3	3	1	2
L2	5	2	5	3	6	6	2	7	5
L3	9	8	9	10	9	10	8	3	8
L4	4	5	3	2	2	4	5	5	7
L5	8	9	8	8	8	9	9	9	10
L6	6	7	6	7	4	7	7	4	9
L7	10	10	10	9	10	8	10	10	6
L8	7	4	7	4	7	2	4	2	4
L9	2	6	1	1	1	1	6	8	3
L11	3	3	4	5	3	5	1	6	1

Figure 47 presents the Kendall's τ coefficients for the eight asphalt mixture evaluation parameters. The two Texas overlay parameters, $N_{f,OT}$ and CCPR, yielded the highest ranking agreement with $\tau = 0.91$ and 0.73 , respectively, with the adjusted ALF fatigue life. The beam fatigue and S-VECD tests provided moderate degrees of agreement compared to the reference ranking, yielding the same τ value of 0.60 , followed by the SCB Jc and Texas overlay CPR parameters ($\tau = 0.56$). The I-FIT and IDT test yielded the lowest τ values, with $\tau = 0.47$ for FI, and 0.16 for DCSE.

Figure 47. Rank correlation coefficients for all mixture evaluation parameters with reference to the adjusted ALF fatigue life



Summary. This section has presented the procedure and results for adjusting the measured fatigue performance of the ALF lanes based on the tensile strain responses computed at the bottom of the asphalt layer. Through this process, discrepancies among the ALF lane structures (except the asphalt mixture properties) were considered, and the resulting adjusted ALF performances were used to correlate with the laboratory performance of the asphalt mixtures. Stronger numerical correlations with the adjusted ALF fatigue data were observed for laboratory results than with the measured fatigue data. Among the six asphalt mixture performance tests, only the S-VECD, Texas overlay, beam fatigue, and SCB tests provided the evaluation parameters that were able to identify the lowest three ALF performers (i.e., L3, L5, L7). The IDT and I-FIT tests could not discriminate one or two of the lowest performers from some of the lanes with moderate field performance.

Additionally, preliminary threshold values for each asphalt mixture performance parameter were determined based on the established relationships. It should be realized that these relationships and parameter thresholds were identified based on the ALF test lanes, which employed an accelerated fatigue loading. The ALF loading condition using a constant temperature and wheel loading is considered much more severe than real loading conditions in field pavements. In addition to the numerical correlation, rank correlation was also investigated between the mixture evaluation parameters and the adjusted ALF fatigue life as the reference. The best ranking agreement was provided by the Texas overlay and beam fatigue tests, followed by S-VECD and SCB tests. The I-FIT and IDT tests yielded the lowest rank correlation with the reference.

Combining the observations made with respect to the numerical and ranking correlations with the ALF field performance, and considering the test efficiency and typical variability, the research team recommended the use of the Texas overlay, S-VECD, and SCB tests as the routine laboratory performance tests for intermediate-temperature cracking resistance of asphalt mixtures. The beam fatigue test also demonstrated to be an adequate method despite its lengthy test time and relatively high variability. The I-FIT and IDT tests were not recommended based on their limited capability in identifying the lowest performers and in ranking the ALF lanes as compared to the field performance.

Score Card ranking for Asphalt Mixture Test Methods

One objective of the research project was to compare the six test methods that are well-established and widely used by state agencies and researchers for assessing the fatigue/fracture resistance of asphalt mixtures. A total of 14 aspects for each test method were evaluated and the results were quantified by the scores of 1, 2, 3, and 4 representing the least desired to most desired characteristics. Therefore, a higher total score suggests the most desired test method to be selected for mixture fatigue/fracture characterization. The following lists the 14 aspects selected in evaluation and the complete table is attached in Appendix A.

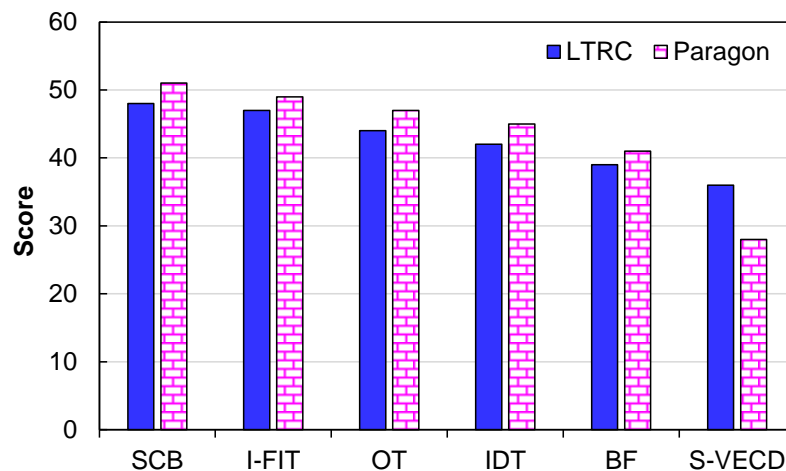
Aspects of test method evaluation:

- specimen preparation time
- instrumentation requirement
- testing oversight

- data interpretation effort
- sensitivity to asphalt grade and mix design parameters
- routine application feasibility
- correlation to field performance
- availability of test standard
- test time
- training requirement
- data analysis requirement
- equipment cost
- technical ability requirement
- test repeatability and variability

The scores were independently developed by the research team as well as the technical and management staff of Paragon Technical Service, Inc., who has testing and analysis experience on each of the six asphalt mixture test methods. The scoring results for each factor are included in Appendix A. Figure 48 summarizes the scores for the six test methods provided by LTRC and Paragon. Note that, in obtaining the final score, no weighting factors were applied.

Figure 48. Summary of scoring results for the asphalt mixture test methods



It is noted that all of the tests were scored 2-3 higher by Paragon than by LTRC, except for the S-VECD test. The score for S-VECD provided by Paragon was considerably lower than the one by LTRC. It is worth pointing out that this test is indeed more difficult in data analysis and interpretation compared to the others. The operator's experience in testing and background in the viscoelastic continuum damage theory are also key factors for successful completion of this test. Compared to all other tests, the S-VECD test employs the uniaxial loading mode which renders a uniform distribution of stress and strain at the cross-section of the test specimen. This testing mode is beneficial for improving test repeatability. Results from this test can be used not only for material evaluation and screening, but also for further mechanistic modeling and finite element analysis.

Out of the six tests, the two monotonic tests using semi-circular specimens (i.e., SCB and I-FIT) were ranked the highest, partly due to the ease in sample preparation, testing, and data analysis. The I-FIT test was scored slightly lower primarily because this test is relatively new and the existing literature documenting its correlation with field performance is limited and mixed. Another potential issue identified during the course of this study is that, because of the high loading rate (50 mm/min), in practice the I-FIT test may require a high data sampling rate (e.g., up to 400 Hz) for stiff mixtures such as those containing RAS or high RAP percentages. In this case, the conventional tabletop loading frame such as those for the Marshall test may not suffice.

Preparation of the OT test specimens, as analogous to the S-VECD test, requires a gluing jig. However, compared to S-VECD, the OT sample has four surfaces that need to be trimmed and the parallelism of the surfaces was found to be an important factor toward the test variability. In the ideal scenario, a double-blade saw should be used to ensure the surface parallelism, but this type of equipment is not available in many asphalt laboratories. Another tricky point in OT sample preparation is that no glue should be present at the gap. This is done by pulling out the spacer after the sample is pressed on to the plates according to the test standard, but in practice, it requires experience to ensure the remaining glue on the specimen at the gap is minimal.

Compared to SCB, I-FIT, and OT tests, the IDT test requires two sets of extensometers mounted at the two surfaces for deformation measurement during testing. Meanwhile, the relatively lower test temperature (i.e., 10°C) may call for a load capacity around 22 kN (5 kips) or even higher. These requirements make the use of the existing AMPT setup unable to accommodate this test. In this study, the IDT test was performed using an MTS machine equipped with an ample environmental chamber, and liquid nitrogen was used as

the cryogenic fluid to maintain the test temperature at 10°C. Another disadvantage compared to the preceding three tests is that the data reduction procedure of the IDT test is cumbersome. This test consists of three steps, i.e., dynamic modulus, creep, and fracture/strength tests, and the data generated by all surfaces of all replicates need to be pooled together and compared for data trimming, a laborious process necessitated to reduce test variability.

The beam fatigue test is the most time-consuming procedure among all the tests evaluated. Without a proper estimate of the initial strain applied, the test can run beyond two to three days. The beam samples are typically obtained by compacting and cutting a slab. Compared to the other tests, beam specimens are usually allowed to have a larger tolerance of $\pm 1.0\%$ in air void. Compared to the other cyclic tests such as OT and S-VECD, fatigue life identified from the beam fatigue test usually has a large variability, but in general, it is still within the threshold specified in ASTM D7460. Data reduction is straightforward by determining the fatigue life and plotting it with respect to the strain applied. Comparison of fatigue resistance is conducted at the same strain level.

Conclusions

The objectives of this project were to investigate the effect of RAP/RAS on the cracking performance of asphalt binders and mixtures, establish mechanistic test criteria that ensure pavement fatigue performance, and compare the existing mixture testing methods for the optimum selection. The plant-produced loose asphalt mixtures contributed from four agencies (FHWA, Colorado DOT, Florida DOT, and Louisiana DOTD) were acquired and characterized in the LTRC asphalt laboratory. Asphalt binders were extracted and recovered from the compacted mixtures that were long-term aged. A suite of asphalt binder and asphalt mixture testing methods were employed to characterize the mechanistic, rheological, and chemical properties. The asphalt mixture test methods for cracking resistance included the S-VECD, Texas overlay, four-point bending beam fatigue, SCB, IDT, and I-FIT tests. The asphalt binder testing consisted of Superpave performance grading, frequency sweep, and LAS for rheological characterization, and SARA fractionation, GPC, and FTIR for chemical characterization. For each test method, a thorough literature review was conducted on the underlying principle and theory to identify and/or develop the test parameters that best suited the objectives of the study. With the obtained parameters, the effects of RAP/RAS content, WMA technologies, and different base binders were assessed. Further, interrelationships among the asphalt binder and mixture parameters, and between the mixture parameters and the ALF lane fatigue performance were also investigated. A score card ranking system for all of the mixture evaluation tests was developed and evaluated independently by two asphalt laboratories. Based on the findings, the following conclusions were drawn:

1) With respect to the asphalt mixture cracking resistance:

- Increase in the RAP content or the use of RAS reduced the cracking resistance. Among the eight asphalt mixture evaluation parameters, all ranked the cracking resistance from best to lowest as L1 (control) > L6 (20% RAP) > L5 (40% RAP), except the Texas overlay CCPR parameter. Only the S-VECD, beam fatigue, Texas overlay, and SCB tests reasonably compared the cracking resistance between L6 (20% RAP) and L3 (20% RAS) as L6 > L3, considering the RAS binder was more oxidatively aged than that from the RAP.
- In general, the two WMA technologies (water foaming and Evotherm) produced mixtures that were similar in cracking performance compared to the counterpart HMA mixtures. Different asphalt mixture evaluation parameters yielded different

ranking results for the two WMA processes compared to each other and to the HMA process, and the result was not conclusive.

- Use of soft base binder was found to be more effective with (high) RAP than with RAS in accommodating the recycled asphalt binders. All asphalt mixture evaluation parameters consistently led to this observation, except $N_{f,BF}$ (beam fatigue), FI (I-FIT), and CPR (Texas overlay).
- In evaluating the relationships among the mixture evaluation parameters, the MFS (S-VECD) parameter exhibited overall the best correlations with the remaining parameters, followed by CPR, $N_{f,OT}$, and SCB J_c . The $N_{f,BF}$ parameter presented overall the lowest correlation with the other parameters. Out of all the comparisons evaluated, relationship between J_c and MFS from two different tests was the strongest with an R^2 value of 0.85.

2) With respect to the rheological and chemical properties of the extracted asphalt binders in relation to cracking resistance:

- In general, asphalt binders extracted from mixtures containing higher RAP percentage or RAS yielded higher values of PG temperatures, rheological index R , asphaltenes fraction, HMW component, Carbonyl index, lower A_{LAS} , and more negative ΔT_c , all suggesting lower cracking resistance within the scope of this study. All rheological and chemical parameters provided reasonable trends with increase in the asphalt mixture RAP content (i.e., within L1, L6, and L3). Only the proposed A_{LAS} parameter, which was an immediate indicator of fatigue resistance, was able to properly rank the binders extracted from L6 (20% RAP) and L3 (20% RAS). For the CO and FL materials, all parameters yielded consistent and reasonable comparisons, except for the GPC HMW parameter in evaluating the two CO extracted binders. The asphaltenes fraction, ΔT_c , and R parameters did not properly rank the two LA extracted binders.
- The two WMA technologies did not yield conclusive results in terms of rheological and chemical properties in the extracted binders as compared to each other and to the asphalt binders extracted from the counterpart HMA mixtures. Different parameters provided various ranking results.
- Use of soft base binder was found to be more effective with (high) RAP than with RAS in accommodating the recycled asphalt binders. All the rheological and chemical parameters obtained for the extracted binders consistently led to this conclusion, which agreed with the asphalt mixture test results.

- Relatively good relationships were observed among the three chemical parameters ($R^2 = 0.69$ to 0.77), and good to strong correlations were identified among the three rheological parameters ($R^2 = 0.64$ to 0.95). Among the three chemical parameters, asphaltene fraction determined via the SARA analysis was found to provide the highest correlations with the rheological properties, followed with HMW and Carbonyl index. Among the three rheological parameters, ΔT_c exhibited the highest correlations with the chemical properties, followed by R and A_{LAS} .

3) With respect to the relationship between the asphalt binder and asphalt mixture parameters:

- A number of parameters were selected to investigate the relationship between the properties of asphalt mixtures and the extracted asphalt binders. They were selected such that they reasonably reflected the effect of material composition, especially the RAP content, and that they presented high correlations with the remaining asphalt binder or mixture parameters. The MFS (S-VECD, cyclic testing) and J_c (SCB, monotonic testing) were selected as the two mixture parameters, and asphaltene fraction (SARA, chemistry) and ΔT_c (Superpave performance grading, rheology) were selected as the two asphalt binder parameters. Reasonable trends were observed for all the interrelationships; increase in the asphaltene concentration or when ΔT_c became more negative for the extracted asphalt binders, the asphalt mixtures saw a deterioration in fatigue/fracture resistance as evidenced by the increase in MFS or reduction in J_c . Overall, the MFS parameter exhibited stronger relationships with the asphalt binder parameters compared to J_c . However, a general lack of strong correlation was noted between the parameters of asphalt mixtures and the extracted asphalt binders, which may be attributed to the complicating role of aggregate structure in resisting deformation and cracking.

4) With respect to the relationship between the asphalt mixture parameters, the ALF performance, and the preliminary test criteria:

- The fatigue performance field measurements for the ALF lanes were adjusted to eliminate the effect of discrepancies in structures and material properties of the unbound layers. The obtained adjusted performance was used to correlate with the laboratory mixture testing results. The adjustment was found to improve the correlation in all cases. By identifying the lowest performers of the ALF lanes (i.e., L3, L5, and L7), the following preliminary testing criteria were proposed:
 - S-VECD test: $MFS \leq 9.0$

- Texas overlay test: $N_{f,OT} \geq 65$, $CPR \leq 0.6$, $CCPR \leq 0.15$
- Four-point bending beam fatigue test: $N_{f,BF,340\mu\epsilon} \geq 3.0E+5$
- SCB test: $J_c \geq 0.4 \text{ kJ/m}^2$
- IDT test: $DCSE \geq 2.0 \text{ kJ/m}^3$
- I-FIT test: $FI \geq 0.4$

It should be emphasized that these criteria were based on limited materials from the ALF test lanes that employed an accelerated fatigue loading. More experimental data and field observations on real pavements are needed to confirm and adjust these criteria.

- According to the investigation on the numerical and rank correlation of all the mixture evaluation parameters with reference to the adjusted ALF performance, the Texas overlay, S-VECD, and SCB tests were recommended as routine tests to be used for performance evaluation of the intermediate-temperature cracking resistance. The beam fatigue test also proved to be an adequate tool despite the lengthy test time and relatively high variability. The I-FIT and IDT tests were not recommended given their limited ranking and discriminating capability as noticed in this study.

5) With respect to the score ranking among the asphalt mixture test methods:

- A total of 14 factors covering the aspects of testing, analysis, and correlation with field performance were evaluated for each of the six asphalt mixture test methods. The ranking result from best to the least desired was SCB, I-FIT, OT, IDT, BF, and S-VECD. It should be noted that the factors were not weighted, but some factors (such as sensitivity to material composition, data analysis, and correlation with field performance) would certainly be given more emphasis than others. Development of weighting factors, however, was considered subjective and thus was not attempted. Therefore, the score card ranking result was only for the purpose of complementing the above conclusions on the performance-based comparison of the test methods in selecting the appropriate methodologies.

Recommendations

In this study, the testing criteria for the six asphalt mixture cracking tests were developed based on the pavement fatigue performance from the full-scale ALF test lanes subjected to accelerated fatigue loading. It is recommended that field fatigue performance data on real pavements subjected to actual traffic and environmental conditions be collected and the materials be characterized to further adjust and refine the criteria.

Acronyms, Abbreviations, and Symbols

Term	Description
AASHTO	American Association of State Highway and Transportation Officials
ALF	Accelerated Loading facility
AMPT	Asphalt Mixture Performance Tester
ANOVA	Analysis of Variance
ASTM	American Society of Testing Materials
BBR	Bending Beam Rheometer
BF	beam fatigue
CA	Christensen-Anderson
CAB	crushed aggregate base
CCPR	corrected crack progression rate
CFE	critical fracture energy
CPR	crack progression rate
Cm	centimeter(s)
CO	Colorado
CoV	coefficient of variation
DCSE	dissipated creep strain energy
DMR	dynamic modulus ratio
DOT	Department of Transportation
DOTD	Department of Transportation and Development
DSR	dynamic shear rheometer
ER	energy ratio
FHWA	Federal Highway Administration
FI	flexibility index
FL	Florida
ft.	foot (feet)
FTIR	Fourier transform infrared spectroscopy
FWD	falling weight deflectometer
GPC	gel permeation chromatography

Term	Description
G-R	Glover-Rowe
HMA	hot-mix asphalt
HMW	high molecular weight
IDT	indirect tension
I-FIT	Illinois flexibility index test
In.	inch(es)
LA	Louisiana
LAS	linear amplitude sweep
LMS	large molecular size
LSD	least significant difference
LTRC	Louisiana Transportation Research Center
LVDT	linear variable differential transducer
LVE	linear viscoelastic
lb.	pound(s)
M	meter(s)
MFS	Material Fatigue Sensitivity
MMS	medium molecular size
NMAS	Material Testing System
OT	nominal maximum aggregate size
PAV	Texas overlay test
PG	pressurized aging vessel
RAP	performance grade
RAS	reclaimed asphalt pavement
RBR	recycled binder ratio
RTFO	rolling thin film oven
SARA	saturates, aromatics, resins, asphaltenes
SCB	semi-circular bend
SMS	small molecular size
S-VECD	simplified viscoelastic continuum damage
TCE	Trichloroethylene

Term	Description
VECD	viscoelastic continuum damage
VMA	voids in the mineral aggregate
WMA	warm-mix asphalt

References

- [1] M. Zaumanis and R. Mallick, "Review of Very High-Content Reclaimed Asphalt Use in Plant-Produced Pavements: State of the Art," *International Journal of Pavement Engineering*, vol. 16, no. 1, pp. 39-55, 2015.
- [2] R. Williams, A. Cascione, D. Haugen, W. Buttlar, R. Bentsen and J. Behnke, "Characterization of Hot Mix Asphalt Containing Post-Consumer Recycled Asphalt Shingles and Fractionated Reclaimed Asphalt Pavement," Iowa State University, Ames, Iowa, 2011.
- [3] L. Loria, E. Hajj, P. Sebaaly, M. Barton, S. Kass and T. Liske, "Performance Evaluation of Asphalt Mixtures with High Recycled Asphalt Pavement Content," *Transportation Research Record: Journal of the Transportation Research Board*, vol. 2208, pp. 72-81, 2011.
- [4] X. Shu, B. Huang and D. Vukosavljevic, "Laboratory Evaluation of Fatigue Characteristics of Recycled Asphalt Mixture," *Construction and Building Materials*, vol. 22, no. 7, pp. 1323-1330, 2008.
- [5] J. Daniel, N. Gibson, S. Tarbox, A. Copeland and A. Andriescu, "Effect of Long Term Aging on RAP Mixtures: Laboratory Evaluation of Plant Produced Mixtures," *Journal of Association of Asphalt Paving Technologists*, vol. 82, pp. 327-365, 2013.
- [6] F. Hong, D. H. Chen and M. Mikhail, "Long-Term Performance Evaluation of Recycled Asphalt Pavement Results from Texas," *Transportation Research Record: Journal of the Transportation Research Board*, vol. 2180, pp. 58-66, 2010.
- [7] W. S. Mogawer, A. Austerman, R. Roque, S. Underwood, L. Mohammad and J. Zou, "Ageing and Rejuvenators: Evaluating Their Impact on High RAP Mixtures Fatigue Cracking Characteristics Using Advanced Mechanistic Models and Testing Methods," *Road Materials and Pavement Design*, vol. 16, no. s2, pp. 1-28, 2015.

- [8] S. Zhao, B. Huang, X. Shu, X. Jia and M. Woods, "Laboratory Performance Evaluation of Warm-Mix Asphalt Containing High Percentages of Reclaimed Asphalt Pavement," *Transportation Research Record: Journal of the Transportation Research Board*, vol. 2294, pp. 98-105, 2012.
- [9] F. Zhou, H. Li, S. Hu, R. Lee, T. Scullion, G. Claros, J. Epps and J. Button, "Evaluation of Use of Recycled Asphalt Shingles in HMA," *Journal of Association of Asphalt Paving Technologists*, vol. 82, pp. 367-402, 2013.
- [10] X. Li and N. Gibson, "Comparison of Laboratory Fatigue Characteristics with Full-Scale Pavement Cracking for Recycled and Warm-Mix Asphalts," *Transportation Research Record: Journal of the Transportation Research Board*, vol. 2576, pp. 100-108, 2016.
- [11] "AASHTO," in *Standard Practice for Mixture Conditioning of Hot Mix Asphalt (HMA). AASHTO R 30-02*, Washington DC, 2015.
- [12] AASHTO, "Standard Method of Test for Determining the Dynamic Modulus and Flow Number for Asphalt Mixtures Using the Asphalt Mixture Performance Tester (AMPT). AASHTO T 378-17," Washington DC, 2017.
- [13] J. S. Daniel and Y. R. Kim, "Development of a Simplified Fatigue Test and Analysis Procedure Using a Viscoelastic Continuum Damage Model," *Journal of Association of Asphalt Paving Technologists*, vol. 71, pp. 619-650, 2002.
- [14] B. S. Underwood, Y. R. Kim and M. N. Guddati, "Improved Calculation Method of Damage Parameter in Viscoelastic Continuum Damage Model," *International Journal of Pavement Engineering*, vol. 11, no. 6, pp. 459-476, 2010.
- [15] B. S. Underwood, C. Baek and Y. R. Kim, "Simplified Viscoelastic Continuum Damage Model as Platform for Asphalt Concrete Fatigue Analysis," *Transportation Research Record: Journal of the Transportation Research Board*, vol. 2296, no. 1, pp. 36-45, 2012.
- [16] M. E. Kutay, N. Gibson and J. Youtcheff, "Conventional and Viscoelastic Continuum Damage (VECD)-Based Fatigue Analysis of Polymer Modified

Asphalt Pavements," *Journal of the Association of Asphalt Paving Technologists*, vol. 77, pp. 395-434, 2008.

- [17] W. Cao, A. Norouzi and Y. R. Kim, "Application of Viscoelastic Continuum Damage Approach to Predict Fatigue Performance of Binzhou Perpetual Pavements," *Journal of Traffic and Transportation Engineering (English Edition)*, vol. 3, no. 2, pp. 104-115, 2016.
- [18] T. Hou, B. S. Underwood and Y. R. Kim, "Fatigue Performance Prediction of North Carolina Mixtures Using the Simplified Viscoelastic Continuum Damage Mode," *Journal of the Association of Asphalt Paving Technologists*, vol. 79, pp. 35-80, 2010.
- [19] M. Sabouri, T. Bennert, S. J. Daniel and Y. R. Kim, "A Comprehensive Evaluation of the Fatigue Behaviour of Plant-produced RAP Mixtures," *Road Materials and Pavement Design*, vol. 16, no. sup2, pp. 29-54, 2015.
- [20] A. Norouzi, A. Sabouri and Y. R. Kim, "Fatigue Life and Endurance Limit Prediction of Asphalt Mixtures Using Energy-Based Failure Criterion," *International Journal of Pavement Engineering*, vol. 18, no. 11, pp. 990-1003, 2017.
- [21] "AASHTO," in *Standard Method of Test for Determining the Damage Characteristic Curve of Asphalt Mixtures from Direct Tension Cyclic Fatigue Tests. AASHTO TP 107-14*, Washington DC, 2016.
- [22] R. A. Schapery, "A Theory of Crack Initiation and Growth in Viscoelastic Media II. Approximate Methods of Analysis," *International Journal of Fracture*, vol. 11, no. 3, pp. 369-388, 1975.
- [23] M. Sabouri and Y. R. Kim, "Development of a Failure Criterion for Asphalt Mixtures Under Different Modes of Fatigue Loading," *Transportation Research Record: Journal of the Transportation Research Board*, vol. 2447, pp. 117-125, 2014.
- [24] A. Norouzi and Y. R. Kim, "Mechanistic Evaluation of Fatigue Cracking in Asphalt Pavements," *International Journal of Pavement Engineering*, vol. 18, no. 6, pp. 530-546, 2017.

- [25] J. Lee, A. Norouzi and Y. R. Kim, "Determining Specimen Geometry of Cylindrical Specimens for Direct Tension Fatigue Testing of Asphalt Concrete," *Journal of Testing and Evaluation*, vol. 45, no. 2, pp. 613-623, 2017.
- [26] W. Cao, L. N. Mohammad and M. Elseifi, "Assessing the Effects of RAP, RAS, and Warm-mix Technologies on Fatigue Performance of Asphalt Mixtures and Pavements Using Viscoelastic Continuum Damage Approach," *Road Materials and Pavement Design*, vol. 18, no. s4, pp. 353-371, 2017.
- [27] R. A. Schapery, "A Theory of Mechanical Behavior of Elastic Media with Growing Damage and Other Changes in Structure," *Journal of the Mechanics and Physics of Solids*, vol. 38, no. 2, pp. 215-253, 1990.
- [28] R. A. Schapery, "Correspondence Principles and a Generalized J Integral for Large Deformation and Fracture Analysis of Viscoelastic Media," *International Journal of Fracture*, vol. 25, no. 3, pp. 195-223, 1984.
- [29] S. W. Park , Y. R. Kim and R. A. Schapery, "A Viscoelastic Continuum Damage Model and Its Application to Uniaxial Behavior of Asphalt Concrete," *Mechanics of Materials*, vol. 24, no. 4, pp. 241-255, 1996.
- [30] F. P. Germann and R. L. Lytton, "Methodology for Predicting the Reflection Cracking Life of Asphalt Concrete Overlays. Report No. FHWA-TX-79-09 + 207-5.," Texas State Department of Highways and Public Transportation, Austin, Texas, 1979.
- [31] G. Cleveland, R. L. Lytton and J. Button, "Using Pseudostrain Damage Theory to Characterize Reinforcing Benefits of Geosynthetic Materials in Asphalt Concrete Overlays," *Transportation Research Record: Journal of the Transportation Research Board*, vol. 1849, pp. 202-211, 2003.
- [32] F. Zhou and T. Scullion, "Overlay Tester: A Rapid Performance Related Crack Resistance Test. Report No. FHWA-TX-84+261-1.," Texas Transportation Institute , College Station, Texas, 2005.
- [33] D. L. Pickett and R. L. Lytton, "Laboratory Evaluation of Selected Fabrics for Reinforcement of Asphalt Concrete Overlays. Report No. FHWA-TX-84+261-1.," Texas Transportation Institute, College Station, Texas, 1983.

- [34] F. Zhou, S. Hu, D. H. Chen and T. Scullion, "Overlay Tester: Simple Performance Test for Fatigue Cracking," *Transportation Research Record: Journal of the Transportation Research Board*, vol. 2001, pp. 1-8, 2007.
- [35] V. Garcia, A. Miramontes, J. Garibay, I. Abdallah and S. Nazarian, "Improved Overlay Tester for Fatigue Cracking Resistance of Asphalt Mixtures. Report No. TxDOT 0-6815-1," The University of Texas at El Paso, El Paso, Texas, 2017.
- [36] "TxDOT," in *Test Procedure for Overlay Test*, Austin, Texas, Texas Department of Transportation, 2017.
- [37] L. F. Walubita, A. N. Faruk, G. Das, H. A. Tanvir, J. Zhang and T. Scullion, "The Overlay Tester: A Sensitivity Study to Improve Repeatability and Minimize Variability in the Test Results. Report No. FHWA/TX-12/0-6607-1," Texas Transportation Institute, College Station, Texas, 2012.
- [38] S. Carpenter, K. Ghuzlan and S. Shen, "Fatigue Endurance Limit for Highway and Airport Pavements," *Transportation Research Record: Journal of the Transportation Research Board*, vol. 1832, pp. 131-138, 2003.
- [39] "ASTM," in *Standard Test Method for Determining Fatigue Failure of Compacted Asphalt Concrete Subjected to Repeated Flexural Bending. ASTM D7460-10*, West Conshohocken, Pennsylvania, 2010.
- [40] S. Shen and S. Carpenter, "Development of an Asphalt Fatigue Model Based on Energy Principles," *Journal of Association of Asphalt Paving Technologists*, vol. 76, pp. 525-573, 2007.
- [41] "AASHTO," in *Standard Method of Test for Determining the Fatigue Life of Compacted Asphalt Mixtures Subjected to Repeated Flexural Bending. AASHTO T 321-17*, Washington DC, 2017.
- [42] G. Rowe, P. Blankenship, M. J. Sharrock and T. Bennert, "The Fatigue Performance of Asphalt Mixtures in the Four Point Bending Beam Fatigue Test in Accordance with AASHTO and ASTM Analysis Methods," in *5th Eurasphalt & Eurobitume Congress*, Istanbul, June 13-15, 2012. <http://www.h-a-d.hr/pubfile.php?id=667>.

- [43] K. P. Chong and M. D. Kuruppu, "New Specimens for Fracture Toughness Determination for Rock and Other Materials," *International Journal of Fracture*, vol. 26, pp. R59-R62, 1984.
- [44] M. A. Mull, K. Stuart and A. Yehia, "Fracture Resistance Characterization of Chemically Modified Crumb Rubber Asphalt Pavement," *Journal of Materials Science*, vol. 37, no. 3, pp. 557-566, 2002.
- [45] E. Mahmoud, S. Saadeh, H. Hakimelahi and J. Harvey, "Extended Finite-Element Modelling of Asphalt Mixtures Fracture Properties Using the Semi-Circular Bending Test," *Materials and Pavement Design*, vol. 15, no. 1, pp. 153-166, 2014.
- [46] S. Cooper, L. N. Mohammad and M. Elseifi, "Laboratory Performance of Asphalt Mixtures Containing Recycled Asphalt Shingles," *Transportation Research Record: Journal of the Transportation Research Board*, vol. 2445, pp. 94-102, 2014.
- [47] L. N. Mohammad, M. Kim and H. Challa, "Development of Performance-Based Specifications for Louisiana Asphalt Mixtures. Report No. FHWA/LA.14/558," Louisiana Transportation Research Center, Baton Rouge, Louisiana, 2016.
- [48] "ASTM," in *Standard Test Method for Evaluation of Asphalt Mixture Cracking Resistance using the Semi-Circular Bend Test (SCB) at Intermediate Temperatures. ASTM D8044-16*, ASTM International, West Conshohocken, Pennsylvania, 2016.
- [49] W. G. Buttlar and R. Roque, "Development and Evaluation of the Strategic Highway Research Program Measurement and Analysis System for Indirect Tensile Testing of Asphalt Mixtures at Low Temperatures," *Transportation Research Record: Journal of Transportation Research Board*, vol. 1454, pp. 163-171, 1994.
- [50] R. Roque and R. G. Buttlar, "The Development of a Measurement and Analysis System to Accurately Determine Asphalt Concrete Properties Using the Indirect Tensile Mode," *Journal of Association of Asphalt Paving Technologists*, vol. 61, pp. 304-332, 1992.

- [51] R. Roque, B. Birgisson, B. Sangpetgnam and Z. Zhang, "Hot Mix Asphalt Fracture Mechanics: a Fundamental Crack Growth Law for Asphalt Mixtures," *Journal of Association of Asphalt Paving Technologists*, vol. 71, pp. 816-827, 2002.
- [52] Z. Zhang, R. Roque, B. Birgisson and B. Sangpetgnam, "Identification and Verification of a Suitable Crack Growth Law for Asphalt Mixtures," *Journal of the Association of Asphalt Paving Technologists*, vol. 70, pp. 206-241, 2001.
- [53] Y. R. Kim, Y. Seo, M. King and M. Momen, "Dynamic Modulus Testing of Asphalt Concrete in Indirect Tension Mode," *Transportation Research Record: Journal of the Transportation Research Board*, vol. 1891, pp. 163-173, 2004.
- [54] Y. R. Kim and H. Wen, "Fracture Energy from Indirect Tension Testing," *Journal of Association of Asphalt Paving Technologists*, vol. 71, pp. 779-793, 2002.
- [55] R. Roque, B. Birgisson, C. Drakos and B. Dietrich, "Development and Field Evaluation of Energy-Based Criteria for Top-down Cracking Performance of Hot Mix Asphalt," *Journal of Association of Asphalt Paving Technologists*, vol. 73, pp. 229-260, 2004.
- [56] I. L. Al-Qadi, H. Ozer, J. Lambros, A. E. Khatib, P. Singhvi, T. Khan, J. Rivera-Perez and B. Doll, "Testing Protocols to Ensure Performance of High Asphalt Binder Replacement Mixes Using RAP and RAS. Report No. FHWA-ICT-15-017," Illinois Center for Transportation, Urbana, Illinois, 2015.
- [57] C. Ling, D. Swiertz, T. Mandal, P. Teymourpour and H. Bahia, "Sensitivity of the Illinois Flexibility Index Test to Mixture Design Factors," *Transportation Research Record: Journal of the Transportation Research Board*, vol. 2631, pp. 153-159, 2017.
- [58] R. C. West, "NCHRP 9-55: Recycled Asphalt Shingles in Asphalt Mixtures with Warm Mix Asphalt Technologies," in *Presented at the 2017 spring meeting of the Asphalt Mix Expert Task Groups*, Ames, Iowa, May -12, 2017.

- [59] A. Hanz, "Effect of Polymer Modification on I-FIT Parameters," in *Presented at the 2017 fall meeting of the Asphalt Binder Expert Task Groups*, Bozeman, Montana, September 19-20, 2017.
- [60] "AASHTO," in *Standard Method of Test for Determining the Fracture Potential of Asphalt Mixtures Using the Illinois Flexibility Index Test (I-FIT)*. AASHTO TP124-16, Washington, DC, 2016.
- [61] "AASHTO," in *Standard Method of Test for Quantitative Extraction of Asphalt Binder from Hot Mix Asphalt (HMA)*. AASHTO T 164-14, Washington DC, p. 2014.
- [62] "AASHTO," in *Standard Practice for Recovery of Asphalt Binder from Solution by Abson Method*. AASHTO R 59-11, Washington DC, 2015.
- [63] "AASHTO," in *Standard Practice for Grading or Verifying the Performance Grade (PG) of an Asphalt Binder*. AASHTO R 29-15, Washington DC, 2015.
- [64] "AASHTO," in *Standard Method of Test for Determining the Flexural Creep Stiffness of Asphalt Binder Using the Bending Beam Rheometer (BBR)*. AASHTO T 313-12, Washington DC, 2016.
- [65] "AASHTO," in *Standard Method of Test for Effect of Heat and Air on a Moving Film of Asphalt Binder (Rolling Thin-Film Oven Test)*. AASHTO T 240-13, Washington DC, 2017.
- [66] "AASHTO," in *Standard Practice for Accelerated Aging of Asphalt Binder Using a Pressurized Aging Vessel (PAV)*. AASHTO R 28-12, Washington DC, p. 2016.
- [67] "AASHTO," in *Standard Specification for Performance-Graded Asphalt Binder*. AASHTO M 320-17, Washington DC, 2017.
- [68] "ASTM," in *Standard Practice for Determining the Continuous Grading Temperatures and Continuous Grades for PG Graded Asphalt Binders*. ASTM D7643-16, ASTM International, West Conshohocken, Pennsylvania, 2016.
- [69] C. J. Glover, R. R. Davison, C. H. Domke, Y. Ruan, P. Juristyarini, D. B. Knorr and S. H. Jung, "Development of a New Method for Assessing Asphalt Binder

Durability with Field Validation. Report No. FHWA/TX-05/1872-2," Texas Transportation Institute, College Station, Texas, 2005.

- [70] R. M. Anderson, G. N. King, D. I. Hanson and P. B. Blankenship, "Evaluation of the Relationship between Asphalt Binder Properties and Non-load Related Cracking," *Journal of Association of Asphalt Paving Technologists*, vol. 80, pp. 615-649, 2011.
- [71] P. Kandhal, "Low-temperature Ductility in Relation to Pavement Performance. In: Marek, C.R. (Ed.), ASTM STP 628: Low-Temperature Properties of Bituminous Materials and Compacted Bituminous Paving Mixtures," *American Society for Testing and Materials, Philadelphia, PA*, pp. 95-106, 1977.
- [72] G. M. Rowe, "Prepared Discussion Following the Paper by Anderson et al. Titled Evaluation of the Relationship between Asphalt Binder Properties and Non-Load Related Cracking," *Journal of Association of Asphalt Paving Technologists*, vol. 80, pp. 649-662, 2011.
- [73] D. W. Christensen and D. A. Anderson, "Interpretation of Dynamic Mechanical Test Data for Paving Grade Asphalt Cements," *Journal of Association of Asphalt Paving Technologists*, vol. 61, pp. 67-116, 1992.
- [74] D. W. Christensen, D. A. Anderson and G. M. Rowe, "Relaxation Spectra of Asphalt Binders and the Christensen–Anderson Rheological Model," *Road Materials and Pavement Design*, vol. 18, no. s1, pp. 382-403, 2017.
- [75] F. Moutier, G. Ramond, C. Such and J. Bonnot, "Influence of the Nature of Asphalt Cements on the Fatigue Strength of Asphalt-Aggregate Mixtures under Imposed Strain," in *Conference of Highway Research: Sharing the Benefits, The United States Strategic Highway Research Program*, Thomas Telford, London.
- [76] W. S. Mogawer, A. Booshehrian, S. Vahidi and A. J. Austerman, "Evaluating the Effect of Rejuvenators on the Degree of Blending and Performance of High RAP, RAS, and," *Road Materials and Pavement Design*, vol. 14, no. s2, pp. 193-213, 2013.
- [77] W. S. Mogawer, T. Bennert, A. Austerman and C. Ericson, "Investigating the Aging Mitigation Capabilities of Rejuvenators in High RAP Mixtures Using

- Black Space Diagrams, Binder Rheology and Mixture Tests," *Journal of Association of Asphalt Paving Technologists*, vol. 84, pp. 705-736, 2015.
- [78] J. C. Petersen, R. E. Robertson, J. F. Branthaver, P. M. Harnsberger, J. J. Duvall, S. S. Kim, D. A. Anderson, D. W. Christiansen and H. U. Bahia, "Binder Characterization and Evaluation: Volume I. SHRP-A-367," Transportation Research Board, Washington, D.C, 1994.
- [79] "AASHTO," in *Standard Method of Test for Estimating Fatigue Resistance of Asphalt Binders Using the Linear Amplitude Sweep. AASHTO TP 101-12*, Washington DC, 2016.
- [80] C. Hintz, R. Velasquez, C. Johnson and H. Bahia, "Modification and Validation of Linear Amplitude Sweep Test for Binder Fatigue Specification," *Transportation Research Record: Journal of the Transportation Research Board*, vol. 2207, pp. 99-106, 2011.
- [81] F. Safaei, C. Castorena and Y. R. Kim, "Linking Asphalt Binder Fatigue to Asphalt Mixture Fatigue Performance Using Viscoelastic Continuum Damage Modeling," *Mechanics of Time-Dependent Materials*, vol. 20, no. 3, pp. 299-323, 2016.
- [82] C. Wang, C. Castorena, J. Zhang and Y. R. Kim, "Unified Failure Criterion for Asphalt Binder under Cyclic Fatigue Loading," *Road Materials and Pavement Design*, vol. 16, no. sup2, pp. 125-148, 2015.
- [83] W. Cao, L. N. Mohammad and P. Barghabany, "Use of Viscoelastic Continuum Damage Theory to Correlate Fatigue Resistance of Asphalt Binders and Mixtures," *International Journal of Geomechanics*, vol. 18, no. 11, p. 04018151, 2018.
- [84] W. H. Daly, "Relationship between Chemical Makeup of Binders and Engineering Performance: A Synthesis of Highway Practice. Report No. NCHRP Synthesis 511," Transportation Research Board, Washington DC, 2017.
- [85] J. C. Petersen, P. M. Harnsberger and R. E. Robertson, "Factors Affecting the Kinetics and Mechanisms of Asphalt Oxidation and the Relative Effects of

- Oxidation Products on Age Hardening," *American Chemical Society Division of Fuel Chemistry Preprints*, vol. 41, no. 4, pp. 1232-1244, 1996.
- [86] J. C. Petersen, "Chemical Composition of Asphalt as Related to Asphalt Durability: State of the Art," *Transportation Research Record: Journal of the Transportation Research Board*, vol. 999, pp. 13-30, 1984.
- [87] F. J. Nellenstyn, "The Constitution of Asphalt," *Journal of the Institution of Petroleum Technologists*, vol. 10, pp. 311-325, 1924.
- [88] F. J. Nellenstyn, "Relation of the Micelle to the Medium in Asphalt," *Journal of the Institution of Petroleum Technologists*, vol. 14, pp. 134-138, 1928.
- [89] L. Loeber, G. Muller, J. Morel and O. Sutton, "Bitumen in Colloid Science: A Chemical, Structural and Rheological Approach," *Fuel*, vol. 77, no. 13, pp. 1443-1450, 1998.
- [90] "ASTM," in *Standard Test Method for n-heptane Insolubles. ASTM D3279-12*, ASTM International, West Conshohocken, PA, 2012.
- [91] K. W. Kim, J. L. Burati and S. N. Amirkhanian, "Relation of HP-GPC Profile with Mechanical Properties of AC Mixtures," *Journal of Materials in Civil Engineering*, vol. 5, no. 4, pp. 447-459, 1993.
- [92] M. A. Plummer and C. C. Zimmerman, "Asphalt Quality and Yield Predictions from Crude Oil Analysis," *Journal of Association of Asphalt Paving Technologists*, vol. 53, pp. 138-159, 1984.
- [93] M. M. Hattingh, "The Fraction of Asphalt," *Journal of Association of Asphalt Paving Technologists*, vol. 53, pp. 197-215, 1984.
- [94] J. C. Petersen, "Quantitative Functional Group Analysis of Asphalts Using Differential Infrared Spectrometry and Selective Chemical Reactions-Theory and Application," *Transportation Research Record: Journal of the Transportation Research Board*, vol. 1096, pp. 1-11, 1986.
- [95] S. B. Cooper, I. Negulescu, S. S. Balamurugan, L. N. Mohammad and W. H. Daly, "Binder Composition and Intermediate Temperature Cracking

- Performance of Asphalt Mixtures Containing RAS," *Road Materials and Pavement Design*, vol. 16, no. s2, pp. 275-295, 2015.
- [96] M. Kim, L. N. Mohammad, T. Jordan and S. B. Cooper, "Fatigue Performance of Asphalt Mixture Containing Recycled Materials and Warm-mix Technologies under Accelerated Loading and Four Point Bending Beam Test," *Journal of Cleaner Production*, vol. 192, pp. 656-664, 2018.
- [97] G. M. Rowe and D. A. Anderson, "Binder Rheology 101 – Relaxation Spectr," in *Asphalt Binder ETG Meeting*, 2014.
- [98] M. Eslaminia, S. Thirunavukkarasu, M. N. Guddati and Y. R. Kim, "Accelerated Pavement Performance Modeling Using Layered Viscoelastic Analysis," in *Scarpas, A., Kringos, N., Al-Qadi, I. (Eds.), 7th RILEM International Conference on Cracking in Pavements*, Springer, Dordrecht, 2012.
- [99] R. C. West, C. W. Winkle, S. Maghsoodloo and S. Dixon, "Relationships between Simple Asphalt Mixture Cracking Tests Using Ndesign Specimens and Fatigue Cracking at FHWA's Accelerated Loading Facility," *Road Materials and Pavement Design*, vol. 18, no. s4, pp. 428-446, 2017.
- [100] T. Pellinen, D. W. Christensen, G. Rowe and M. J. Sharrock, "Fatigue-Transfer Functions: How Do They Compare?," *Transportation Research Record: Journal of the Transportation Research Board*, vol. 1896, pp. 77-87, 2004.
- [101] M. G. Kendall, "A New Measure of Rank Correlation," *Biometrika*, vol. 30, no. 1/2, pp. 81-93, 1938.

Appendix

Score Card System for Asphalt Mixture Test Methods

A. Specimen preparation

1. Very long preparation time (7+ days)
2. Long preparation time (5-6 days)
3. Short preparation time (3-4 days)
4. Minimal preparation required (1-2 days)

B. Instrumentation requirement

1. Instrumenting the specimen is tedious and requires significant gauges
2. Instrumenting the specimen is moderate and requires significant gauges
3. Instrumenting the specimen is simple and requires some significant gauges
4. Instrumenting the specimen is simple and does not require significant gauges

C. Testing oversight

1. Testing is very involved and requires substantial oversight
2. Testing requires heavy oversight
3. Testing requires moderate oversight
4. Testing is very straightforward and requires little oversight

D. Data interpretation effort

1. Data requires substantial interpretation to be usable
2. Data requires heavy interpretation
3. Data requires moderate interpretation

4. Data requires little interpretation to be usable

E. Sensitivity to asphalt grade and mix design parameters

1. The outcome of this test is not dependent on the AC grade and mix design
2. The outcome of this test is slightly dependent on the AC grade and mix design
3. The outcome of this test is moderately dependent on the AC grade and mix design
4. The outcome of this test is highly dependent on the AC grade and mix design

F. Routine application feasibility

1. Application cannot be done routinely
2. Application can be done routinely but very slowly
3. Application can be done routinely with moderate speed
4. Application can be done routinely with great speed

G. Correlation to field performance

1. No field correlation in the literature
2. Few papers/reports in the literature
3. Some papers/reports in the literature
4. Well documented in the literature

H. Availability of test standard

1. No plans are available for the development of the method
2. The method is to be developed
3. The method is under development
4. The method has been standardized and adopted by AASHTO, ASTM, or state agency

I. Test time

1. Very long test time (6+ days)
2. Long test time (4-5 days)
3. Medium test time (2-3 days)
4. Short test times (1 day)

J. Training requirement

1. Intensive training (heavy consequence from failure)
2. Moderate training (light consequence from failure)
3. Simple training (some guidance required)
4. Minimal training (slim chance of failure)

K. Data analysis requirement

1. Analysis is extremely difficult and requires an experienced operator
2. Analysis is difficult and will require initial guidance
3. Analysis is moderately involved; can be performed with minimal experience
4. Analysis is easy and can be performed by any operator

L. Equipment cost

1. Very expensive equipment cost
2. Moderately expensive equipment cost
3. Cheap equipment cost
4. No equipment cost

M. Technical ability requirement

1. Excellent technical ability required to complete test

2. Good technical ability required to complete test
3. Little technical ability required to complete test
4. No technical ability required to complete test

N. Test repeatability and variability

1. This procedure is hard to repeat and has many changing variables
2. This procedure is hard to repeat but has few changing variables
3. This procedure is easy to repeat but has many changing variables
4. This procedure is easy to repeat and has few changing variables

Tables A-1 and A-2 present the scoring results provided by the research team of this project and Paragon Technical Service, Inc., respectively. Table A-3 provides the equipment pertinent to the evaluation.

Table A-1. Score card ranking results from LTRC asphalt laboratory

Factors	SCB	I-FIT	OT	IDT	BF	S-VECD
A	4	4	2	3	3	2
B	4	4	4	3	4	2
C	4	4	4	3	4	3
D	3	3	3	4	3	2
E	3	3	3	3	3	3
F	4	4	3	3	2	3
G	3	2	3	3	3	3
H	4	4	4	4	4	4
I	4	4	3	4	2	2
J	3	3	3	2	2	2
K	3	3	4	3	3	2
L	2	2	2	1	1	2
M	3	3	3	2	2	2
N	4	4	3	4	3	4

Table A-2 Score card ranking results from Paragon Technical Service, Inc.

Factors	SCB	I-FIT	OT	IDT	BF	S-VECD
A	4	4	3	3	3	2

Factors	SCB	I-FIT	OT	IDT	BF	S-VECD
B	4	4	4	4	4	2
C	4	4	4	3	4	3
D	4	3	4	4	3	2
E	3	3	3	3	3	3
F	4	4	4	3	3	2
G	3	3	3	3	3	3
H	4	4	4	4	4	3
I	4	4	4	4	4	1
J	4	4	3	3	2	1
K	4	4	4	3	2	1
L	1	1	1	1	1	1
M	4	4	3	3	2	1
N	4	3	3	4	3	3

Table A-3 Equipment for the test methods pertinent to the score card evaluation

Test	AMPT	AST	MTS	Cox & Sons
SCB	L	P	--	--
I-FIT	L	P	--	--
OT	L P	--	--	--
IDT	--	P	L	--
BF	--	P	--	L
S-VECD	L	P	--	--

Note: L = LTRC; P = Paragon; -- = not applicable; AST = Asphalt Standard Tester; AMPT = Asphalt Mixture Performance Tester; MTS = Material Testing System.